
# SEDIMENT TRANSPORT

# IN THE

# MACKENZIE RIVER PLUME

prepared for:

The Atlantic Geoscience Centre
of
The Geological Survey of Canada
Bedford Institute of Oceanography
Dartmouth, Nova Scotia

by

Susan Davidson
Sylvain de Margerie
Karen Lank

**ASA Consulting Ltd.**
P.O. Box 2025
Dartmouth East, Nova Scotia
B2W 3X8

JANUARY 1988

**GEOLOGICAL SURVEY OF CANADA, OPEN FILE NO.** 2303

**Sediment Transport in the Mackenzie River Plume; Prepared by S. Davidson, S.de Margerie and K. Lank; ASA Consulting Ltd. Dartmouth, Nova Scotia; January 1988; 92p plus 2 appendices.**

This report was prepared under contract to:

Atlantic Geoscience Centre
Geological Survey of Canada
Energy Mines and Resources
Bedford Institute of Oceanography
Dartmouth, Nova Scotia.

**Scientific Authority:** P.R. Hill

Funding was provided under the Northern Oil and Gas Action Plan program (NOGAP) Project D.1: Beaufort Sea Coastal Zone Geotechnics.

*Acknowledgements*

*The authors of this report would like to thank Esso Resources Canada Ltd. for the use of their data for this study. Geoff Spedding of Esso was instrumental in obtaining this data for our use. We would also like to thank Natalie Sutterlin of the Environmental Studies Revolving Funds for her assistance, as well as Jean Gagnon of MEDS for his prompt response to our data requests.*

TABLE OF CONTENTS

LIST OF FIGURES

LIST OF TABLES

# 1.0 INTRODUCTION

## 1.1 Background

The continental shelf of the Canadian Beaufort Sea (Figure 1.1) is an area of offshore oil and gas exploration with potential for future development of hydrocarbon resources. Both exploration and development activities require seabed structures which, for safe design, necessitate an understanding of the regional sedimentary processes.

The Canadian Beaufort Sea consists of a broad continental shelf extending up to 150 km offshore from the coastline to the shelf break, located in water depths of about 100 m. The deep waters of the Mackenzie Trough, where water depths exceeding 100 m approach within 30 km of the coast, divide the shelf into two main areas. A series of shallow, gently sloped valleys traverse the continental shelf to the east of the Mackenzie Trough.

The Mackenzie River enters the Beaufort Sea through several main channels interconnected in a complex manner. These channels discharge into Shallow Bay, Mackenzie Bay and Kugmallit Bay (Figure 1.1). The Mackenzie River is the largest North American river draining into the Arctic Ocean, with a drainage basin of approximately 1.8 million square kilometers extending into British Columbia, Alberta, Saskatchewan, and the Yukon and Northwest

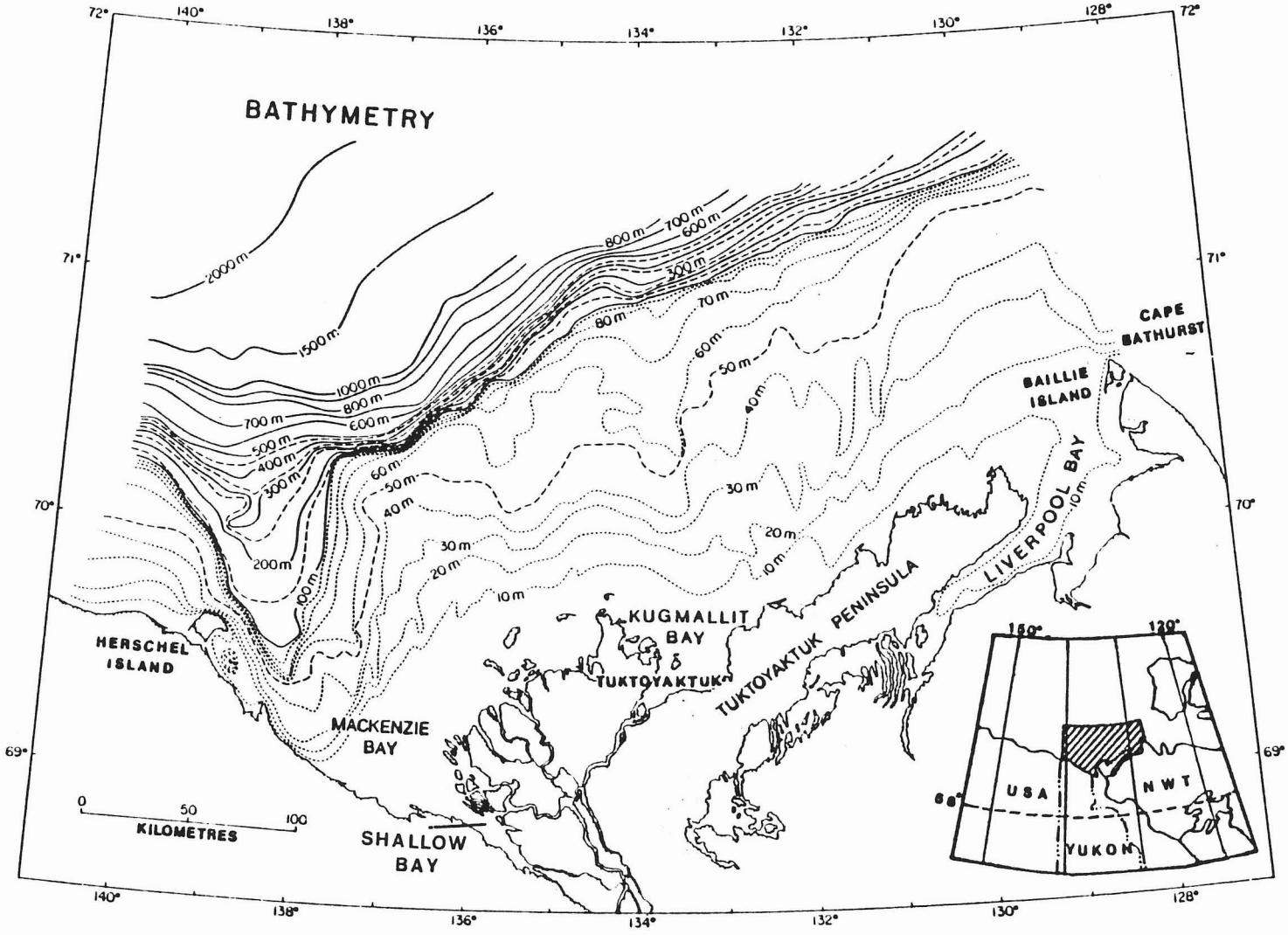


Figure 1.1 The Canadian Beaufort Sea (after Pelletier, 1975).

Territories. It has been estimated that the Mackenzie River is the largest single source of riverine sediments in the Arctic Ocean (Milliman and Meade, 1983).

Surficial seabed sediments on the Beaufort Shelf range from clays to sands and gravels (Figure 1.2). Most of the shelf area is covered with clay and silty clay deposits, with coarser silt deposits occurring inside the 10 m contour and offshore from Liverpool Bay. Isolated patches of sand and gravel occur on the eastern portion of the shelf; previous studies have concluded that these sediments are relict (e.g. Fissel and Birch, 1984). The coarser sediments to the west of Herschel Island are also probably relict, but those in the nearshore zone of the Mackenzie Delta can be attributed to the more dynamic hydrodynamic regimes of the areas (Harper and Penland, 1982).

The Beaufort Shelf differs from most other Canadian continental shelves in that it is ice-covered for most of the year. As well as directly disturbing the seabed through ice scouring, ice may be responsible for minor amounts of sediment transport through ice-rafting and by the selective concentration of suspended sediments during the freezing process (Harper and Penland, 1982). In addition, the location of the offshore ice edge during the open water season significantly affects the wave climate through limiting the effective fetch for wave generation. Typical ice edge positions for late August are shown in Figure 1.3.

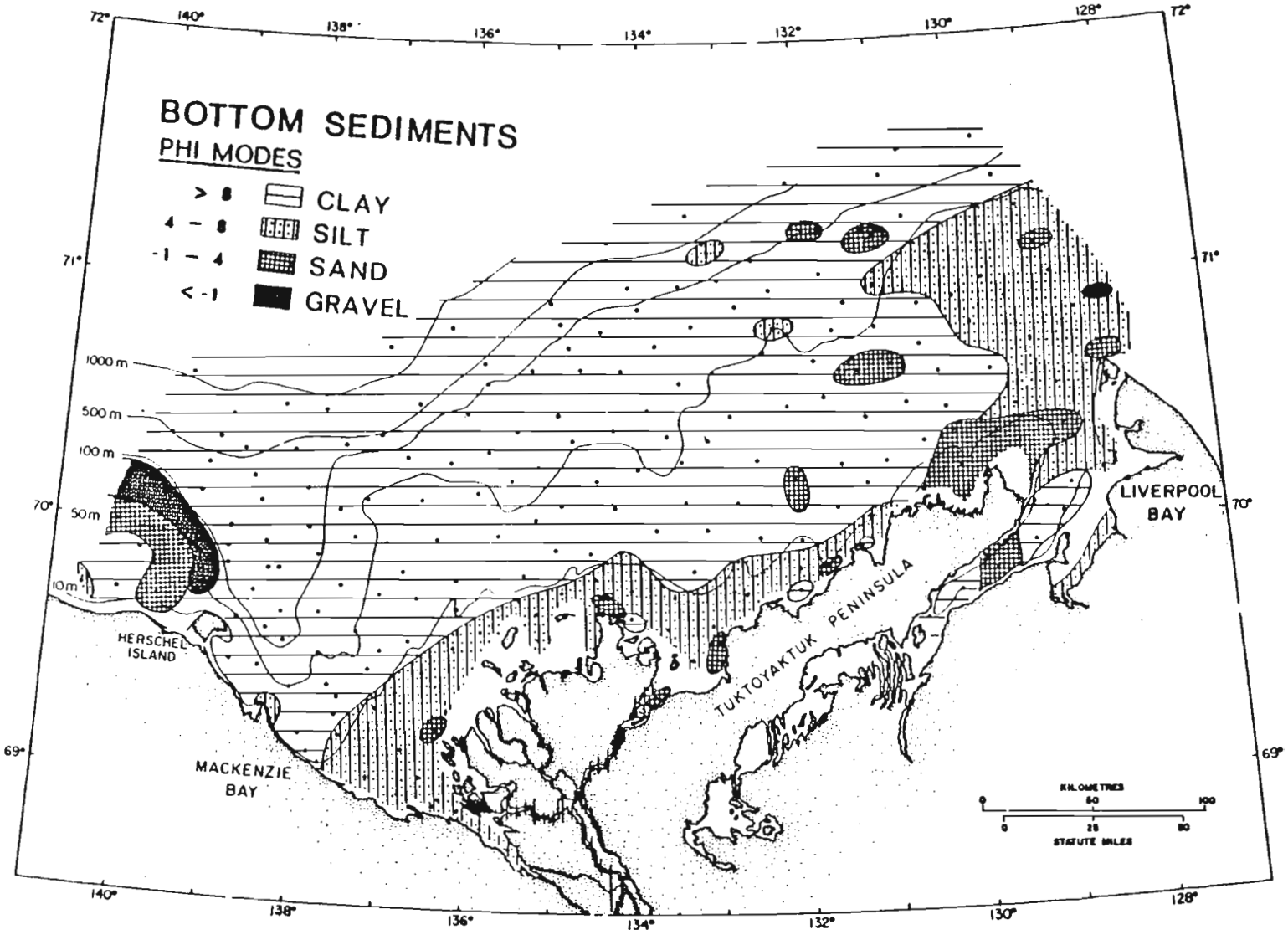


Figure 1.2 Surficial seabed sediments on the Beaufort Shelf (after Pelletier, 1975)

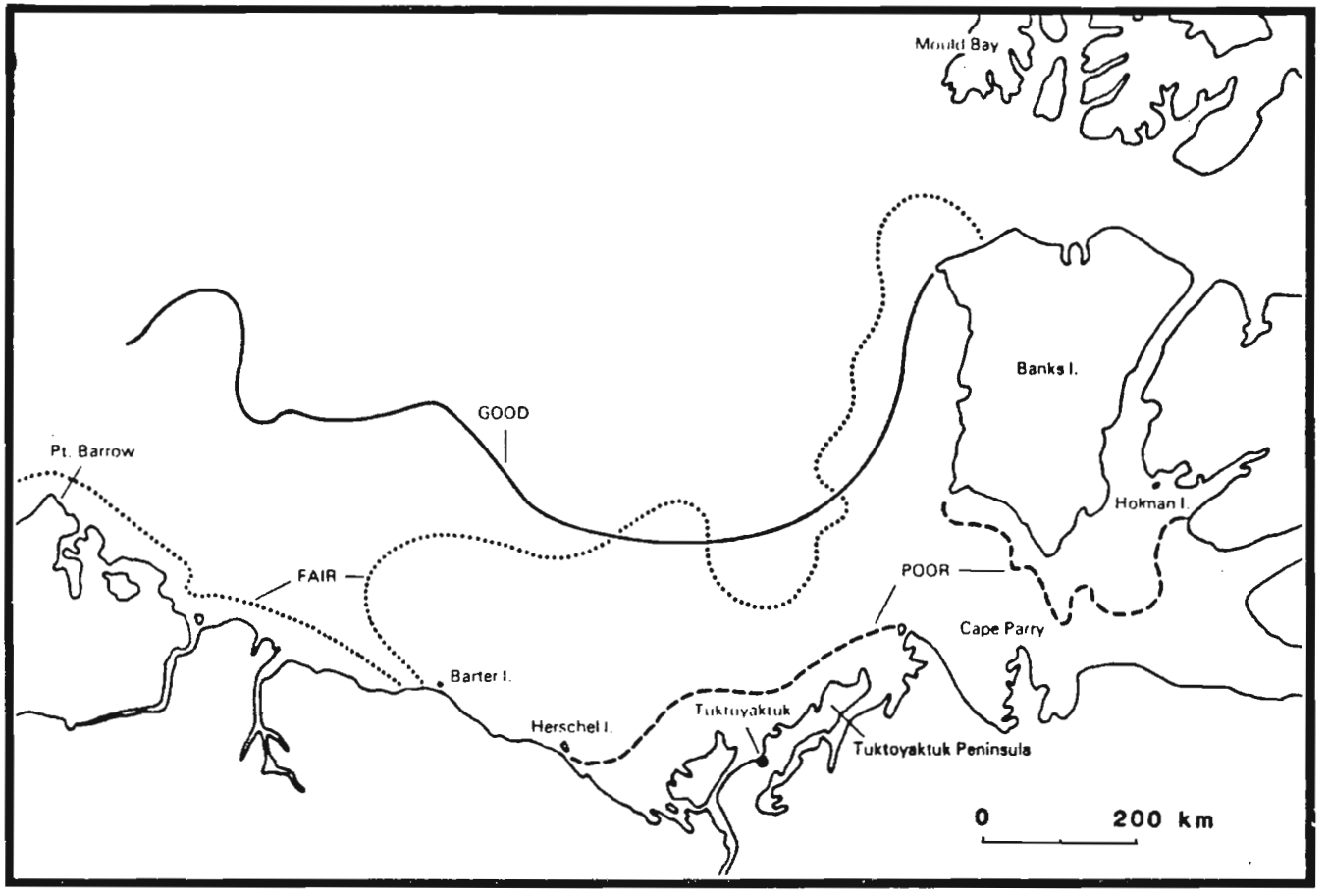


Figure 1.3 Typical ice edge positions for late August (after Harper and Penland, 1982).

The Beaufort Sea ice cover can be divided into three zones: the landfast ice, which is essentially immobile and extends out to about 20 m water depth by mid-winter; the Beaufort Sea pack ice which covers most of the deep water of the Canadian Basin and moves in a roughly clockwise direction with the ambient water currents; and the transition ice zone which provides a buffer zone between the mobile pack ice and the relatively stationary landfast ice.

The landfast ice zone is characterized by numerous ice ridges and underwater keels. These keels can scour the seabed, leading to extensive bottom sediment disturbance and reworking. Actual sediment transport and dispersion, however, will depend on the ambient under-ice currents which are significantly reduced from those present during the open water season. Inadequate information is available to assess the magnitude of scouring related transport, but Harper et al. (in prep.) consider it to be insignificant. Minor amounts of sediment may also be transported through ice-rafting and the selective concentration of suspended sediments during the freezing process.

## 1.2 Sediment Transport Processes

Sediment transport processes in any marine environment depend on the ambient hydrodynamic and geological conditions, in that the hydrodynamic conditions provide the forces which lead to sediment

suspension and movement while geological factors influence the supply and type of sediment available for transport. The relative importance of various transporting mechanisms varies with location in the offshore.

Harper et al. (in prep.) considered four main sediment transport processes for the Beaufort shelf. These include: ice-related transport, surface plume dispersal, wave-generated transport and bottom current transport. Since wave- and current-generated transport are not generally independent (due to wave current interactions), they will be considered together in this study.

The major effect of sea ice in modifying sediment transport processes is in limiting the effective fetch during the open water season. Figure 1.3 shows the extreme variation in ice edge position for late August; the open water fetch in a northwesterly direction ranges from about 100 km during a poor ice year to almost 1000 km during a good year. Both the surface wave and storm-driven current climates on the shelf will be severely affected by the available fetch.

The Mackenzie River is thought to be the largest single source of riverine sediments to the Arctic Ocean (Milliman and Meade, 1983). An analysis of surface suspended sediment concentrations using LANDSAT images (Harper and Penland, 1982) showed that the surface plume consists of two parts: a

concentrated inner plume separated by a sharp concentration gradient from a much larger, diffuse outer plume. This sharp concentration gradient generally occurs within the 10 m or even the 5 m isobath. The plume responds to the ambient winds, being deflected to the east along the coastline under westerly winds and to the west and northward under easterlies. Thus, plume advection and dispersion processes lead to the distribution of fluvial sediments over a wider area of the Beaufort shelf.

As well as supplying sediments to the Beaufort Shelf, the estuarine circulation patterns induced by the fresh river water may provide a significant contribution to the nearshore and inner shelf current regime. The typical estuarine pattern consists of an outward surface current coupled with a shoreward return current at the seabed.

Sediment transport occurs when seabed or suspended sediments are carried away from the point of origin by the ambient currents. Sediment resuspension from the seabed occurs when the seabed shear stress exceeds the critical value for the in situ sediments. Once sediments are resuspended, they will be transported by the currents until the stress level decreases to the point where deposition can occur.

The shear stress acting on the seabed results from the combined influence of all the hydrodynamic processes creating bottom currents. These processes can include large scale oceanic

circulation and related features such as eddies and meanders, atmospherically forced motions including inertial oscillations, tides, internal tides and internal waves and surface waves and wave-generated currents. All of these processes can lead to both surface and near-bed currents. In addition, nonlinear interactions between currents of different frequencies (i.e. surface waves and longer period tidal currents) can lead to greatly increased bottom stresses.

The critical shear stress for mobilizing sediments also varies temporally and spatially, due to sediment grain size, composition, degree of consolidation and biological component (McCave, 1984). To add to the complexity of the system, the critical shear stress can actually depend on the hydrodynamic forces and in extreme cases the cyclic wave loading may lead to total loss of shear strength (i.e. sediment liquefaction). Sediments will tend to settle where they are in equilibrium with respect to the hydrodynamic environment, and their local properties will often provide a valuable clue to the intensity of hydrodynamic disturbances.

The relative importance of the various hydrodynamic processes in creating currents large enough to lead to sediment motion varies with location on the continental shelf. In general, large scale currents and internal tides and waves predominate near the shelf break and outer shelf with atmospherically forced currents, tidal currents and surface wave effects increasing in

importance as the water depth decreases. Within the nearshore zone, oscillatory wave-induced currents and lower frequency currents generated by wave breaking and frictional dissipation of wave energy largely govern the rates and directions of sediment movement.

## 1.3 Previous Studies

The first sediment dispersion model for the Beaufort Sea was developed by Pelletier (1975), based on measured surficial sediment distributions (Figure 1.2). Pelletier identified fine-grained fluvial sediments extending from Herschel Island to the eastern end of the Tuktoyaktuk Peninsula and offshore to the continental shelf. The coarser sediments to the west and east of this area suggest a reduced fluvial sediment component (Fissel and Birch, 1984). The conceptual model developed by Pelletier is presented in Figure 1.4. The main elements of this and later models include:

(1) a nearshore area of the shelf dominated by the presence of the Mackenzie River sediment plume,

(2) a net eastward deflection of the plume along the Tuktoyaktuk Peninsula, and

(3) various energy zones, with zones of highest energy generally located near the coastline and energy level decreasing across the continental shelf.

Harper and Penland (1982) interpreted all available oceanographic, hydrological and geological data to produce a

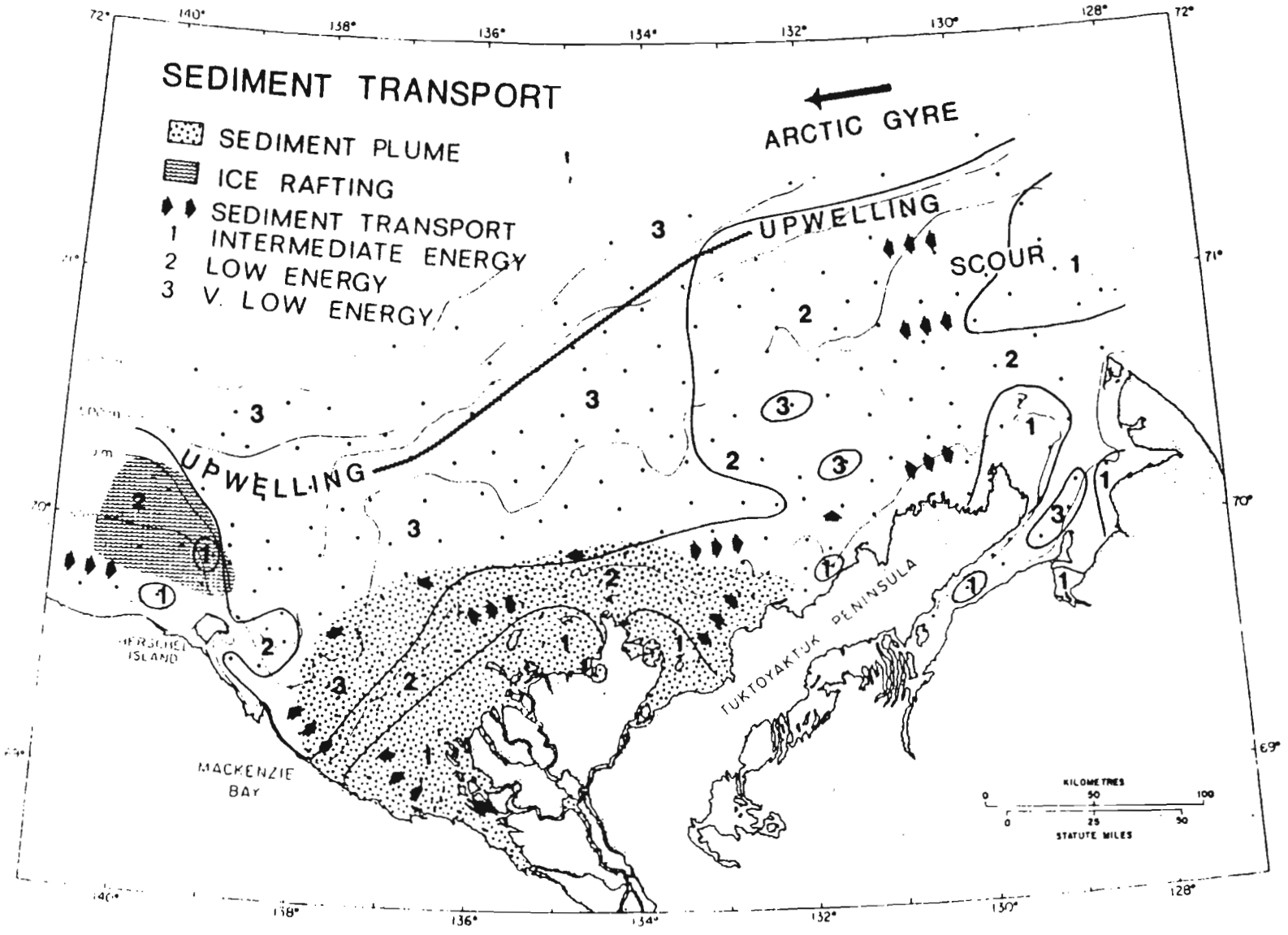


Figure 1.4 Conceptual model of shelf sediment transport developed by Pelletier (1975).

sediment budget and a modified model for sediment transport and dispersion on the Canadian Beaufort Shelf. The sediment budget with the major sources and sinks of sedimentary material is summarized in Table 1.1. As can be seen from this table, the Mackenzie River provides over 95% of the total sediment input to the Canadian Beaufort Sea. The major sediment sink appears to be sediment accumulation on the continental shelf, although insufficient information was available to estimate sediment losses to the continental slope and Arctic basin or to sediment accumulation in estuaries. Discrepancies between estimates of sediment sources and sinks could also be attributed to errors in the estimates of shelf sediment accumulations (Harper et al., in prep.).

The conceptual model for sediment dispersion on the Beaufort Shelf as developed by Harper et al. (in prep.) is presented in Figure 1.5. This model extends that of Pelletier (1975) to include the results of the analyses conducted in the later study. Harper et al. found that surface waves provide the major source of energy for sediment transport; these authors divide the shelf into three energy zones depending on the frequency of resuspension of bottom sediments by surface waves. Most of the wave energy was found to be concentrated in westerly storms; these storms also drive eastward currents and deflect the surface plume of the Mackenzie River to the east.

TABLE 1.1

Sediment budget for the Beaufort Sea shelf
(Harper and Penland, 1982)

| Sediment Sources | | $m^3/yr$ |
|---|---|---|
| Fluvial | | |
| Mackenzie River | | $8.56 \times 10^7$ |
| Yukon Rivers | | $4.53 \times 10^5$ |
| Coastal Erosion | | $<2.94 \times 10^6$ |
| | TOTAL | $8.89 \times 10^7$ |
| **Sediment Sinks** | | |
| Estuaries | | ? |
| Coastal Landforms | | $>2.96 \times 10^4$ |
| Shelf | | $4.2$ to $5.2 \times 10^7$ |
| Offshore | | ? |
| | TOTAL | $4.2$ TO $7.1 \times 10^7$ |

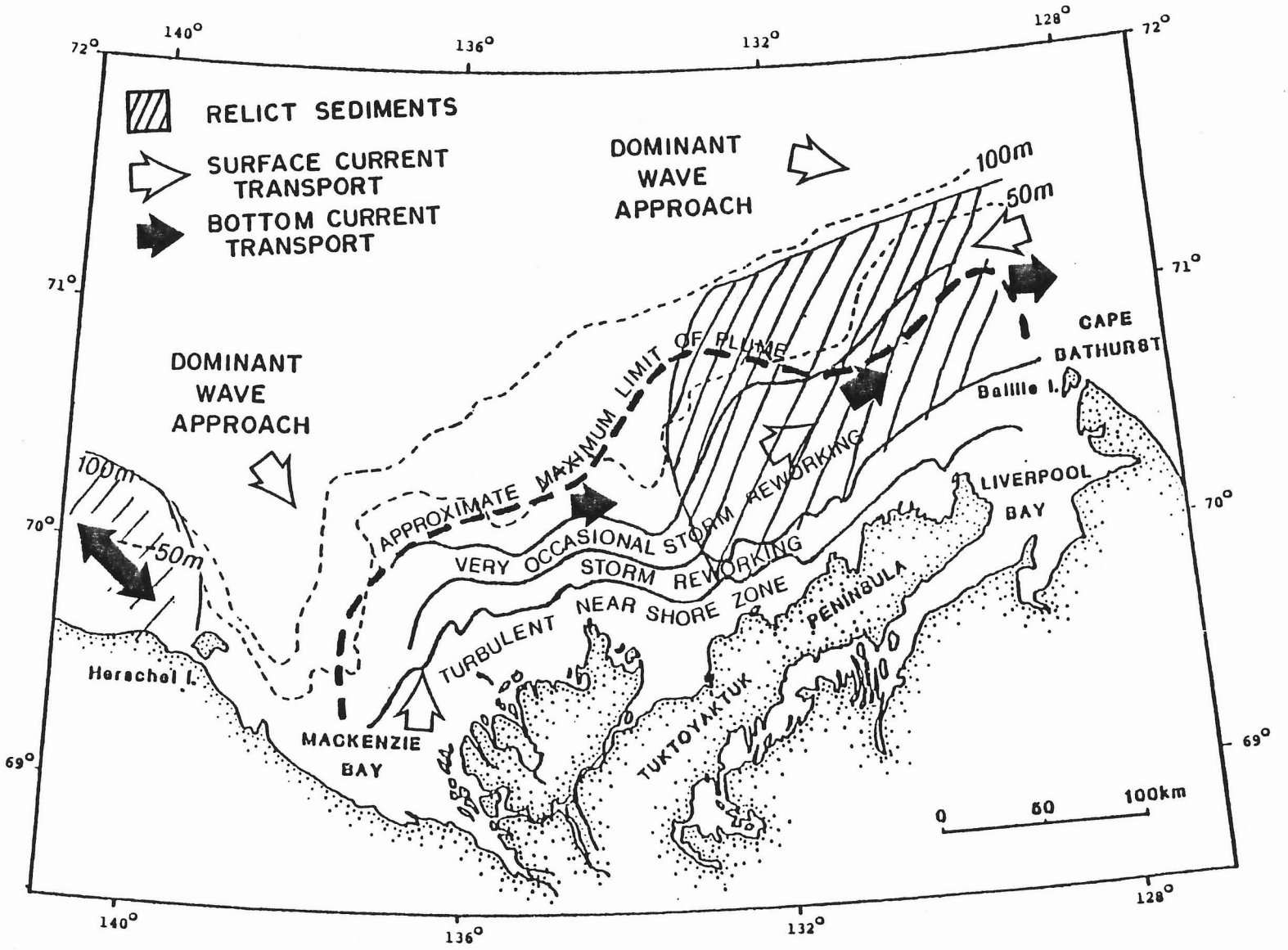


Figure 1.5 Conceptual model of shelf sediment transport developed by Harper et al. (in prep.).

Further data analyses were conducted by Fissel and Birch (1984) in order to more fully quantify the processes responsible for shelf sediment transport, with emphasis on the middle and outer portions of the shelf. Again, the shelf area is divided into three spatial units with varying energy levels and sedimentation characteristics: the nearshore shelf, the mid-depth shelf and the outer shelf (Figure 1.6). The Alaskan and Yukon Trough, the Mackenzie Trough, the continental slope and the Amundsen Gulf Trough are considered to be sediment sinks. The major characteristics of the three shelf zones are:

(1) the nearshore zone: this zone is characterized by high levels of sediment accumulation, suspended sediment concentrations and bottom resuspension by both wave-induced and steady currents. This zone extends to 10 to 20 m water depth.

(2) the mid-depth zone: sediment accumulation and suspended sediment concentrations are greatly reduced from the levels in the near-shore zone. Currents are also reduced and wave disturbance of the bottom is infrequent but occurs at least once each summer season. This zone extends offshore from the nearshore zone to a water depth of 50 to 75 m.

(3) the outer shelf zone: this zone differs from the mid-shelf zone primarily in terms of energy levels, in that the steady bottom current component is greater but wave-induced bottom oscillations are less than in the mid-shelf zone.

These studies have indicated a general lack of data and information concerning the sedimentary processes in the nearshore zone, particularly in water depths of less than 10 m. Hill and Nadeau (in prep.) describe additional data analyses for this inner shelf zone and describe a preliminary model based on interpretations of both oceanographic data and the near surface

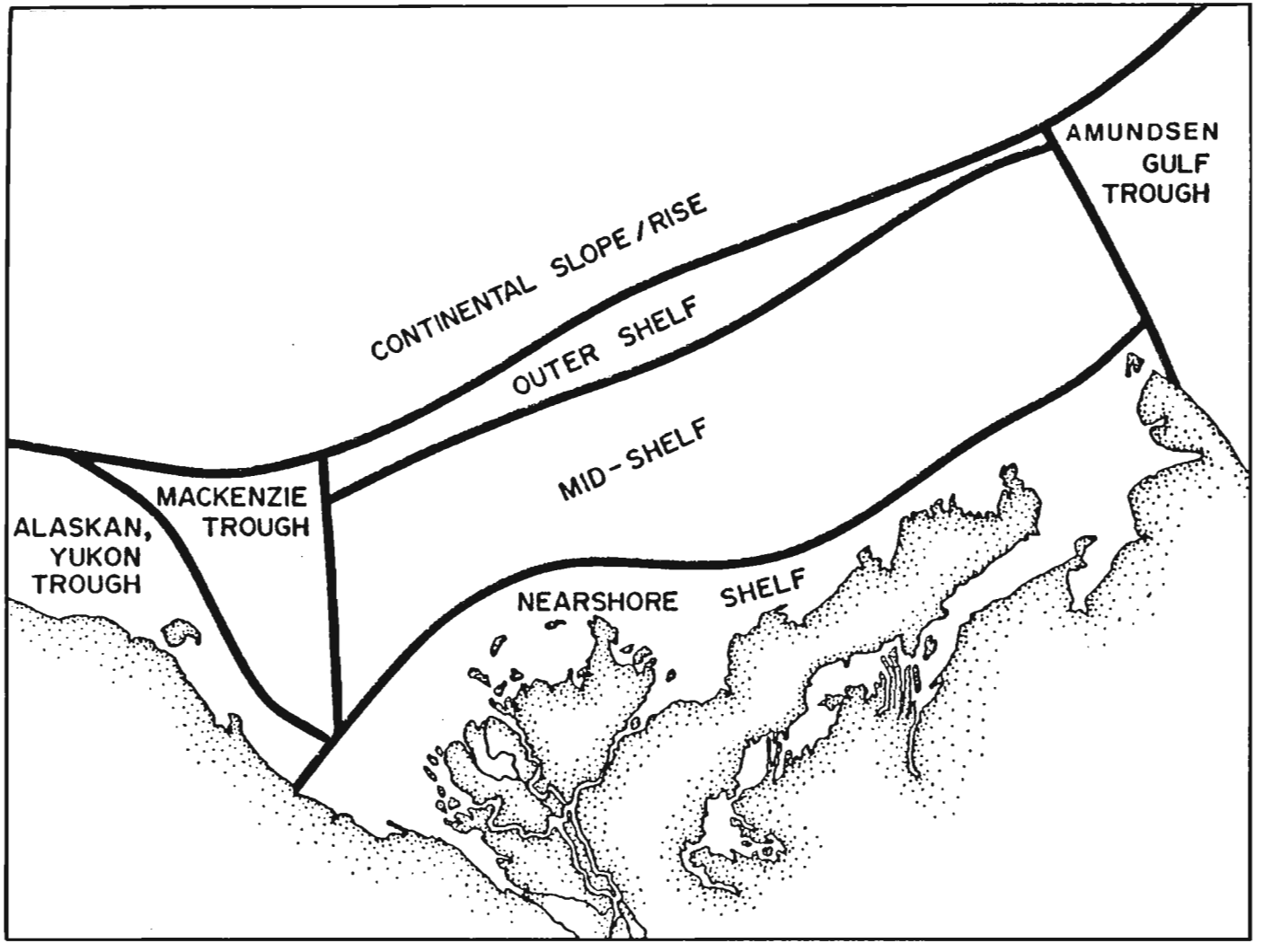


Figure 1.6 Spatial units for the conceptual model of sediment transport developed by Fissel and Birch (1984).

facies distributions. They conclude that a combination of wave-, wind- and circulation-driven currents results in maximum energy and high suspended sediment concentrations near the seabed at about 5 m water depth, with the intensity of bottom sediment reworking decreasing in both the onshore and offshore directions.

## 1.4 Study Objectives and Report Organization

The main objective of this study was to develop a conceptual model which quantifies the relative importance of estuarine circulation, wind-induced currents and wave-induced oscillatory currents in the reworking of bottom sediments on the inner Beaufort Shelf. Analyses were conducted of current, wind and wave records for the inner shelf for 1984, 1985 and 1986. Temperature and salinity data were also considered where appropriate, as were several case studies of individual storm events. Chapter 2 of this report describes the analysis procedures and results of the individual analyses, while Chapter 3 discusses these results in terms of sediment transport and resuspension processes while Chapter 4 summarizes the findings and gives recommendations for future studies.

# 2.0 DATA ANALYSES

This chapter describes the sources and quality of the data used for this study, as well as the types of analyses conducted and the basic results of these analyses.

## 2.1 Available Data

The main purpose of this study was to quantify the relative importance of estuarine circulation, wind- and wave-induced steady currents and wave-induced oscillatory currents in the reworking of bottom sediments on the inner Beaufort shelf and nearshore zone. This study considered recent data collected in the years 1984, 1985 and 1986, focussing on the study area defined by Figure 2.1.

### *2.1.1 Currents and Waves*

The oceanographic data sets used in this study are summarized in Tables 2.1 to 2.3, with station locations shown in Figure 2.1. The 1986 data were obtained as part of an Environmental Studies Revolving Funds (ESRF) project as described by Hodgins et al. (1987). Current velocities were measured at two sites, T1.1 and T1.2, with suspended sediment concentrations also being measured at the shallow water site, T1.2. The burst sampling strategy used for current velocity measurements provided direct observations of wave orbital velocities as well as mean current components.

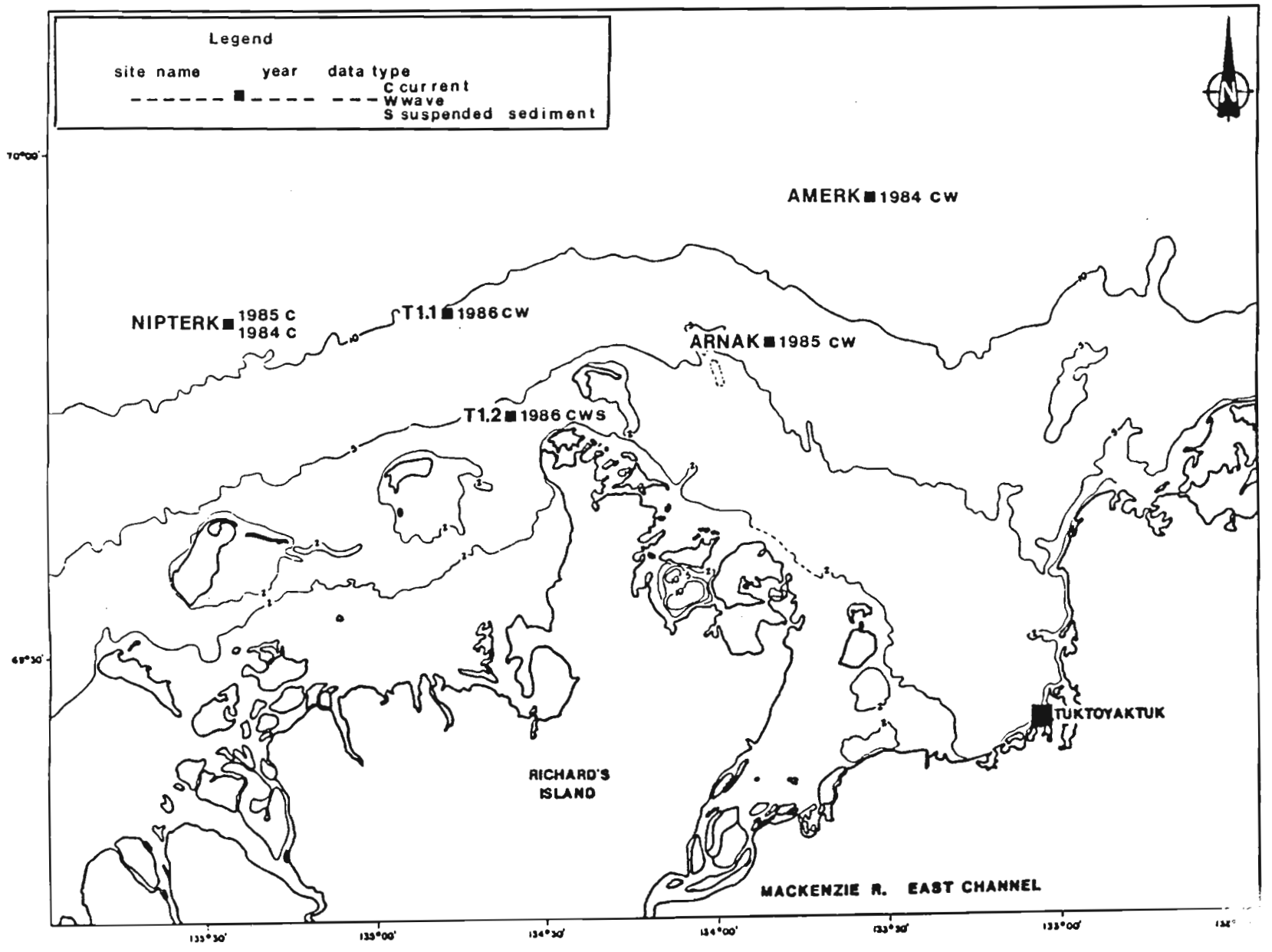


Figure 2.1 Study area with current meter locations.

TABLE 2.1

Oceanographic Data for 1986

| Location | Water Depth (m) | Dates | Data Description |
|---|---|---|---|
| T1.1 | 10.5 | 18 Aug. - 24 Sept. | 0.5 m above seabed:<br>-burst velocity data (1024 values of u and v at 1 Hz) every 4 hours<br>-derived wave parameters $H_{sig}$ and $T_p$ every 4 hours<br>-mean current components u and v every 15 minutes |
| T1.2 | 5.9 | 18 Aug. - 24 Sept. | 0.5 m above seabed:<br>-burst velocity data (1024 values of u and v at 1 Hz) every 4 hours<br>-derived wave parameters $H_{sig}$ and $T_p$ every 4 hours<br>-derived mean current components u and v every 4 hours<br>1.0 m above seabed:<br>-suspended sediment concentrations every 4 hours |

TABLE 2.2

Oceanographic Data for 1985

| Location | Water Depth (m) | Dates | Data Description |
|---|---|---|---|
| ARNAK | 7.6 | 28 Aug. - 3 Oct. | 2.8 m above seabed:<br>-burst velocity data (60 values of u and v at 1 Hz) every 90 minutes<br>- derived mean current components u and v every 90 minutes<br>1.6 m above seabed:<br>-temperature and salinity every 30 minutes |
| NIPTERK | 12.2 | 26 Aug. - 14 Oct. | 4.4 m above seabed:<br>-mean current components u and v every 30 minutes<br>2.6 m above seabed:<br>-mean current components u and v every 30 minutes<br>-temperature and salinity every 30 minutes |

TABLE 2.3

Oceanographic Data for 1984

| Location | Water Depth (m) | Dates | Data Description |
|---|---|---|---|
| AMERK | 20.5 | 31 July - 26 Sept. | 13.4 m above seabed:<br>-mean current components u and v every 15 minutes |
| | 22.5 | 24 July - 27 Sept. | 3.0 m above seabed:<br>-mean current components u and v every 30 minutes |
| | 21.0 | 5 Aug. - 5 Oct. (many data gaps) | -$H_{sig}$ and $T_p$ every 3 hours (surface wave rider) |
| NIPTERK | 14.6 | 5 Aug. - 26 Sept. | 7.6 m above seabed:<br>-mean current components u and v every 15 minutes |
| | 14.3 | 24 July - 26 Sept. | 3.3 m above seabed:<br>-mean current components u and v every 30 minutes |

Currents were measured by Esso Resources Canada Ltd. at the Arnak and Nipterk sites during the 1985 open water season (Arctic Laboratories Ltd., 1985a and 1985b). These data records were obtained through the Marine Environmental Data Service (MEDS) of Environment Canada. Two instruments were moored at each site, however, data recovery was poor in some cases. The near-bed Aanderaa meter used at the Arnak site was damaged by ice and thus provided only temperature and salinity data.

The burst sampling strategy used by the Inter Ocean S4 meter at the Arnak site was sufficient to provide estimates of wave orbital velocities. The raw data were obtained from Arctic Laboratories Ltd. for this purpose; analysis techniques will be described later in this chapter. This data provided the only source of wave climate information for 1985.

Esso also measured currents at the Nipterk and Amerk sites during the summer of 1984 (Birch et al., 1984a and 1984b). The near-bed meters at both sites were Endeco 105 current meters, for which Birch et al. state the direction data were poor at low current speeds. However, the current patterns were found to be consistent with other observations so all directional data were employed for this study. Nondirectional surface wave measurements near the Amerk site were obtained through a MEDS program; these data were somewhat sporadic.

### 2.1.2 *Wind Observations*

Wind and weather data from Tuktayuktuk and the Molikpak and Kulluk drilling locations were obtained from Seaconsult Ltd. for the 1986 season. All three records are relatively continuous, except for the drill ship Kulluk which changed location near mid-season. For 1984 and 1985, weather observations from Tuktoyaktuk, as well as all offshore observations collected in the area north of 58° and west of 120° were acquired from the Atmospheric Environment Service (AES) of Environment Canada. Most of these data records are fragmented and discontinuous, but relatively continuous records were extracted for Havik (1984 and first part of 1985) and Molikpak (last part of 1985). The locations of the wind observation stations are given in Figure 2.2.

The analysis procedures described in the following sections of this report used the offshore wind stations since land effects can be significant in the Tuktoyaktuk wind data. For 1986, the Molikpak data were selected over the Kulluk data due to greater continuity of the data record. Correlation analyses showed a high correlation among offshore wind observations ($R^2 > 0.8$).

### 2.1.3 *Mackenzie River Discharge*

River flow data were acquired from the Canada Center for Inland Waters (CCIW) and station locations are listed in Table 2.4

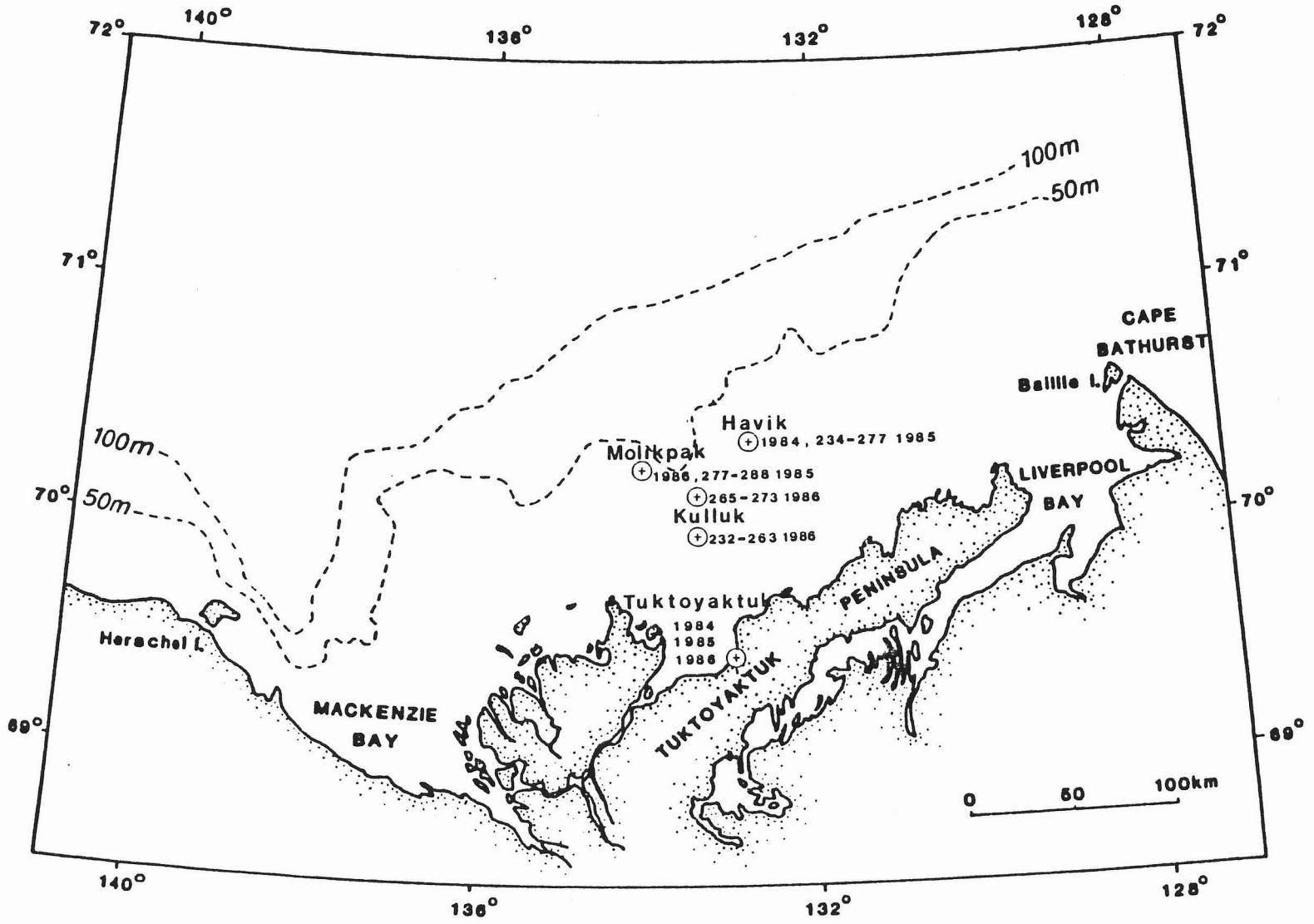


Figure 2.2 Locations and dates of wind observations.

TABLE 2.4

River flow monitoring stations

| Station number | CCIW ref. number | Location | August mean flow ($m^3/s$) | years available |
|---|---|---|---|---|
| 1 | 10LA002 | Arctic Red River near Mouth 66° 47' 10"N, 133° 06' 00"W | 526 | 1984, 85, 86 |
| 2 | 10LA003 | MacKenzie above Arctic Red 67° 21' 30"N, 133° 33' 30"W | 14 500 | 1984 |
| 3 | 10LA004 | Weldon Creek near mouth 66° 23' 10"N, 132° 39' 00"W | 5 | 1984, 85 |
| 4 | 10LC002 | East Channel at Inuvik 68° 22' 33"N, 133° 45' 46"W | 266 | 1984, 85, 86 |
| 5 | 10LC003 | Rengleng River below highway 67° 45' 25"N, 133° 51' 25"W | 1 | 1984, 85 |
| 6 | 10LC007 | Caribou Creek above highway 68° 04' 15"N, 133° 28' 30"W | 1 | 1984, 85, 86 |
| 7 | 10LC009 | Cabin Creek above highway 68° 15' 00"N, 133° 15' 00"W | 1 | 1984, 85 |
| 8 | 10LC010 | Boot Creek near Inuvik 68° 21' 23"N, 133° 40' 15"W | 0 | 1985, 86 |
| 9 | 10MC002 | Peel above Fort MacPherson 67° 13' 15"N, 134° 56' 45"W | 1 180 | 1984, 85, 86 |
| 10 | 10MC007 | Rat River at Fort MacPherson 67° 40' 45"N, 135° 42' 30"W | 27 | 1984, 85, 86 |

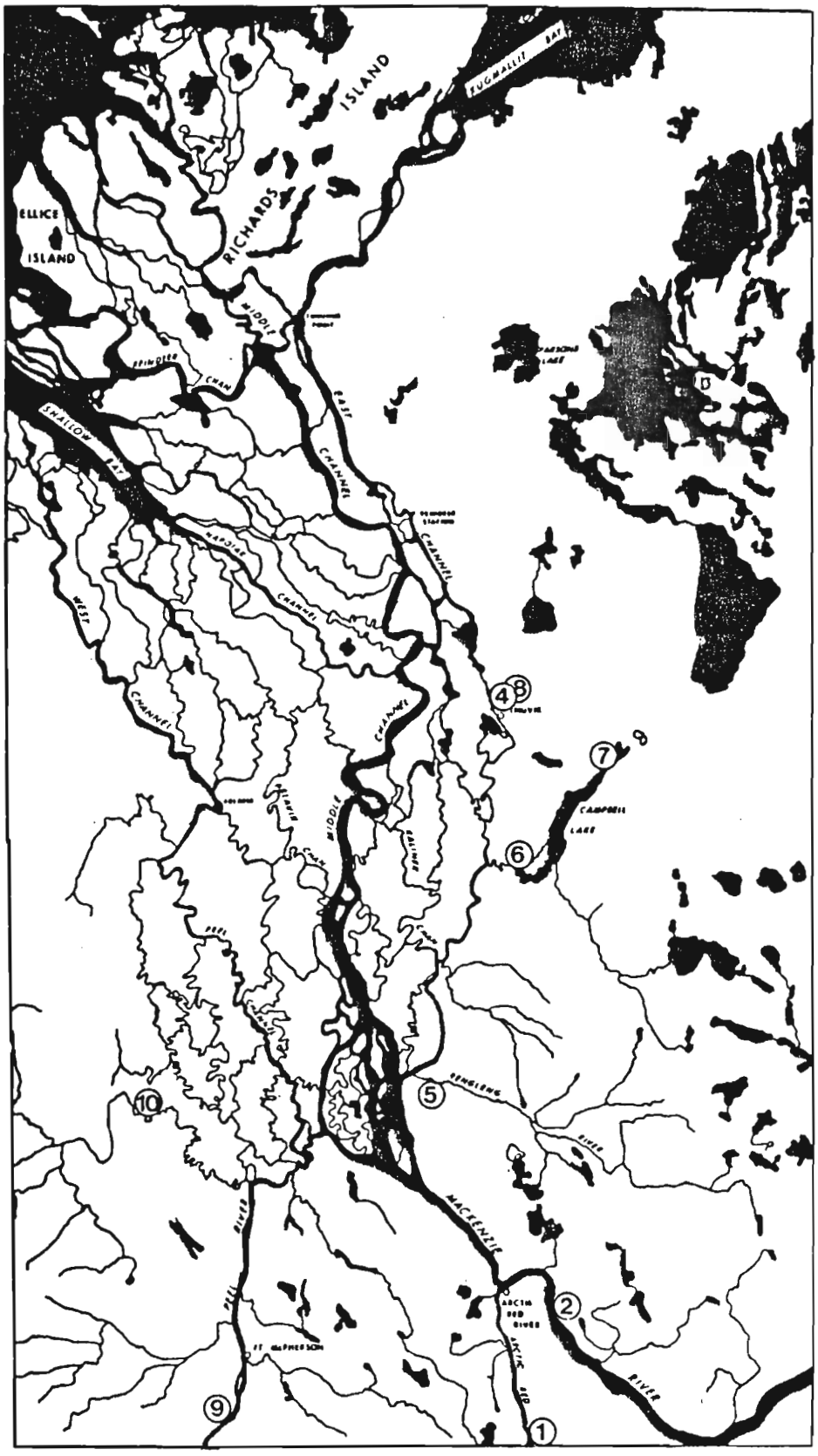


Figure 2.3 River flow measuring station locations.

and plotted in Figure 2.3. Only data from stations 1, 2, 4 and 9 were used since the other locations represent a very small proportion of the flow into the Mackenzie Delta system.

### *2.1.4 Sea Ice*

Weekly ice charts produced by AES were obtained for 1984 and 1985 through the Bedford Institute of Oceanography. Similar charts for 1986 were obtained from Hodgins et al. (1987).

### *2.1.5 Temperature and Salinity*

Although not used extensively in this study, temperature and salinity data were obtained from Nadeau (1984) for the 1984 season and from Hill (pers. comm.) for 1986.

## 2.2 Mean Flows and Velocity Variance

All time series used in this study have been plotted and are shown in Appendix A. The current velocities have been divided into directional components, with the eastward component denoted as u and the northward component as v.

As a first step in data analysis, mean flows and velocity variances were calculated for each of the current records and are

given in Table 2.5. This data is presented graphically in Figures 2.4 and 2.5, where each cluster represents a current meter time series with each dot representing one velocity observation. The mean current velocity is indicated by the position of the centre of the cluster with respect to the station location and the magnitude of the velocity variance is related to the scatter of the cluster. From these plots it can easily be seen that the variable component of motion is much greater than the mean flow.

The mean flow velocities given in Table 2.5 range from approximately 2 to 10 cm/s, with the standard deviation of the velocity (square root of the variance) ranging between 9 and 26 cm/s. These estimates are subject to statistical uncertainty; using a time scale of 4 days to assess the number of independent samples in the time series, it is found that the mean velocities are not statistically significant at the 64% level.

The current variance can be seen to increase in shallow water as well as to increase with distance away from the seabed. Considering data sets taken within the same year, it is found without exception that the near bottom current variance is greater in shallower water. Similarly, currents measured at the same location are always greater further off the bottom. This can be expected for wave-generated currents as well as for direct wind forcing, both of which are more effective in shallow water. Boundary layer and stratification effects will also tend to decrease currents with distance from the surface. The available

TABLE 2.5

Mean currents, current variance and standard deviations

| year / station | water depth (m) | instrument depth (m) | U / V mean (m/s) | total variance ($m^2/s^2$) | standard deviation (m/s) |
|---|---|---|---|---|---|
| 1986 | | | | | |
| T1.1 | 10.5 | 10.0 | 0.019 | 0.0086 | 0.093 |
| | | | 0.002 | | |
| T1.2 | 5.9 | 5.4 | 0.054 | 0.0431 | 0.208 |
| | | | 0.044 | | |
| 1985 | | | | | |
| ARNAK | 7.6 | 4.8 | -0.025 | 0.0408 | 0.202 |
| | | | 0.013 | | |
| NIPTERK | 12.2 | 7.8 | 0.027 | 0.0525 | 0.229 |
| | | | 0.005 | | |
| | 12.2 | 9.6 | 0.009 | 0.0233 | 0.153 |
| | | | 0.014 | | |
| 1984 | | | | | |
| AMERK | 20.5 | 7.1 | -0.0579 | 0.0654 | 0.256 |
| | | | 0.0026 | | |
| | 22.5 | 19.5 | 0.0071 | 0.0070 | 0.084 |
| | | | -0.0062 | | |
| NIPTERK | 14.6 | 7.0 | -0.0873 | 0.0385 | 0.196 |
| | | | -0.0096 | | |
| | 14.3 | 11.0 | 0.0234 | 0.0259 | 0.161 |
| | | | 0.0124 | | |

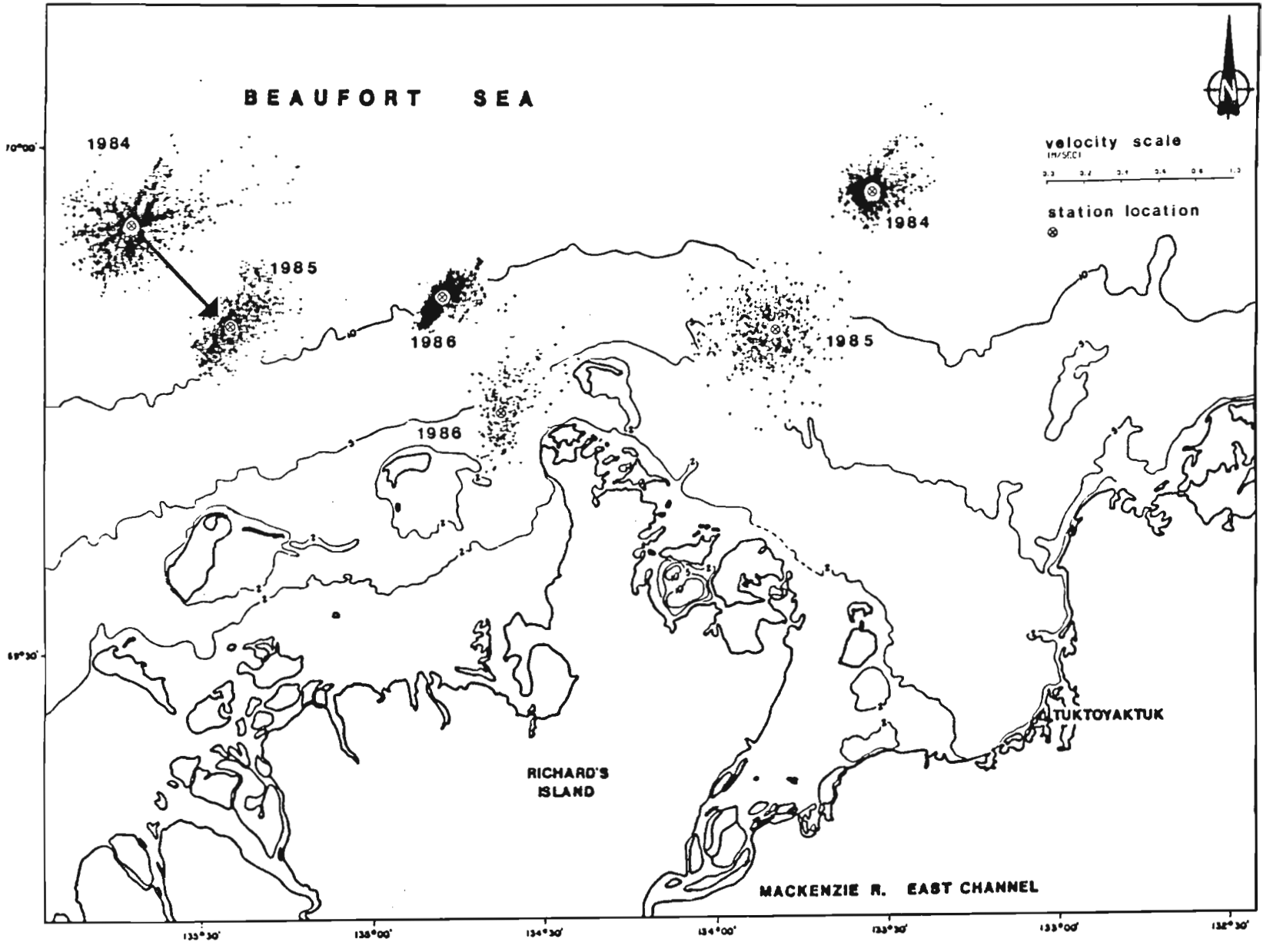


Figure 2.4 Spatial distribution of currents.

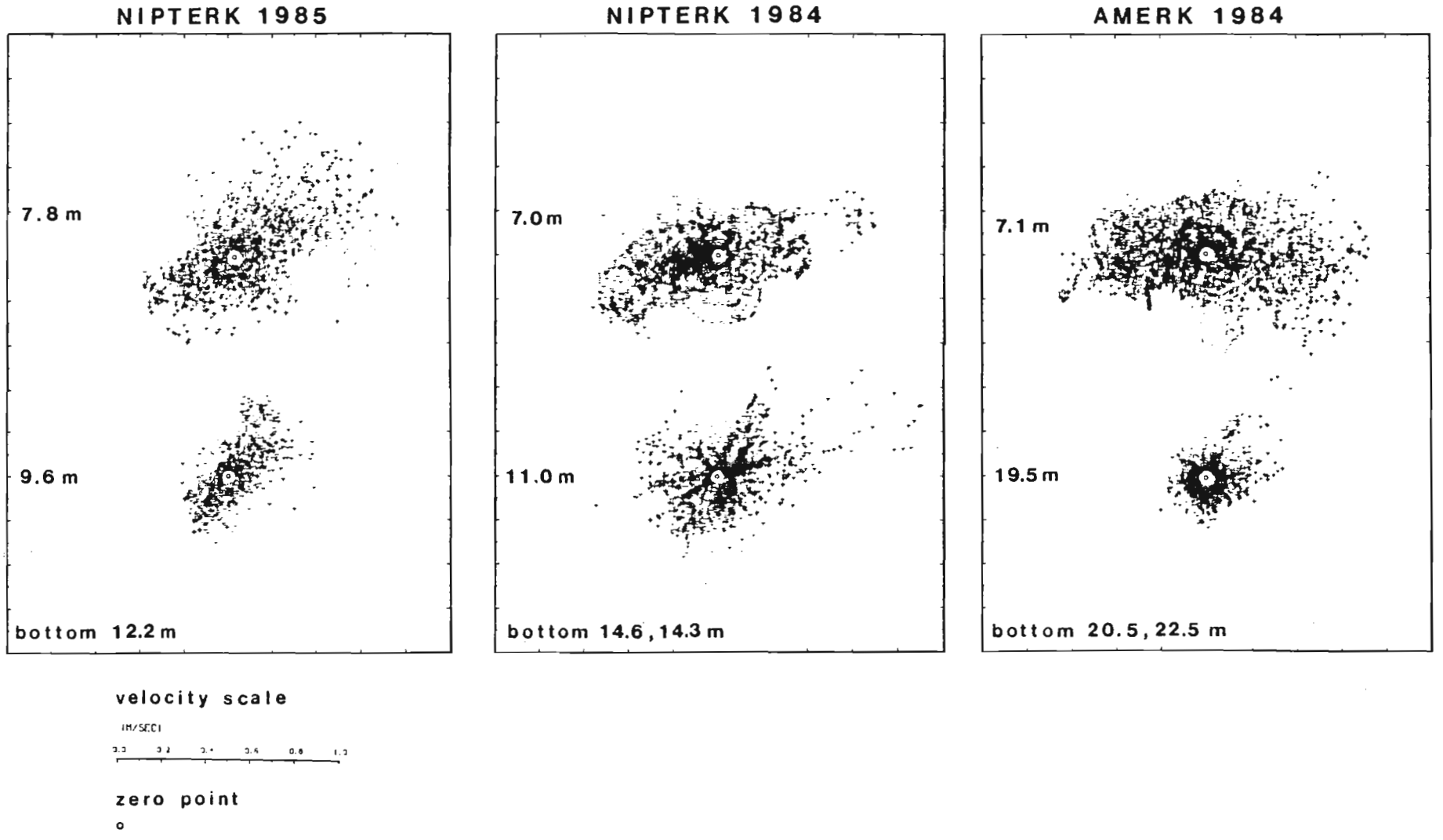


Figure 2.5 Vertical distribution of currents.

data suggest that, to a first approximation, the standard deviation of the current speed increases linearly with the inverse of distance from the surface (Figure 2.6).

## 2.3 Frequency Distribution of Velocity Variance

As described earlier in this report, several hydrodynamic processes can be responsible for current generation on the continental shelf. These processes can include large scale oceanic circulation and related features such as eddies and meanders, atmospherically forced motions including inertial oscillations, tides, internal tides, internal waves and surface waves and wave-generated currents. These forcing mechanisms can often be identified in the current record by their characteristic frequencies. For example, the principally semi-diurnal tidal currents will be characterized by a dominant 12.42 hour cycle, while wind driven currents would be expected to have a similar time scale as the wind climate itself, usually in the order of several to tens of days.

Tidal analyses were conducted for all current meter time series using standard least square techniques. However, the similarity between the inertial period and the semi-diurnal tidal period introduces a potentially large degree of error into the results. Inertial motions result from the free oscillation of the ocean following any transient forcing; the inertial period depends

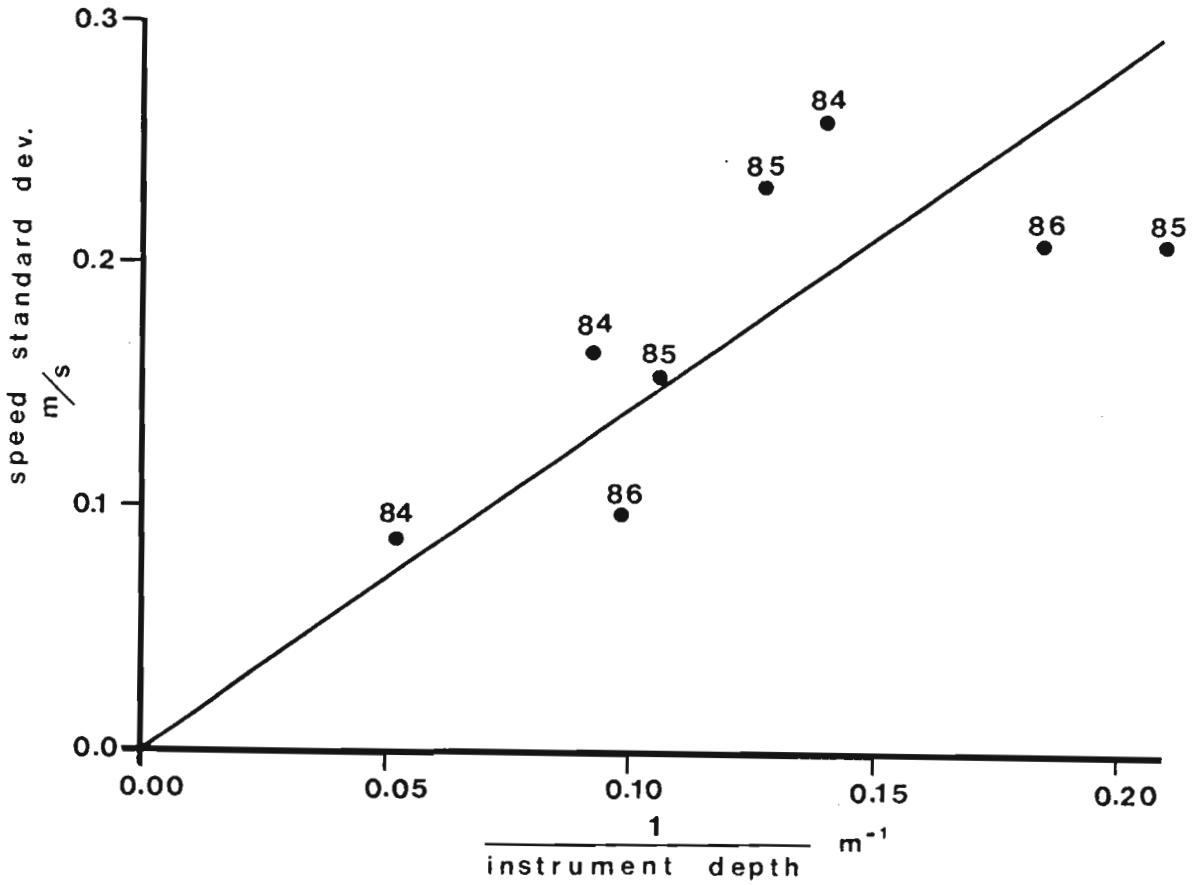


Figure 2.6 Standard deviation of current speed as a function of distance from the sea surface.

on latitude and is about 12.7 hours in the study area. Under ideal conditions, the minimum recording period required to separate the two signals would be 23 days, but a much longer data record is required if current variability is high and other signals are also present. Due to the short ice-free season, most of the current meter records from the Beaufort Sea are too short to adequately resolve these two signals.

For all the current meter time series, the amount of variance explained by tidal analysis was small, roughly 10%, most of which was in the principal fortnightly constituent (14 day period) as opposed to the semi-diurnal band, as expected. This is probably an artifact of the analysis which misinterprets part of the low frequency motion of nontidal origin. This is not surprising, as the low frequency signal is large and the duration of the current time series does not allow good resolution at a 14 day period. Removing the fortnightly signal reduces the variance due to tides to less than 5%.

Computed semidiurnal currents are between 0.02 m/s and 0.07 m/s which is of the right magnitude to account for the 0.25 m tidal range in Tuktoyaktuk.

Spectral analyses were conducted on all the residual current (tides removed) time series in order to determine the frequency dependent variance distribution. Two sample spectra are presented in Figure 2.7; these are characteristic of all the current time

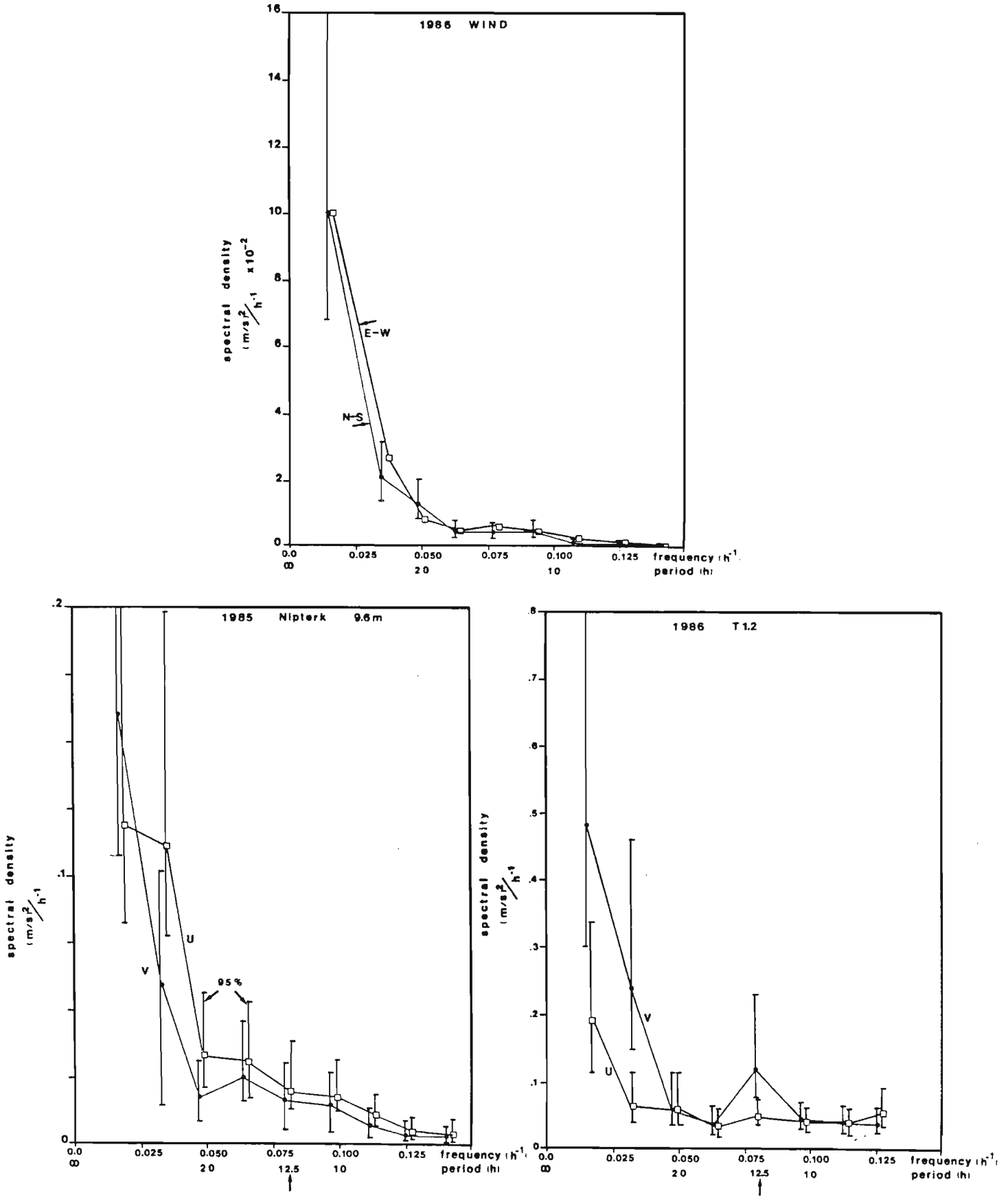


Figure 2.7 Typical frequency spectra for currents and wind.

series. All spectra display a relatively smooth decrease in signal with increase in frequency, with the only significant peak occurring at the tidal or inertial frequency. Most of the energy is concentrated in frequencies lower than one cycle per day. This corresponds to the frequency distribution for wind energy, suggesting that atmospheric forcing may play an important role in driving the coastal circulation.

To examine the temporal behaviour of currents at different frequencies, all time series were digitally filtered using three Cartwright filters. The three filters are complementary (the original signal can be recovered, except for small losses, by recombining the three filtered time series) and no part of the data is missed by examining each of the filtered time series. The three filters correspond to:

- low pass, effectively passing energy with periods longer than 24 hours, corresponding to directly forced wind motion, runoff effects, oceanic eddies, etc.,

- band pass, admitting energy with periods between 6 and 24 hours and primarily intended to capture tidal and inertial motions,

- high pass , for signals with periods shorter that 6 hours but not including wave motions; this is generally a quiet band in the spectrum of ocean variability with the occasional exception attributable to the presence of internal waves.

Table 2.6 shows the distribution of current variance between low, middle and high frequencies. These results agree with the spectral analysis results with, on the average, 75% of the total variance occurring in the low frequency band. Wind forcing acts

TABLE 2.6

Frequency distribution of currents

| year station | water depth (m) | inst. depth (m) | VELOCITY VARIANCE ($m^2/s^2$) FREQUENCY DISTRIBUTION total (no waves) | low T>24 | med. 24>T>6 | high T<6 | waves |
|---|---|---|---|---|---|---|---|
| 1986 | | | | | | | |
| T1.1 | 10.5 | 10.0 | 0.0086 | 0.0068 | 0.0011 | 0.0006 | 0.0069 |
| T1.2 | 5.9 | 5.4 | 0.0431 | 0.0357 | 0.0076 | * | 0.0207 |
| 1985 | | | | | | | |
| ARNAK | 7.6 | 4.8 | 0.0408 | 0.0096 | 0.0169 | 0.0115 | 0.0124 |
| NIPTERK | 12.2 | 7.8 | 0.0525 | 0.0386 | 0.0103 | 0.0029 | |
| | 12.2 | 9.6 | 0.0233 | 0.0175 | 0.0029 | 0.0004 | |
| 1984 | | | | | | | |
| AMERK | 20.5 | 7.1 | 0.0654 | 0.0538 | 0.0098 | 0.0015 | 0.0002** |
| | 22.5 | 19.5 | 0.0070 | 0.0036 | 0.0013 | 0.0012 | |
| NIPTERK | 14.6 | 7.0 | 0.0385 | 0.0303 | 0.0078 | 0.0008 | |
| | 14.3 | 11.0 | 0.0259 | 0.0064 | 0.0041 | 0.0024 | |

* For this record, the medium band frequency band corresponds to periods ranging from 4 to 24 hours instead of 6 to 24 hours, no high frequency band was processed since the instrument sampling interval was 4 hours.

** Based on 20 days of data, of which only 10 overlap the current time series.

principally at low frequencies. The only exception is the 1985 Arnak data, where the velocity variance is spread fairly evenly across the frequency bands. This data, however, may be contaminated by movement of the surface mooring or may have been affected by sea ice as was the nearby Aanderaa meter.

## 2.4 Wave Induced Bottom Currents

No direct wave measurements were available for the 1985 season, however, the burst sampling strategy employed for current measurement at the Arnak site was adequate to infer wave orbital velocities as well as the steady current components. The Inter Ocean S4 current meter used at this site measured both u and v velocity components at 1 Hz for 60 seconds every 90 minutes. This frequency was high enough to resolve the wave orbital velocities.

For each burst, the mean current components were computed and subtracted from the velocity record. The wave period was calculated as the mean zero crossing period of the resulting velocity record. The root-mean-square wave-induced orbital velocity ($U_{rms}(z)$ ) was then calculated. Using linear wave theory (U.S. Army, 1973), a simple transfer function was applied in order to calculate the wave-induced orbital velocity at the seabed ($U_{rms}(0)$ ):

$$U_{rms}(0) = \frac{U_{rms}(z)}{\cosh(kz)} \qquad (2.1)$$

where z is the height of the velocity record above the seabed and $k = 2\pi/L$ is the wave number with L as the wavelength. The wave number, k, can be determined from the wave orbital frequency, $\omega = 2\pi/T$ where T is the wave period, and the water depth, d, through the linear wave theory dispersion equation:

$$\omega^2 = gk \tanh (kd) \qquad (2.2)$$

Although equation 2.1 is strictly valid only for unidirectional monochromatic wave fields, in general it provides a first order estimate of the magnitude of bottom orbital velocities.

The velocity variance due to wave-induced currents ($U^2_{rms}$) is given in Table 2.6 for the four sites where wave information was available. For the three shallowest sites, bottom wave orbital velocity variances are similar in magnitude to the current variance. Although there is little wave data available for sites deeper than 10.5 m, it is expected that the longer period currents will dominate over wave-induced oscillatory currents in deeper water due to the attenuating effects of increasing water depth on bottom wave orbital velocities.

Time series of surface wave heights were also calculated from the burst velocity data using linear wave theory, where

$$H = \frac{U(z)T}{\pi} \frac{\sinh (kd)}{\cosh (kz)} \qquad (2.3)$$

In order to convert the wave height based on $U_{rms}(z)$ to the significant wave height, $H_s$, the wave heights obtained from equation 2.3 were multiplied by a factor of 2 (U.S. Army, 1973). Time series of $H_s$ are given in Appendix A for all sites where wave information was available.

In order to check the validity of this procedure, the same analysis technique was applied to the burst current meter data obtained by Hodgins et al. (1987). Figure 2.8 shows comparisons between surface wave heights obtained using the above formula and those obtained by Hodgins et al. using spectral information provided by pressure as well as velocity sensors. Although the agreement is excellent for the T1.2 site in shallow water, the present wave height estimates underestimate by up to about 25% those computed by Hodgins et al. for the T1.1 site in deeper water. This discrepancy cannot be explained by the use of linear theory, as higher order calculations can only bring a change of a few percent, for the wave conditions observed. The difference can be due to other factors, including the different assumptions made concerning wave period and calibration errors in one of the sensors. One should note that our estimates rely primarily on the velocity measurement while Hodgins et al. (1987) rely primarily on the pressure signal to compute the surface wave height. In deeper water, the wave signal is attenuated near the bottom, and any estimate of the surface wave climate based on these will be more sensitive to error.

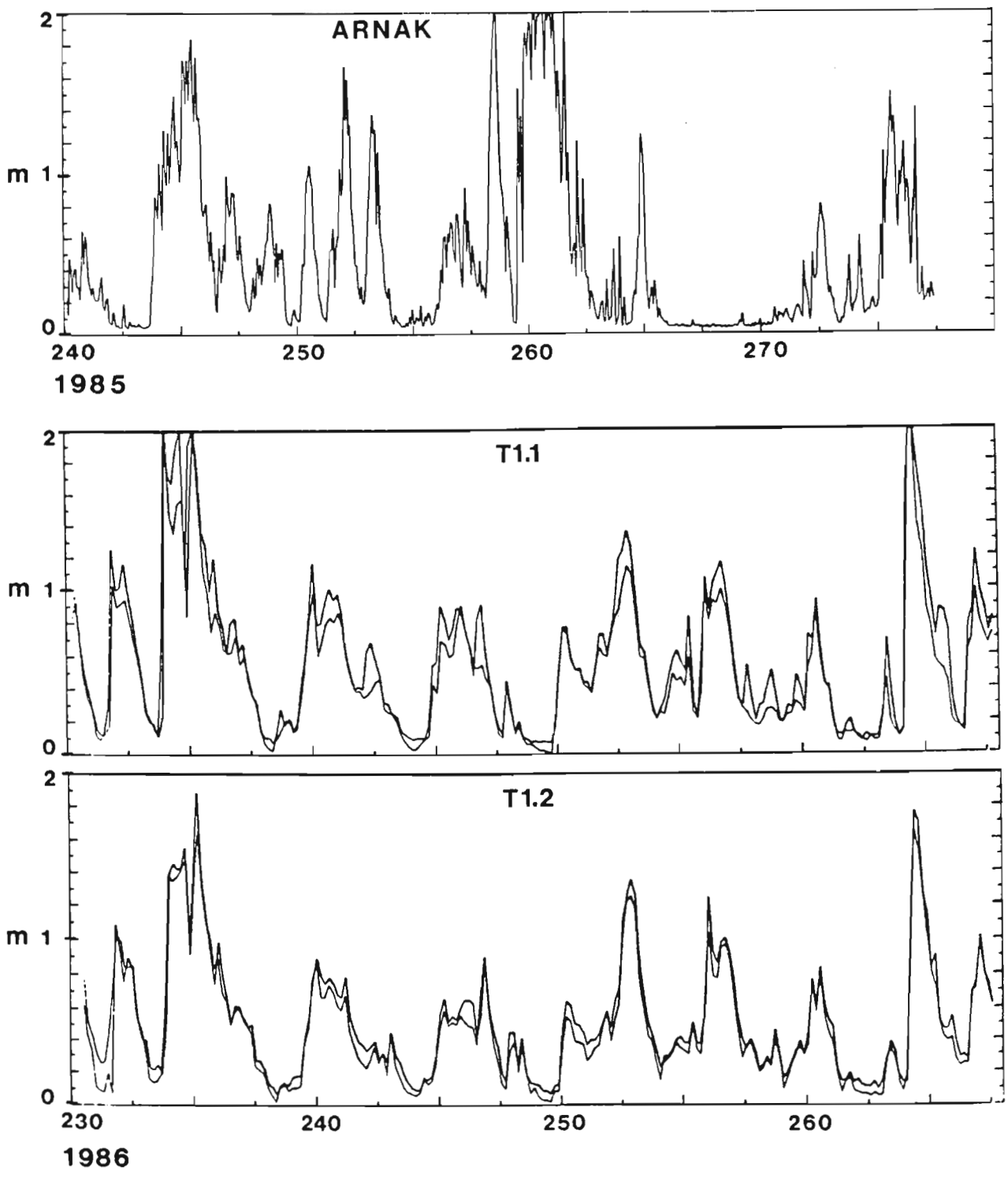


Figure 2.8 Significant wave heights computed from burst current meter data using equation 2.3 and using spectral information provided by pressure as well as velocity sensors (two lower graphs only) from Hodgins et al. (1987).

As discussed in Chapter 1 of this report, the critical hydrodynamic parameter for sediment transport considerations is the bottom shear stress acting on the seabed. Non-linear interactions between wave-induced currents and currents of lower frequencies can greatly increase the shear stress over that present under the low frequency currents alone; this topic will be further discussed in Section 2.6 of this report.

## 2.5 Correlation Analyses

Figure 2.9 shows concurrent time series of wind, surface waves, bottom currents and river flow rate; this provides a visual impression of the relationships between the various time series. A comparison of these times series indicates that bottom currents are at times associated with strong winds or shifts in the wind, but that there is little correlation between bottom currents and river runoff. Surface waves are similarly related to wind events.

Quantitative analyses of correlations between wind and bottom currents and between surface waves and bottom currents were conducted using a least square estimation technique to determine the coefficients of a linear equation fitting the variables of concern. For the relationship between wind and bottom currents, the component equations are of the form:

$$u = u_o + \Sigma \ (\alpha_i U_i + \beta_i V_i) + \varepsilon \qquad (2.4)$$

$$v = v_o + \Sigma \ (\varkappa_i U_i + \lambda_i V_i) + \varepsilon \qquad (2.5)$$

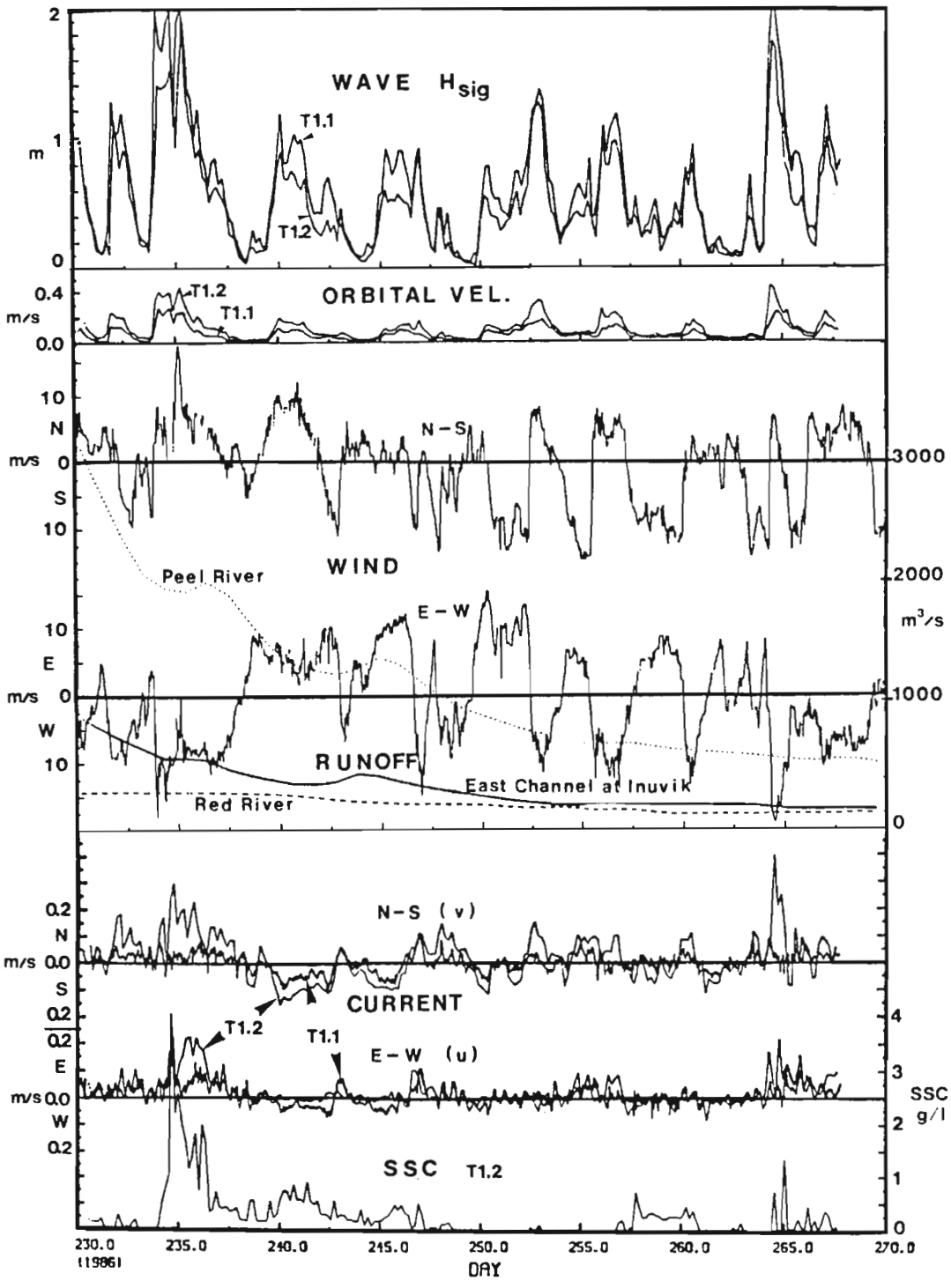


Figure 2.9 Concurrent time series of currents, significant wave height, wind, river runoff and suspended sediment concentration for 1986.

where u and v are the eastward and northward components of bottom current velocity; U and V are eastward and northward wind components; $u_o$ and $v_o$ are constant background currents which arise from the correlation analysis; $\alpha$, $\beta$, $\kappa$ and $\lambda$ are the fitted coefficients; and $\varepsilon$ is a residual error term.

The summation over the index i represents a consideration of lagged response. For example, $U_0$ and $V_0$ are the wind components coincident in time with u and v, while $U_1$ and $V_1$ represent the wind components measured 12 hours previously to the current measurement. Similarly, $U_2$ and $V_2$ are the wind components measured 24 hours prior to the current. The lag analysis determines if there is a significant delay between the wind forcing and the ocean current response.

The current to wind correlation analyses showed that the lagged coefficients ($i \geq 1$) were not significant and their inclusion in equations 2.4 and 2.5 did not reduce the error term, $\varepsilon$. Thus, the following discussion will refer to the unlagged correlation analyses. These correlations were undertaken for the low passed currents which contain most of the directly forced wind response. Since only low frequencies were considered, both current and wind time series were subsampled to 12 hours using a box car filter.

The correlation between low passed currents and winds are highly significant (> 90% level); Table 2.7 shows the regression

TABLE 2.7

Regression of winds on observed currents

To facilitate interpretation, the regression coefficients for the east and west component of velocity were resolved along the direction of maximum response. Wind blowing toward the direction shown (oceanographic direction convension) generate the largest currents. The direction of minimum response is always at 90° to the maximum response.

| year station | water depth (m) | inst. depth (m) | Maximum response: Wind dir. true | Current dir. true | resp. coef. % | minimum resp. coef. % | % low freq. variance explained |
|---|---|---|---|---|---|---|---|
| 1986 | | | | | | | |
| T1.1 | 10.5 | 10.0 | 57 | 39 | 0.87 | 0.12 | 47 |
| T1.2 | 5.9 | 5.4 | 80 | 17 | 1.73 | 0.26 | 35 |
| 1985 | | | | | | | |
| ARNAK | 7.6 | 4.8 | 43 | 81 | 0.49 | 0.00 | 12 |
| NIPTERK | 12.2 | 7.8 | 60 | 64 | 2.29 | 0.08 | 64 |
| | 12.2 | 9.6 | 46 | 36 | 1.58 | 0.11 | 60 |
| 1984 | | | | | | | |
| AMERK | 20.5 | 7.1 | 69 | 85 | 2.36 | 0.15 | 30 |
| | 22.5 | 19.5 | 57 | 27 | 0.47 | 0.06 | 15 |
| NIPTERK | 14.6 | 7.0 | 55 | 55 | 1.27 | 0.44 | 13 |
| | 14.3 | 11.0 | 68 | 55 | 0.66 | 0.15 | 9 |

analysis results. For 1986 and 1985, typically 50% of the low frequency variance can be explained directly by the simple regression. The regression is less successful for 1984, however, the lower winds and increased runoff of that year may have led to an increase in water column stratification, decoupling the bottom currents from direct wind forcing. The interannual differences do not seem related to station location or water depth.

The results given in Table 2.7 indicate that the maximum current response always occurs for winds blowing from the west to southwest, roughly parallel to the shore. The current response averages 1.3% of the wind speed, ranging from 0.49% to 2.36%, and is in the same general direction as the wind. There is no consistent rotational shift. The current response in the across shore direction is an order of magnitude lower than in the shore parallel direction, averaging 0.15% of the wind speed. The spatial distribution of response amplitude closely follows that of the current variance itself, with larger responses occurring away from the seabed and in shallow water.

For surface waves, correlations between wave height and wind were examined. Since the wave height response will, due to fetch effects, depend on the wind direction, the following equation was used:

$$H_{sig} = H_o + \alpha N + \beta E + \varkappa S + \lambda W + \varepsilon \qquad (2.6)$$

where $H_o$ is a constant background wave height; $\alpha$, $\beta$, $\gamma$ and $\lambda$ are the fitted coefficients; and N, E, S, W are wind speeds corresponding to the principal compass directions (i.e. if the wind is blowing from the North quadrant, N equals the wind speed and E = S = W = 0). For this analysis, the wind time series was subsampled to the same interval as the wave data.

It can be seen from the regression analysis results given in Table 2.8 that northerly and westerly winds were the most effective in generating surface waves during the 1986 season. This is consistent with the large ice free fetches north of Mackenzie Bay for this season. The 1985 data, collected in the northern area of Kugmallit Bay, reflects the more open station location with stronger responses from both the east and the south. The 1984 data were collected the furthest offshore, in a median ice year, and the wave-wind response is relatively uniform for all directions. The regression coefficients are such that, on the average, a 10 m/s wind will generate a significant wave height of about 1 m.

The effects of surface waves and winds on generating long period currents are analogous and in the fetch limited environment of the Beaufort Sea they are always in the same direction. They cannot readily be separated, and wind-correlated currents, which include wave-induced mean flows, will be globally referred to as wind forced. It should be noted, however, that this distinction may be important in the numerical modelling of the circulation in the study area (Dolata and Rosenthal, 1984).

TABLE 2.8

Regression of winds on waves

| year | station | water depth (m) | regression coefficients (m)/(m/s) * for wind directions N | S | E | W | % explained variance |
|---|---|---|---|---|---|---|---|
| 1986 | | | | | | | |
| | T1.1 | 10.5 | 0.119 | 0.047 | 0.059 | 0.106 | 56 |
| | T1.2 | 5.9 | 0.078 | 0.029 | 0.036 | 0.082 | 60 |
| 1985 | | | | | | | |
| | ARNAK | 7.6 | 0.098 | 0.053 | 0.096 | 0.104 | 50 |
| 1984 | | | | | | | |
| | AMERK | 20.5 | 0.116 | 0.059 | 0.092 | 0.082 | 58 |

* Wind direction follows meteorological convention (eg. a North wind blows from the North towards the south).

Most of the variance in the current records is from the low frequency band, but the amount of energy left in the higher frequencies (T < 24 hours) remains significant (about 25%). Visual examination indicates that these higher frequency fluctuations are sometimes associated with wind events. Although the intensity of the fluctuations increases during strong wind events, no one-to-one relationship is evident for individual features. This is not surprising since the source of the signal can either be from mesoscale atmospheric features (gusts, squalls, etc.) which vary over the distance separating the current and wind measurements, or inertial oscillations which for bottom currents are indirectly coupled with the wind due to the effects of stratification.

Regression analyses relating high frequency (T < 24 hours) current motion to winds were not successful, with many of the coefficients not significant, and the explained variance not exceeding 16%, and often near 0%. This may be partly due to the wind itself which may lose its autocorrelation at high frequencies over distances comparable to that separating wind and current observations. For sediment transport the currents in this band are probably best considered as a continuous background on which the low frequency wind driven motion is superimposed.

## 2.6 Bottom Stress Calculations

As discussed in Chapter 1 of this report, sediment resuspension from the seabed occurs when the seabed shear stress exceeds the critical value for the in situ sediments. This shear stress results from the combined influence of all the hydrodynamic processes leading to bottom currents. Of these processes, the previously described analyses have indicated that low frequency wind-driven currents and surface waves provide the major components of the near-bed current climate.

The bottom stresses resulting from the near-bed currents were calculated using the method developed by Grant and Madsen (1979), which considers the nonlinear interactions between surface waves and a steady current in the generation of bottom shear stresses. The oscillatory wave-induced currents greatly increase the bottom stress over that due to the steady current alone (Grant and Madsen, 1986, present an excellent review of continental shelf bottom boundary layer mechanics). Calculations were performed assuming that the seabed was essentially flat with no bedforms; this assumption allows bottom stresses to be calculated without requiring separate calculations of form drag and skin friction components.

Time series of bottom stresses were calculated for all sites; these are included in Appendix B. A sample bottom stress time series, for site T1.2 in 1986, is given in Figure 2.10. In all

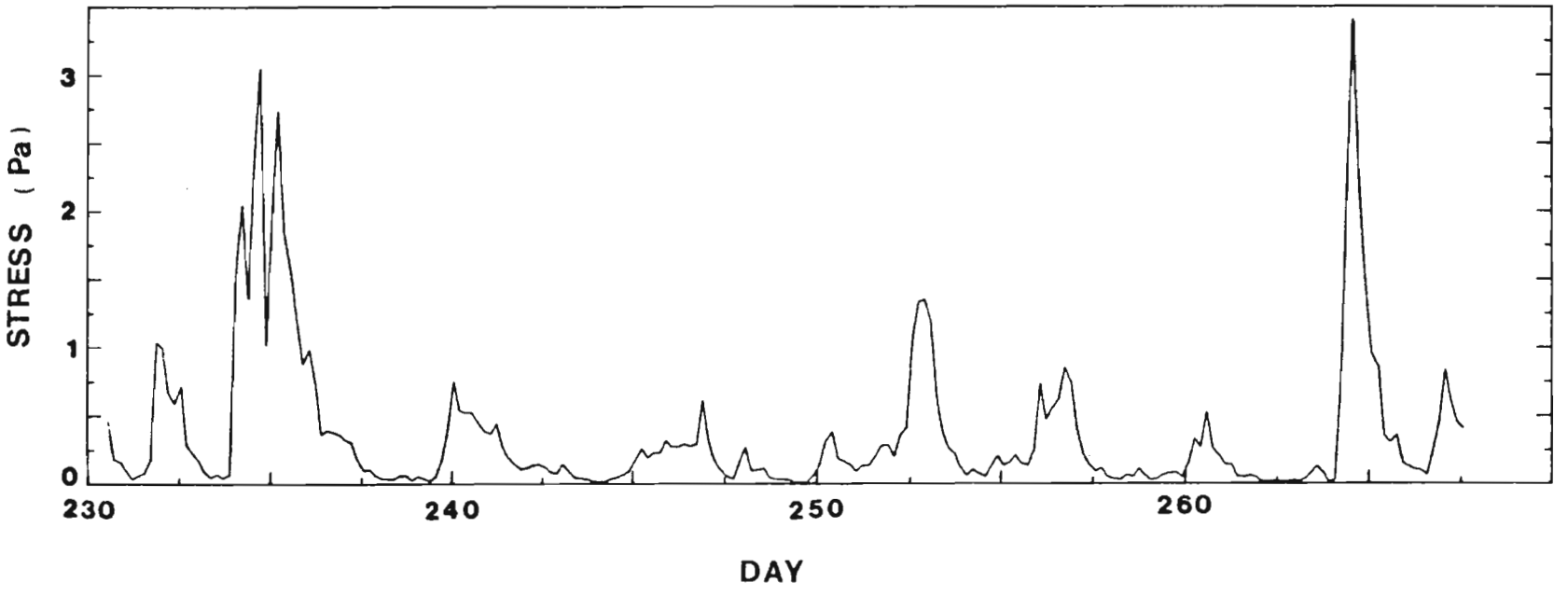


Figure 2.10 Bottom stress time series for T1.2 in 1986.

cases, the unfiltered current records were used to represent the steady current component of near-bed flow. For the sites where wave data were not available, bottom shear stress was calculated assuming a quadratic drag law with a constant drag coefficient, $C_d$, of 0.003, as in Sternberg (1972). The grain size values were given by Hodgins et al. (1987) for the T1.1 and T1.2 measurement sites ($D_{50}$ = 0.0034 mm and 0.0074 mm respectively); bottom sediment grain size measurements for the 1985 and 1984 study sites were not available so a grain size corresponding to silty clay was assumed.

The calculated mean and standard deviation of bottom stress is given in Table 2.9 for each of the study sites. In general, the mean stress increases as the water depth decreases. The importance of waves can be seen in the higher stress values for the sites where wave information was available; the low values given for the Nipterk and Amerk sites reflect only a portion of the total stress values (neglect of waves using the quadratic drag law).

The relative importance of waves and currents in generating bottom stresses can also be estimated by examining the oscillatory and steady portions of total shear stress. Although these do not directly represent the wave- and current-induced portions of bottom stress since both the wave and current fields are interactively modified within the bottom boundary layer, they do give an estimate of the relative orders of magnitude of each component. Table 2.10 shows that the oscillatory component of

TABLE 2.9

Bottom shear stresses

| year | site | water depth (m) | grain size (mm) | BOTTOM STRESS mean (Pa) | std. dev (Pa) |
|---|---|---|---|---|---|
| 1986 | | | | | |
| | T1.1 | 10.5 | 0.003 | 0.17 | 0.66 |
| | T1.2 | 5.9 | 0.007 | 0.35 | 0.52 |
| 1985 | | | | | |
| | Arnak * | 7.6 | 0.002 | 0.21 | 0.38 |
| | Nipterk * | 12.2 | 0.002 | 0.065 | 0.090 |
| 1984 | | | | | |
| | Amerk * ** | 22.5 | 0.002 | 0.019 | 0.045 |
| | Nipterk ** | 14.3 | 0.002 | 0.071 | 0.18 |

* No wave data is available for these sites

** Available wave data were insufficient to use in these calculations.

TABLE 2.10

Steady and oscillatory components of bottom shear stress under combined wave and current flows.

| year | site | water depth (m) | BOTTOM STRESS total (Pa) | steady (Pa) | oscillatory (Pa) |
|---|---|---|---|---|---|
| 1986 | | | | | |
| | T1.1 | 10.5 | 0.17 | 0.03 | 0.14 |
| | T1.2 | 5.9 | 0.35 | 0.09 | 0.26 |
| 1985 | | | | | |
| | Arnak | 7.6 | 0.21 | 0.05 | 0.15 |

bottom stress is 3 to 4 times larger than the steady component for all sites where wave information was available.

## 2.7 Suspended Sediment Concentrations

Suspended sediment concentration measurements were made at the T1.2 site as part of the 1986 ESRF study in the Mackenzie Delta (Hodgins et al., 1987). The concentration values shown in Figure 2.11 represent measurements 100 cm above the seabed obtained using optical backscatter techniques including calibration with in situ bottom sediments. These values represent averages of the burst data collected by Hodgins et al. Concentration values were quite high, with a mean value of 247 mg/l, a standard deviation of 476 mg/l and a maximum of 4049 mg/l measured during the storm of 22-23 August 1986.

In order to examine the relationship between bottom shear stresses and suspended sediment concentrations, correlations between these variables were done using an equation of the form

$$C = C_o + \sum \alpha \tau_b + \varepsilon \qquad (2.7)$$

where C represents the suspended sediment concentration in mg/l, $C_o$ is a constant background concentration which arises from the correlation analysis, $\alpha$ is the fitted coefficient, and $\tau_b$ is the total bottom shear stress, and as before $\varepsilon$ is the residual error. The subscript i indicates that time lags were considered.

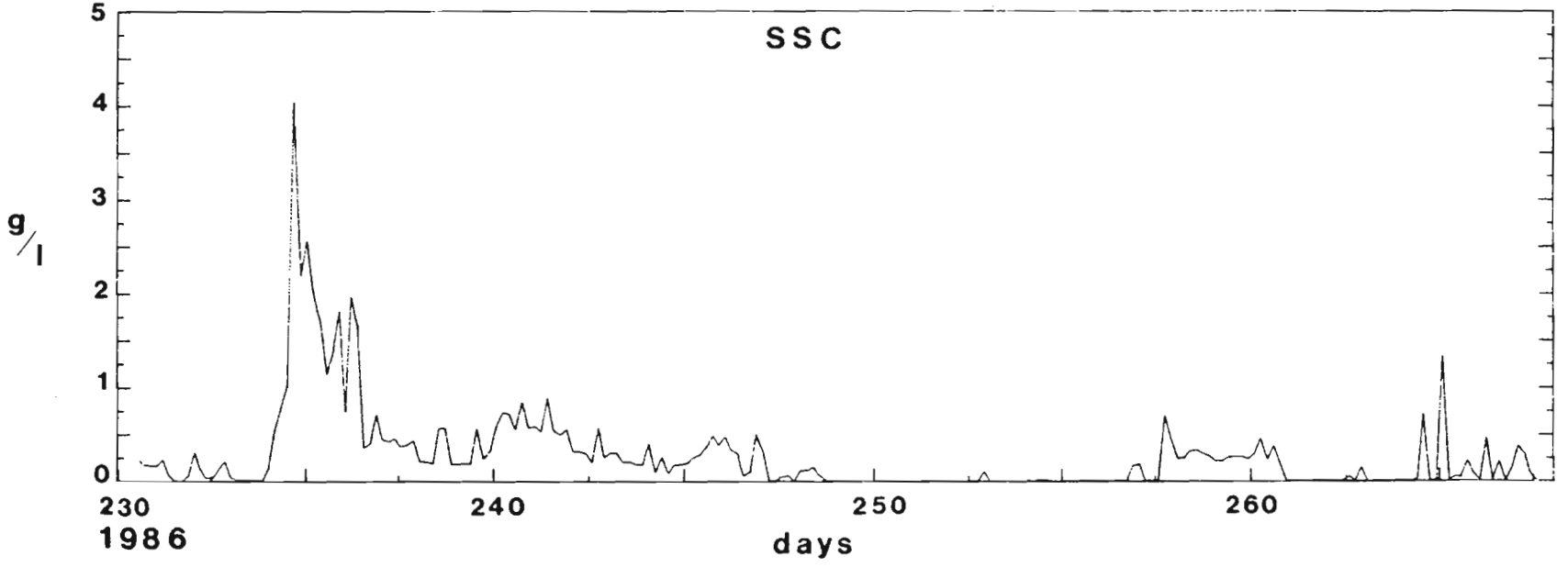


Figure 2.11 Suspended sediment concentration time series for T1.2 in 1986.

The results of this analysis showed that the lagged coefficients ($i \geq 1$) were not significant. The correlation between bottom stress and suspended sediment concentration is highly significant, with 33% of the concentration variance explained by this regression. The remainder of the variance in the concentration time series may perhaps be explained by other sedimentary processes such as the advection of sediment past the measuring device rather than direct resuspension of seabed sediments and changes in the supply of such advected sediments, or time-varying changes in the characteristics of the seabed sediments (i.e. critical shear stress for erosion).

Spectral analyses were also conducted for the concentration data and the bottom stress time series for this site; spectra are plotted in Figure 2.12. Similarly to the current spectra presented in Figure 2.7, both the concentration and bottom stress spectra decrease as the frequency increases, with a relatively minor peak at the tidal or inertial frequency. The great majority of the energy in both cases is contained in frequencies lower than one cycle per day, although the sampling frequency was not high enough to resolve the energy at surface wave frequencies. The concentration of energy in the low frequency band corresponds to atmospherically forced events, the major source of currents in the coastal zone (see Section 2.3).

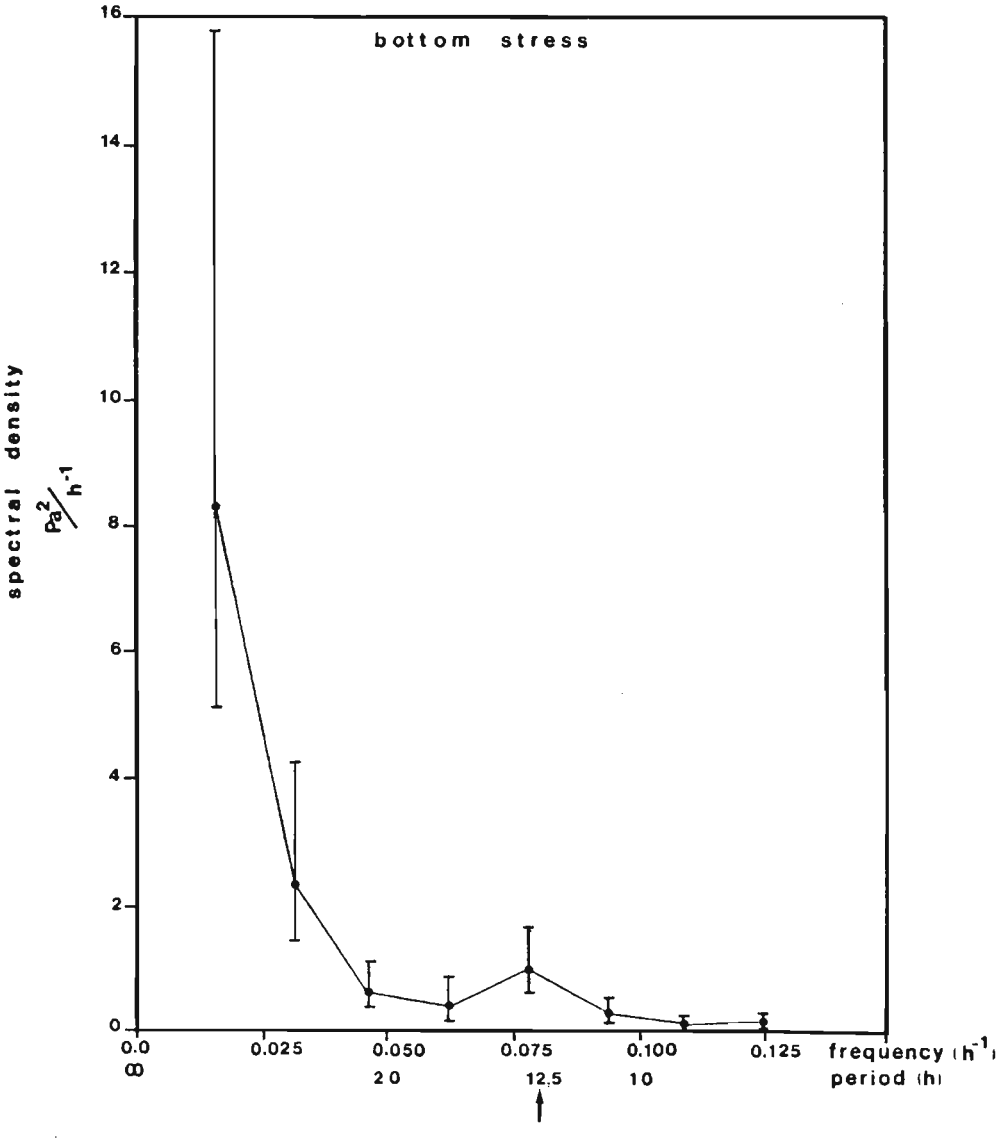


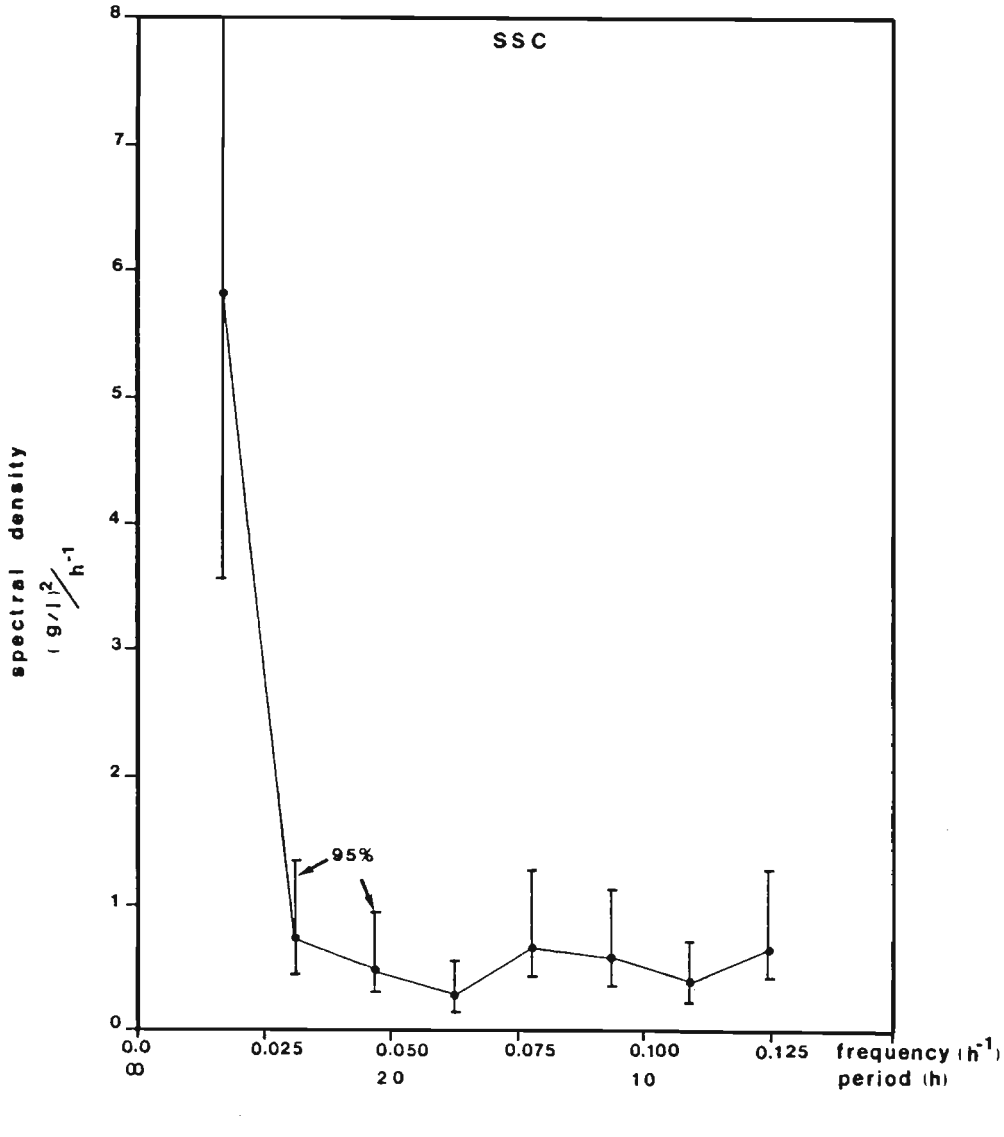


Figure 2.12 Frequency spectra for bottom stress and suspended sediment concentration at site T1.2 in 1986.

## 2.8 1986 Event Analysis

The 1986 season offers the most comprehensive and reliable data set of the three years covered by this study; this data was selected for more detailed analyses. Figure 2.13 presents time series plots of available data for 1986. At the top of the figure, the wave data for stations T1.1 and T1.2 are presented. The two stations can easily be distinguished, as the shallower station has consistently smaller significant wave heights (as derived from the pressure data) and larger bottom orbital velocities. Wave data at the two sites are very well correlated.

The wind data from Molikpak is shown decomposed into east and north components, according to the direction the wind is blowing from. The correlation between the two wind components reflects the bimodal nature of the predominant winds, blowing mostly from the northwest or the southeast. These data are atypical in that southeast winds are generally rare in the summer months. The increased southerly wind component would tend to push the sea ice offshore and may explain the unusually good ice year.

The time series of mean currents are similarly decomposed into east and north components, according to the direction the current is flowing towards. The two time series can be distinguished by the smaller sampling interval at site T1.1; this appears as an apparent high frequency component to the signal. The time series from the two sites are somewhat correlated but do

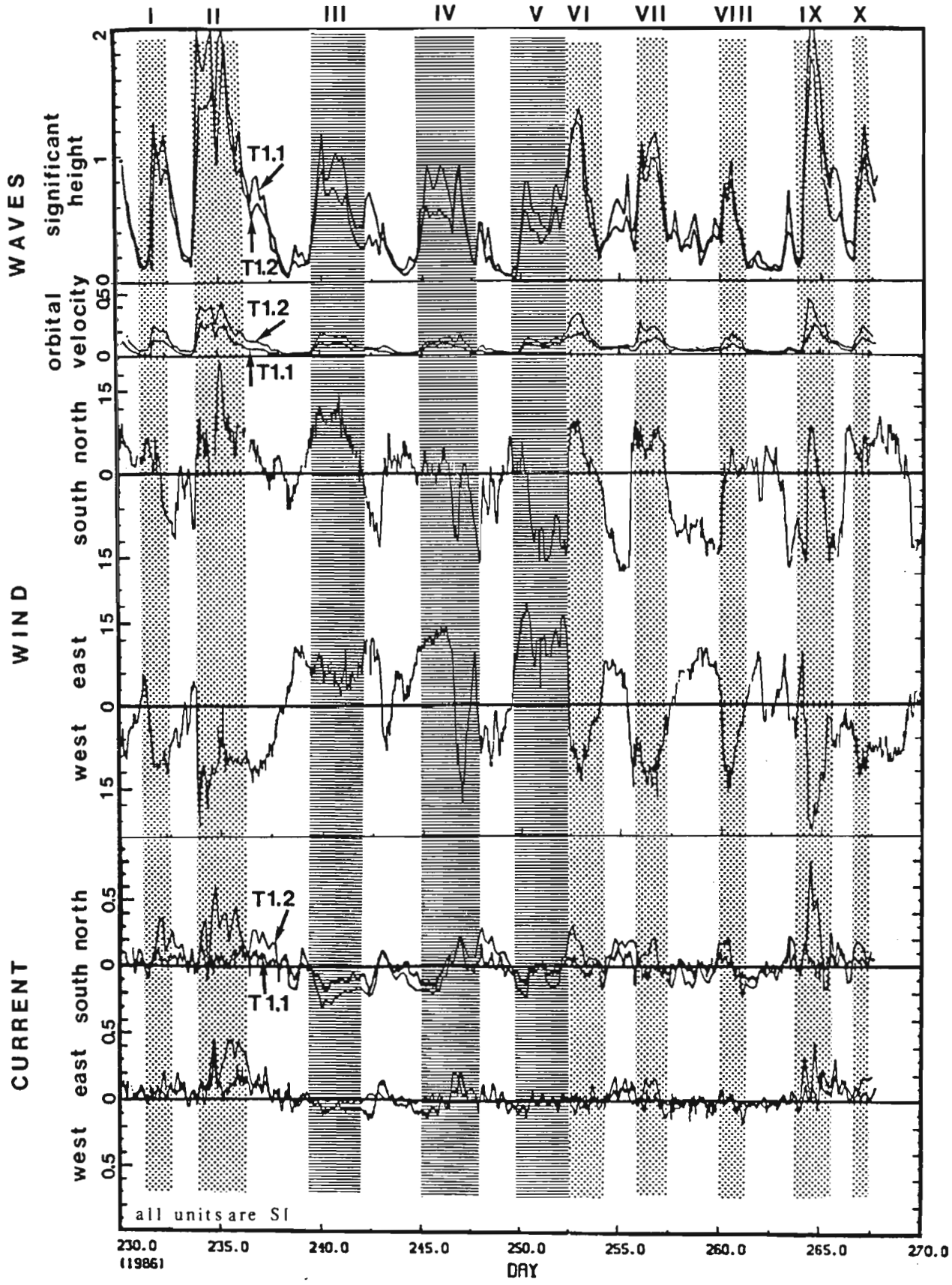


Figure 2.13 Time series plots for 1986.

show significant differences. Currents at the shallower site, T1.2, show more variability in the north-south direction, corresponding to the channel direction between nearby North Head and Hooper Island. The current components at the deeper site are correlated, reflecting a predominant flow alignment in the northeast-southwest direction, approximately parallel to the local isobaths.

Three ice charts characterizing the beginning, middle and end of the observation period are shown in Figures 2.14 to 2.16. These figures show that maximum ice free fetches are from the northwest and northeast. The position of the 9/10 ice boundary does not change significantly during the study period, but an examination of daily ice charts shows the direct effects of wind on the 1/10 ice edge. The measurement period covers an exceptionally good ice season with large ice free areas.

Ten distinct storm events can be identified in the 38 day time series. Although these events have been selected on the basis of wave activity, they also correspond to peaks in winds and mean currents. Most events correspond to westerly and northwesterly winds and result in large waves and strong northeasterly currents. The two most important events, II and IX, occurred for the highest westerly wind speeds during the measurement period and also occur in the direction of strongest response determined from the regression analysis.

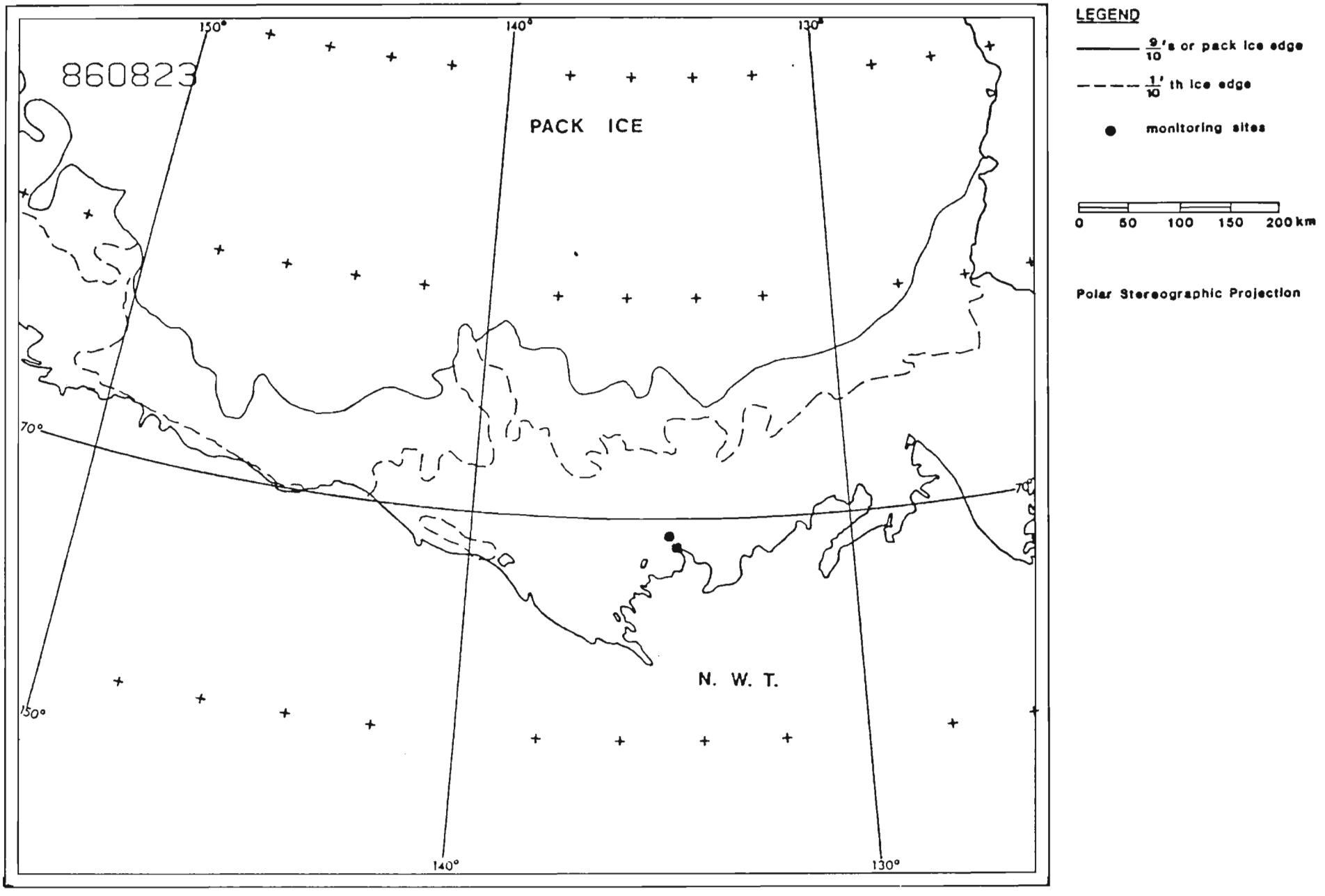


Figure 2.14 Beaufort Sea ice chart for 23 August 1986.

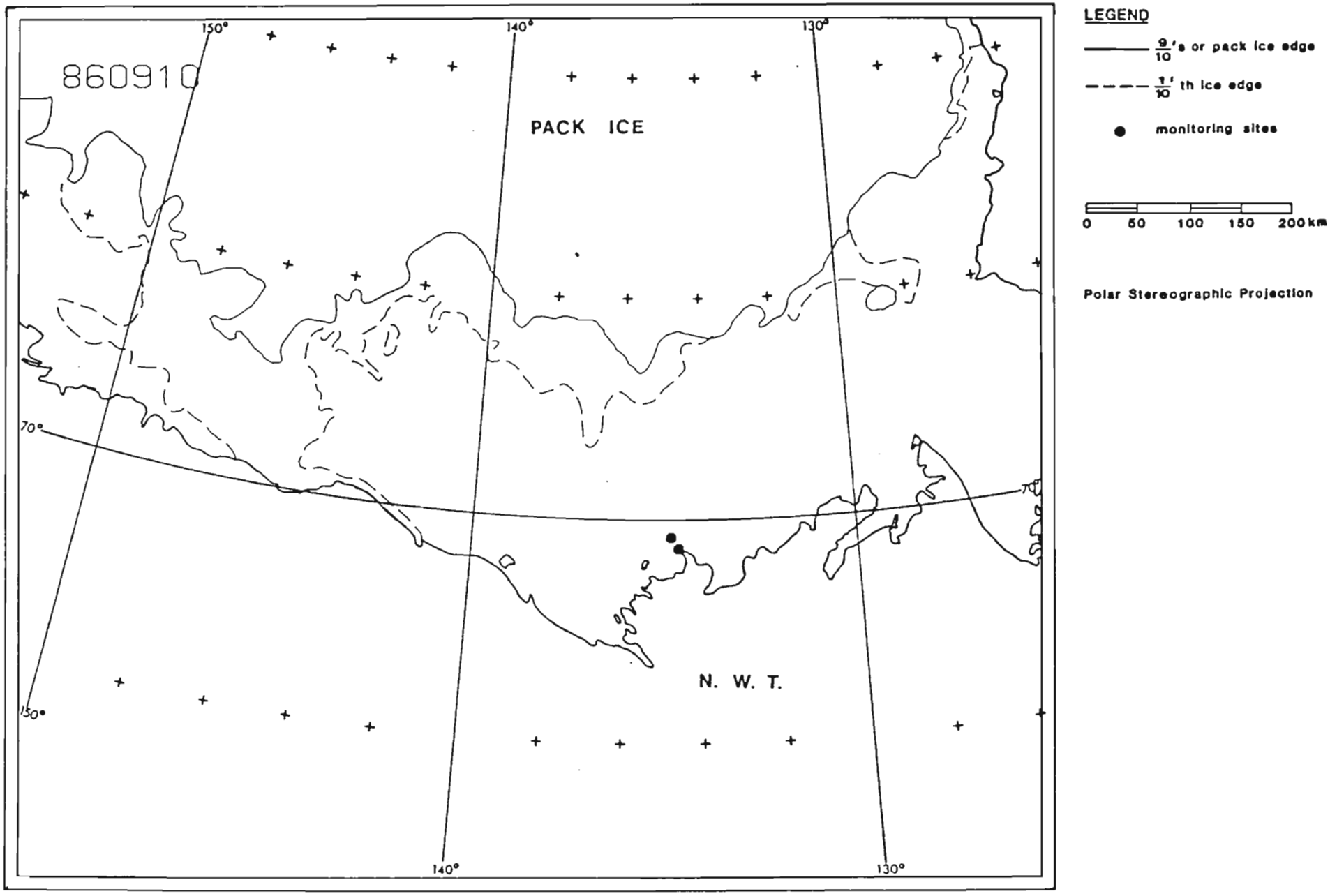


Figure 2.15 Beaufort Sea ice chart for 10 September 1986.

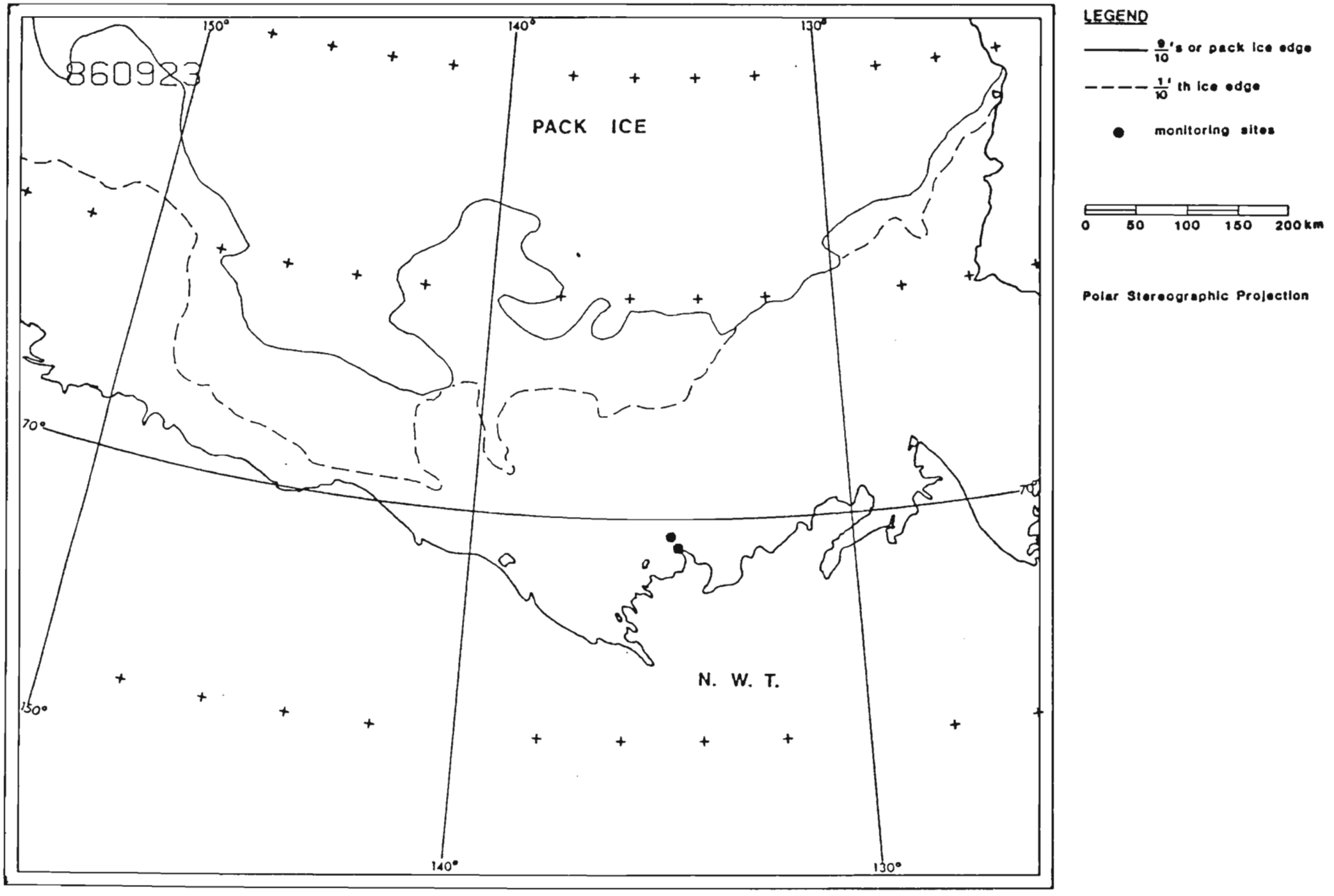


Figure 2.16 Beaufort Sea ice chart for 23 September 1986.

The current response at the shallow site seems disproportionately high for these two events, perhaps representing a nonlinear response, as would be expected from wave-induced flows which depend on wave energy or wave height squared. The response at the shallower site is noteworthy in that westerly winds generate a northward component of flow, contrary to what would be expected from the Coriolis effect. This is probably due to the deflection by North Head of flow trapped between Hooper Island and the shore. At the deeper site, the current flows in the same general direction as the wind.

Although strong currents toward the south and west can be found corresponding to winds with an easterly component (events III, IV, V, as well as days 239, 259 and 262), the wave response for most of these is limited by fetch effects. Since, as discussed previously, the bottom stress regime and sediment resuspension potential depend largely on waves rather than on currents, we can conclude that the northwest wind events would have dominated sediment resuspension in 1986. This is confirmed by the bottom stress time series given in Figure 2.10, where the stress for events II and IX far outweighs the rest of the events. Associated with these northwest wind events leading to sediment resuspension are relatively strong northeast currents; these currents would result in a net sediment drift in this direction.

Examining the sediment concentration time series at T1.2 (Figures 2.9 and 2.11), we find concentration peaks corresponding

to events II, III, IV, VII-VIII and IX. High concentrations on day 259 are associated with southeasterly flows and relatively small wave heights. High concentrations occur for southeast as well as northeast flows and no predominant transport direction can be inferred. Events V and VI are marked by the total absence of response in the suspended sediment signal, although the hydrodynamic forcing is comparable to other events. Intensity of response bears no direct relationship with forcing; for example, the peak suspended load in event II is about three times higher than for event IX which had a higher peak stress.

In general, background sediment concentrations, as well as the response to the storm events, tend to be higher before day 250, a time when the runoff from the Mackenzie River is also significantly higher. This may reflect the advection of the sediment laden plume past the sensor and/or the resuspension of unconsolidated materials recently deposited. Therefore, the observed sediment concentrations appear to be only partly related to the direct effect of wave and current events, and suspended sediment supply from the Mackenzie River as well as plume behaviour and depositional history very likely play a major role in determining the suspended load. The small data sets available (a few events during one season) do not allow quantification of these complex relationships based on data analysis alone (too few degrees of freedom). Quantitative modelling techniques offer a

powerful means of integrating the spotty knowledge of the southern Beaufort Sea, provided by the data, with our general understanding of sedimentary and hydrodynamic processes, in order to develop these quantitative relationships.

# 3.0 DISCUSSION

The main purpose of this study has been to quantify, through analyses of recent data, the relative importance of wind-induced currents, estuarine circulation and wave-induced oscillatory currents on the reworking of bottom sediments in the inner shelf and nearshore zone of the Beaufort Sea. The available data, analysis procedures and results of these analyses are described in Chapter 2 of this report.

In general, the analysis results provide insight into two factors: the spatial distribution of velocity variance attributable to the various forcing mechanisms and the oceanic response to individual atmospheric events. These results will be discussed in the following sections and then related to sediment transport and resuspension phenomenae.

## 3.1 Wind-induced Currents

The spectral analysis results show that, on the average, 75% of the total current variance occurs in the low frequency band, corresponding to atmospheric forcing. Thus, the inner shelf region can truly be said to be storm dominated, particularly when the importance of storm-driven waves, to be discussed later in this chapter, is considered. The spatial distribution of current variance is such that the variance increases in shallow water and also increases with distance above the seabed. A preliminary

estimate of the current variance at a given water depth or location can be obtained by using the plot given in Figure 2.6.

The ocean current response to individual storms is determined through the results of the correlation analyses. Approximately 50% of the current variance is explained by the simple current to wind relationship given by equations 2.4 and 2.5. Although a more complicated relationship including the effects of stratification and depth would probably account for a higher percentage of the current variance, for a first estimate, it can be assumed that the current response in the shore parallel direction is approximately 1.3% of the wind speed while the response in the across shore direction averages 0.15%. In general, larger responses occur away from the seabed and in shallow water.

## 3.2 Estuarine Circulation

Estuarine circulation patterns generally involve an outward surface flow coupled with an inward return flow along the seabed. These flows should be reflected in the current meter records as non-zero mean flows, with the direction and magnitude dependent on height above the seabed. Although mean flows ranging from 2 to 10 cm/s were observed in the current meter records, these were not statistically significant. The current meter data were also found to be uncorrelated with river flow rate. Thus, the estuarine

circulation appears to be an insignificant factor in the bottom current regime and therefore to have little effect on sediment resuspension.

The Mackenzie River is much more important as a source of sediment to the nearshore and inner shelf zone, with the plume behaviour a crucial factor in the initial distribution of sediments in the study area. Although satellite imagery can provide some insight into plume behaviour, it does not provide information on the three-dimensional plume structure. Synoptic profiling surveys would provide the most useful information; however, very little of this type of data is available for the Beaufort Shelf.

A first estimate of estuarine currents can be obtained through simple salt flux calculations based on the observed salinity distributions. Assuming an idealized 2 layer estuary where the dilution of freshwater is entirely due to vertical rather than horizontal diffusion, a mean bottom return flow of about 4 cm/s at the 5 m depth contour is required to account for the observed salinities (the reader is referred to Officer, 1976 for a discussion of estuarine salt balance). This value will decrease in deeper water and increase at shallower depths, and represents a maximum, since consideration of horizontal dispersion will reduce the mean flow required for salt balance.

A very important difference between the Mackenzie estuary and most other estuaries is the dominance of wind forcing over that due to tides. Applying the Hansen-Rattray estuarine classification (Fischer et al., 1979) to the Mackenzie estuary, using $U_{rms}$ instead of a tidal velocity, the classification system predicts a well stratified estuary for a $U_{rms}$ value of 0.1 m/s and a partially mixed estuary for a value of 0.2 m/s. The lower value is characteristic of calm conditions while the higher value is more typical of storms. Thus, the amount of energy available for mixing of the plume water with the shelf water is not constant, depending on atmospheric events rather than tides. This may explain the variability in the plume observed in CTD surveys (Hill and Nadeau, in prep.).

For both storm and calm conditions, the Hansen-Rattray diagram predicts that mean estuarine flows are small and the horizontal dispersion processes dominate over vertical mixing processes. It is the vertical mixing processes which lead to the classical estuarine circulation system composed of an outward surface flow coupled with an inward return flow along the seabed and their minor role is confirmed by the absence of significant mean flows in the current meter data. The dominance of horizontal mixing processes, where ocean water is entrained into the plume through horizontal exchanges, is qualitatively supported by satellite images which show the presence of eddies with sizes comparable to the plume extent from shore.

During storm events, vertical mixing will increase the plume dilution and its thickness, forming a thick layer of brackish water overlying the saltier shelf water. In the following calm period, a secondary plume of lower salinity can develop over the brackish layer. Repetitive storm events will lead to the multiple layer, staircase stratification observed in many salinity profiles, as well as the multiple plume fronts evident in satellite imagery.

Satellite images and salinity data indicate that the variability in plume characteristics along the coastline can be large. Hill and Nadeau (in prep.), for example, show large changes in salinity values measured along a transect at a one week interval. These changes could be explained by lateral plume displacement, although there is insufficient data to resolve the spatial plume characteristics. Although the plume behaviour is insignificant in terms of sediment resuspension due to bottom currents, it plays a major role in determining the distribution of sediments initially deposited from the plume. Numerical modelling may provide additional insight into the plume behaviour; this technique has been successfully applied to the Fraser River by Royer and Emery (1985).

### 3.3 Wave-induced Oscillatory Currents

Table 2.6 gives the velocity variance for wave-induced oscillatory currents for the four sites with available wave

information. In general, these are similar in magnitude to the current variances for the same sites, with velocity variance increasing as water depth decreases.

Figure 3.1 shows the RMS current velocity for both wave-induced oscillatory currents and mean currents, plotted as a function of water depth. This figure also shows the theoretical increase in wave-induced orbital velocity as a function of water depth. This curve is based on linear wave theory, where the increase in bottom orbital velocity with decreasing water depth is given by the factor (U.S. Army, 1973)

$$\left[\frac{2\cosh^2(kd)}{2kd + \sinh(2kd)}\right]^{1/2} \frac{1}{\sinh(kd)} \qquad (3.1)$$

where kd is determined from the linear wave theory dispersion equation given in equation 2.2. This curve does not include wave growth due to wind forcing or dissipation due to bottom stress or wave breaking, nor are wave refraction or diffraction, which depend on local topography, included. Wave shoaling effects are, however, considered in this equation. A six second wave period, corresponding to storm conditions, was used to develop the curve given in Figure 3.1.

In a shallow water environment such as the Beaufort shelf, wave dissipation may be very important in determining the spatial characteristics of the wave field during a storm event. Hodgins

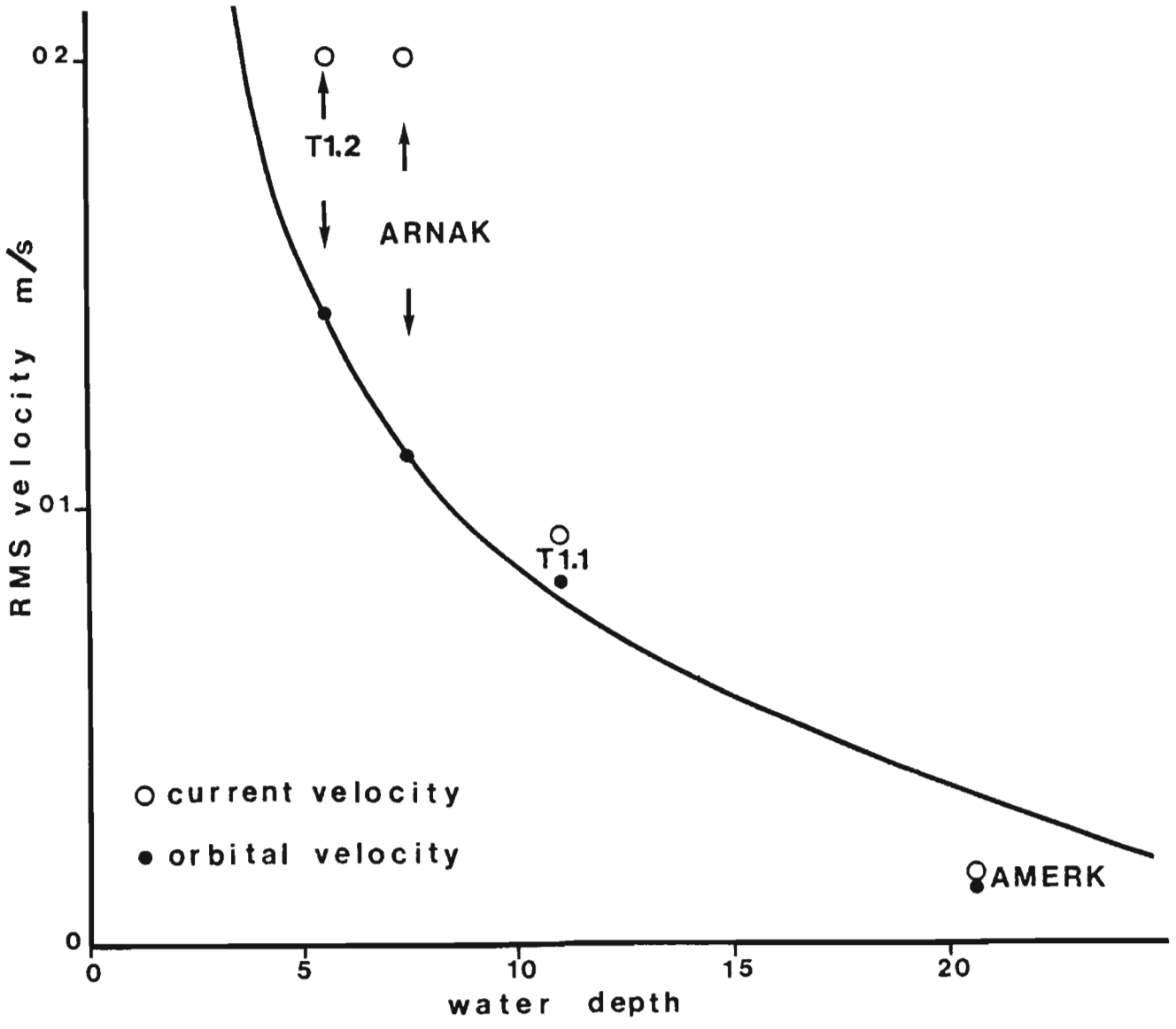


Figure 3.1 RMS current velocity for wave-induced oscillatory currents and mean currents, with theoretical depth dependency of oscillatory currents.

et al. (1987) suggest that wave dissipation was responsible for the differences in wave heights between sites T1.1 and T1.2, however, the effects of dissipation are not evident in the simple comparison presented in Figure 3.1. Energy losses to wave breaking and frictional dissipation likely play an important role in such shallow waters, but may largely be balanced by local wind energy input.

The correlation analyses presented in Section 2.5 of this report indicate that, on the average, a 10 m/s wind speed will generate a significant wave height of about 1 m, although the actual value will be direction and fetch dependent. The response of bottom orbital velocities to storm events can be approximated using the above correlation (10 m/s wind speed for each 1 m of significant wave height), coupled with linear wave theory (equations 2.2 and 2.3) to calculate the bottom orbital velocity for the water depth of interest. This calculation requires an estimate of wave period; the available data shows that storm wave periods are approximately 5 to 6 seconds for the study area.

### 3.4 Wave-induced Steady Currents

In addition to the high frequency oscillatory currents, surface waves can generate low frequency currents with periods similar to those of the direct wind-induced currents. These currents essentially arise from the non-zero fluxes of momentum

associated with surface waves, and can be divided into shore parallel and shore perpendicular components.

Wave-generated longshore currents within the surf zone have been considered by Longuet-Higgins (1970) among others, where wave breaking leads to significant currents capable of transporting sediments. Similar principles have been applied outside of the breaker zone by Dolata and Rosenthal (1984), who have shown that substantial currents can be generated whenever surface wave dissipation occurs.

Although these wave-generated currents cannot be easily separated from direct wind-driven currents, a rough order of magnitude estimate can be made. Assuming that the mean stress due to wave dissipation is balanced by a frictionally controlled steady flow, the mean current can be estimated using (Dolata and Rosenthal, 1984):

$$u^2 \approx \frac{g\, c_g\, H_{sig}^2}{16\, c\, L\, C_d} \qquad (3.2)$$

where c is the wave celerity, $c_g$ is the wave group velocity and $C_d$ is a bottom drag coefficient. Using a value of $C_d$ of 0.003, typical for steady currents on the continental shelf, indicates that surface wave generated mean currents exceeding 10 cm/s can be generated. The effect of wave generated mean wind stress is analogous to the surface wind stress, and cannot easily be

distinquished from it since they both act in the same direction in the Beaufort Sea, due to fetch limitation. Wave effects would appear as an increase in wind drag coefficient when considering the wind driven circulation.

## 3.5 Sediment Transport and Bottom Sediment Reworking

The previous discussion indicates that bottom currents are dominated by wind forcing, acting to generate both low frequency motion and surface waves. This response is consistent with a frictionally dominated flow near a coastline. The time required for bottom frictional dissipation to adjust to a change in forcing is on the order of a few hours for the water depths and current speeds considered here, implying that the flow rapidly adjusts to changes in wind forcing. Assuming that the surface wind stress is balanced by a quadratic bottom shear stress, currents are roughly proportional to the wind speed, as are the wave heights. Apart from the influence of local topography, which influences the flow direction at the T1.2 site, the presence of the coastline restricts the mean currents mainly to the shore parallel direction, although the waves are not so restricted.

As discussed in the first chapter of this report, sediment resuspension from the seabed occurs when the bottom shear stress exceeds the critical value for entrainment of the bottom sediments. As well, the rate of sediment transport once

entrainment occurs is generally thought to be a function of the seabed stress. Bottom stress calculations were performed using the method of Grant and Madsen (1979); this approach considers the non-linear interactions between wave-induced oscillatory currents and other lower frequency currents within the bottom boundary layer. In general, the mean stress level increases as the water depth decreases.

These calculations indicated the importance of waves in greatly increasing the bottom stress level over that present for unidirectional currents alone. This shows that, although the magnitude of the velocity variance is similar for both the low frequency currents and the wave-induced oscillatory currents, surface waves have a dominant effect on determining bottom boundary layer dynamics and hence bottom shear stress. Since both surface waves and bottom currents are highly correlated to wind forcing, the inner shelf region covered by this study can be said to be storm dominated in terms of sediment resuspension.

Preliminary estimates of the spatial distribution of bottom stress levels can be obtained by using the RMS orbital velocity and current velocity, calculated from Figures 3.1 and 2.6 respectively as a function of water depth, as input to a bottom boundary layer model such as that developed by Grant and Madsen. Although this greatly oversimplifies the problem, it can provide useful guidance for site comparison purposes. In addition, individual storm events may be compared by using the current

predictions of the correlation analyses previously described as input to the boundary layer calculations.

Suspended sediment concentration measurements at 1 m above the seabed were available for the T1.2 site in 1986. Correlation analyses showed the concentration values to be highly correlated to the bottom stress, although the simple linear relationship given by equation 2.7 explained only 33% of the variance in the concentration record. This indicates that processes other than bottom stress could be influencing the concentration of suspended sediments. These processes could include changes in the critical shear strength of the seabed sediments or advection of fine material past the measuring station without deposition or resuspension occurring.

Large areas of the Beaufort shelf are covered with fine sediments mainly composed of clays and silts. These sediments are cohesive in nature and the flocculation process plays an important role in determining the critical shear stresses for erosion and deposition. The flocculation process depends on characteristics of the flow field such as turbulence level and duration of periods of quiescent flow, as well as on sediment properties such as particle shape and mineralogical composition. As well, the stress history of the seabed sediments will alter the critical stress for sediment erosion, with wave-induced pore pressure changes an important factor. The change in critical stress may be associated to the progressive weathering and transport of materials deposited

earlier in the season, during peak runoff when the southern Beaufort Sea is still largely ice coverd.

Measured values for the critical shear stress for erosion of estuarine sediments range from 0.01 to 3 Pa (Amos and Mosher, 1985). Comparing these values with the bottom stress time series given in Figure 2.10, it can be seen that the seabed shear stress reaches 3 Pa only during the two extreme storm events, while the stress exceeds 0.01 Pa almost all of the time. The actual shear strength of the in situ sediments is probably some intermediate value since the concentration values are strongly correlated with the bottom stress. An accurate determination of the critical shear stress for erosion of the in situ sediments, and its variation in time, is a major factor in determining the extent of sediment resuspension and reworking.

The advection of fine material past the measuring station could also account for a large portion of the variance in the suspended sediment concentration record. This material represents the wash load component of the river discharge and is too fine to be deposited at the measurement site. As well, this material is likely to be supply limited and thus more related to events occurring in the Mackenzie River watershed than to the bottom stress regime. The high concentration values observed in the first twenty days of the the suspended sediment concentration time series given in Figure 2.11 may therefore reflect changes in sediment supply; a comparison with the river runoff shown in

Figure 2.9 indicates the same long term decreasing trend in both time series. The dynamics of the Mackenzie River plume will also affect the distribution of suspended sediment in the water column, without necessarily changing the seabed stress conditions.

# 4.0 CONCLUSIONS AND RECOMMENDATIONS

## 4.1 Summary of Findings

The principal objective of this study was the assessment of the relative importance of various hydrodynamic processes (estuarine circulation, wind induced currents, oscillatory wave motion, etc.) in reworking bottom sediments on the inner Beaufort Shelf. For this, three years of observations including current, wave, temperature, salinity and suspended sediment measurements in shallow water (22.5 m and less) were analysed.

The results show that the hydrodynamic regime is dominated by storm response, inducing both steady currents and waves. Currents generally follow the wind direction but are influenced by topography, with maximum flows occurring along the direction of the coast. Currents are variable and no significant mean drift can be identified from the data.

Wave induced orbital velocities are comparable to the steady component of flow, but their effect on bottom boundary layer dynamics greatly increases the total bottom stress affecting sediment reworking. The importance of wave orbital velocities, as well as steady currents, increases in shallow water.

No evidence of the classical 2 layer estuarine circulation was found, and the available information suggests that horizontal

dispersion caused by varying wind induced currents and eddies in the plume area dominates the transport of fresh water and associated sediments away from the Mackenzie River delta.

Observed suspended sediment concentrations are strongly correlated with bottom stress due to waves and currents. However this relationship accounts for only 33% of the suspended sediment concentration variance. One must therefore conclude that bottom stress only plays a partial role in determining the suspended load. Two other effects likely to be important are:

1- advection of sediment from elsewhere, either directly from the plume or from another erosional zone,

2- changes in critical stress for erosion associated with depositional and weathering history.

The latter does not itself generate a suspended load, but can account for the large variability in the response of suspended sediment to hydrodynamic loading.

From the evidence gathered, a broad conceptual model of sediment transport processes in the Mackenzie River plume area emerges. The three main components of this model identify the primary source of material, the horizontal transport process, and the settling/remobilisation mechanisms as follows:

1 The Mackenzie River is the primary source of sediment, introduced to the coastal area by several channels through the delta. A large part of the fresh water and sediment load is discharged early in the year, when hydrodynamic forcing is reduced by partial ice cover.

2 Dispersive processes dominate the transport of the suspended materials away from its source. Akin to turbulent diffusion, this transport can be represented by the following equation:

$$\frac{dC}{dt} = -\frac{d}{dx} K_x \frac{dC}{dx}$$

where C is a concentration, t is time, x is distance and $K_x$ is the turbulent diffusion coefficient along x. Transport in the offshore direction will result from the observed suspended sediment concentration gradient (dC/dx) but also from the gradient in $K_x$ (inferred from the observed increase in flow variance in shallower water). The increased current variance in the along shore direction would also indicate that transport parallel to the coast is likely more important than on-offshore exchanges.

3 The settling and erosion of materials on the bottom is dominated by storm events, which will intermittently resuspend materials which then drift offshore as explained above, to settle later under calm conditions. The hydrodynamic energy gradient (larger currents in shallower water) will cause more frequent disturbance in shallow water, and will again favour a net offshore drift.

The principal feature of this model is the reliance on diffusive processes (akin to the random walk) rather than mean advection to explain the distribution of sedimentary materials. An important consequence of the ice cover is the creation of a time difference between maximum discharge and maximum hydrodynamic forcing. We therefore expect that sediments initially deposited during the freshet may not be in equilibrium with respect to ice free hydrodynamic conditions. The nature of bottom materials as well as the distribution of suspended material will therefore evolve during the ice free season, until an equilibrium is reached.

This speculative model could readily be formalized numerically to provide predictions of suspended and bottom sediment distributions. Quantitative verification against available data would then be possible.

## 4.2 Recommendations for Future Work

This project has concentrated on the oceanography and sedimentary processes in the inner shelf and nearshore zone of the Canadian Beaufort Sea (water depths less than 20 m). Most of the data were collected in water depths greater than 10 m, with only two sites located in depths between 5 and 10 m. Extensive areas of the shelf are covered by less than 10 m of water, with significant changes in the sedimentary regime occurring at around the 5 m isobath (Harper and Penland, 1982; Fissel and Birch, 1984; and Hill and Nadeau, in prep.). Additional current meters placed in water depths less than 10 m and less than 5 m, if feasible, would greatly enhance the understanding of the dynamics of this region. The sampling frequency of these meters should be such that both mean and wave-induced oscillatory current components may be resolved. Coincident suspended sediment and salinity measurements would also be extremely valuable. The latter would allow the distinction between resuspended materials and those associated with the plume (i.e. less saline water).

As described above, horizontal dispersion dominates over vertical mixing processes in the Mackenzie River plume, leading to a complex eddy structure and large spatial variability in plume characteristics. Synoptic profiling surveys are required in order to provide information on the three-dimensional plume structure; previous surveys suffer from poor spatial coverage as well as not being truly synoptic. Due to the importance of the plume dynamics

in the supply of sediment to the shelf region, it is recommended that future synoptic profiling surveys, including salinity, temperature and suspended sediment measurements, are undertaken, several times in one season.

As discussed previously, one of the problems associated with any study of cohesive sediment dynamics is determining the critical stresses for both erosion and deposition of the in situ sediments. At present, there is no simple, inexpensive way to determine these stresses, although this is certainly a current research topic. The flume testing of undisturbed seabed samples seems to be the most widely applied technique and should be considered for the surficial sediments of the inner Beaufort shelf. One should also attempt to characterize temporal changes, if any, in sediment characteristics, over the duration of the ice free period.

Empirical determination (relying on observations alone) of the complex relationships between the various factors affecting sediment transport in the southern Beaufort Sea would require massive amounts of data. In view of the short ice free season and the extreme logistical difficulties of arctic work, it is doubtful that enough data would be available in the near future. It is therefore imperative that maximum use of available data be made using alternative analytical methods. Numerical modelling offers an excellent tool for the utilization of short and gappy observations. Such models effectively extend the available data

by using our scientific understanding of sediment transport processes and our experience of other, perhaps better-studied, areas. The fundamental difference between numerical modelling and the more empirical approach is that the complex interrelationships of the many variables are determined a priori from scientific knowledge instead of being left as free parameters to be determined. This greatly reduces site specific data requirements.

Two levels of modelling effort can be seen as natural extensions of the present work. First, modelling of underlying processes (wind driven circulation, wave climate, sediment consolidation, etc.) will provide a better understanding of fundamental elements of sediment transport. Secondly, modelling of the combined effect of all these processes will give insight into the overall behaviour of the southern Beaufort Sea sediment regime. Although the latter requires some knowledge of the underlying processes, it is not necessarily dependent on the detailed modelling of individual components, as these details are often insignificant compared to uncertainties in basic input data. The two levels of modelling investigation can and should be undertaken simultaneously. As with any other technique, the limitations of numerical modelling must be recognized, and the complexity of the models considered should reflect the availability of data and our degree of (or lack of) understanding of the basic processes.

Useful modelling of the hydrodynamic environment includes the simulation of wind driven circulation, wave climate and plume dynamics. Past investigations have dealt mainly with the Beaufort Sea shelf as a whole and are only of marginal applicability in the shallow regions adjacent to the coast. The available data is amply sufficient for initial modelling purposes. In particular, the 1986 data collected by Hodgins et al. (1987) can provide valuable information on the generation and dissipation of wave energy on shallow sloping bottoms. It should be noted that apart from the sediment transport interest, the investigation of the hydrodynamic climate is crucial for other applications such as structural loading, navigation and artificial island engineering.

Initial modelling of sediment transport in the Mackenzie River plume area should be based on the results presented herein, as they summarize the most recent knowledge of this environment. The quantitative analysis and correlation results provide sufficient information for estimating the necessary parameters for simple simulations, and the conceptual model presented earlier is a useful starting point. This model can be expanded or modified as necessary, keeping in mind that the available input and verification data cannot support a very complex system. For example, the approximate knowledge of discharge and its distribution among the channels of the Mackenzie delta limit the usefulness of a detailed geometrical representation of the coastline. In view of the few verification data sets, any model

considered should have few, if any, free parameters to be determined by calibration.

Successful models can be used to effectively interpolate and extrapolate the available data to times when no observations are available. This will allow the investigation of long term trends and interannual variability, which is difficult otherwise. The sensitivity of the numerical results to model inputs can be used to identify key processes and hypotheses, and form a rational basis to plan measurement programs which result in the largest reduction of uncertainty.

# REFERENCES


Amos, C. L. and D. C. Mosher, 1985. Erosion and Deposition of Fine-Grained Sediments from the Bay of Fundy. Sedimentology, Vol. 22, p. 815-832.

Arctic Laboratories Ltd., 1985a. Data Report for Current Meter Measurements at Arnak, Summer 1985. Unpublished report to Esso Resources Canada Ltd.

Arctic Laboratories Ltd., 1985b. Data Report for Current Meter Measurements at Nipterk, Summer 1985. Unpublished report to Esso Resources Canada Ltd.

Birch, J.R., D.B. Fissel and G.R. Wilton, 1984a. Physical Oceanographic Data Report: Amerk O-09 Site, Beaufort Sea, Summer 1984 Current Meter Data. Unpublished report to Esso Resources Canada Ltd.

Birch, J.R., D.B. Fissel and G.R. Wilton, 1984b. Physical Oceanographic Data Report: Nipterk L-19/Kaubvik I-43 Site, Beaufort Sea, Summer 1984 Current Meter Data. Unpublished report to Esso Resources Canada Ltd.

Dolata, L.F. and W. Rosenthal, 1984. Wave Setup and Wave-Induced Currents in Coastal Zones. J. Geophys. Res., Vol. 89, No. C2, p. 1973-1982.

Fischer, H.B., E.J. List, R.C.Y. Koh, J. Imberger and N.H. Brooks, 1979. *Mixing in Inland and Coastal Waters*. Academic Press Inc., New York, New York, 483 p.

Fissel, D.B. and J.R. Birch, 1984. Sediment Transport in the Canadian Beaufort Sea, unpublished report to the Geological Survey of Canada by Arctic Sciences Ltd., Victoria, B.C., 165 p.

Grant, W.D. and O.S. Madsen, 1979. Combined Wave and Current Interaction With a Rough Bottom. J. Geophys. Res., Vol. 84, No. C4, p. 1797-1808.

Grant, W.D. and O.S. Madsen, 1986. The Continental Shelf Bottom Boundary Layer. Ann. Rev. Fluid Mech. 1986. Vol. 18, p. 265-305.

Harper, J.R. and S. Penland, 1982. Beaufort Sea Sediment Dynamics. Unpublished report to the Geological Survey of Canada by Woodward-Clyde Consultants, Victoria, B.C., 125 p.

Harper, J.R., S.M. Blasco and P.R. Hill, in prep. Sediment Transport on the Canadian Beaufort Sea Shelf.

Hill, P.R. and O.C. Nadeau, in prep. Characteristics of the Mackenzie Plume and Sedimentation on the Inner Shelf and Nearshore Zone of the Canadian Beaufort Sea.

Hodgins, D.O., O.J. Sayao, E.D. Kinsella and P.W. Morgan, 1987. Nearshore Sediment Dynamics - Beaufort Sea. The 1986 Monitoring Program. Environmental Studies Revolving Funds Report 054. Ottawa, Canada, 195 p.

Longuet-Higgins, M.S., 1970. Longshore Currents Generated by Obliquely Incident Sea Waves 2. J. Geophys. Res. Vol. 75 No. 33.

McCave, I.N., 1984. Erosion, Transport and Deposition of Fine-grained Marine Sediments, In: *Fine-Grained Sediments: Deep-Water Processes and Facies*, D.A.V. Stow and D.J.W. Piper (editors), Geological Society Special Publication No. 15, Blackwell Scientific Publications, Oxford, U.K.

Milliman, J.D. and R.H. Meade, 1983. World-wide Delivery of River Sediments to the Oceans. J. Geol., 91, p. 1-21.

Nadeau, O.C., 1984. Field Operations Report and Data Synthesis for the Beaufort Sea Sediment Dynamics Project: 1983-1984. Unpublished report to the Geological Survey of Canada by Arctic Sciences Ltd.

Officer, C. B., 1976. *Physical Oceanography of Estuaries (and Associated Coastal Waters)*. Wiley Interscience Publication xii, Wiley, New York, New York, 465p.

Pelletier, B.R., 1975. Sediment Dispersal in the Southern Beaufort Sea. Beaufort Sea Technical Report 25a. Institute of Ocean Sciences, Sidney, B.C., 80 p.

Royer, L. and W.J. Emery, 1985. Computer Simulations of the Fraser River Plume. J. Mar. Res., Vol. 43, p. 289-306.

Sternberg, R.W., 1972. Predicting Initial Motion and Bedload Transport of Sediment Particles in the Shallow Marine Environment. In: *Shelf Sediment Transport, Process and Pattern*, D.B. Duane and O.H. Pilkey (editors), Dowden, Hutchinson & Ross, Inc., p. 61-83.

U. S. Army, 1973. *Shore Protection Manual*. U. S. Army Coastal Engineering Research Center, Fort Belvoir, Virginia.

# Appendix A: Raw data time series

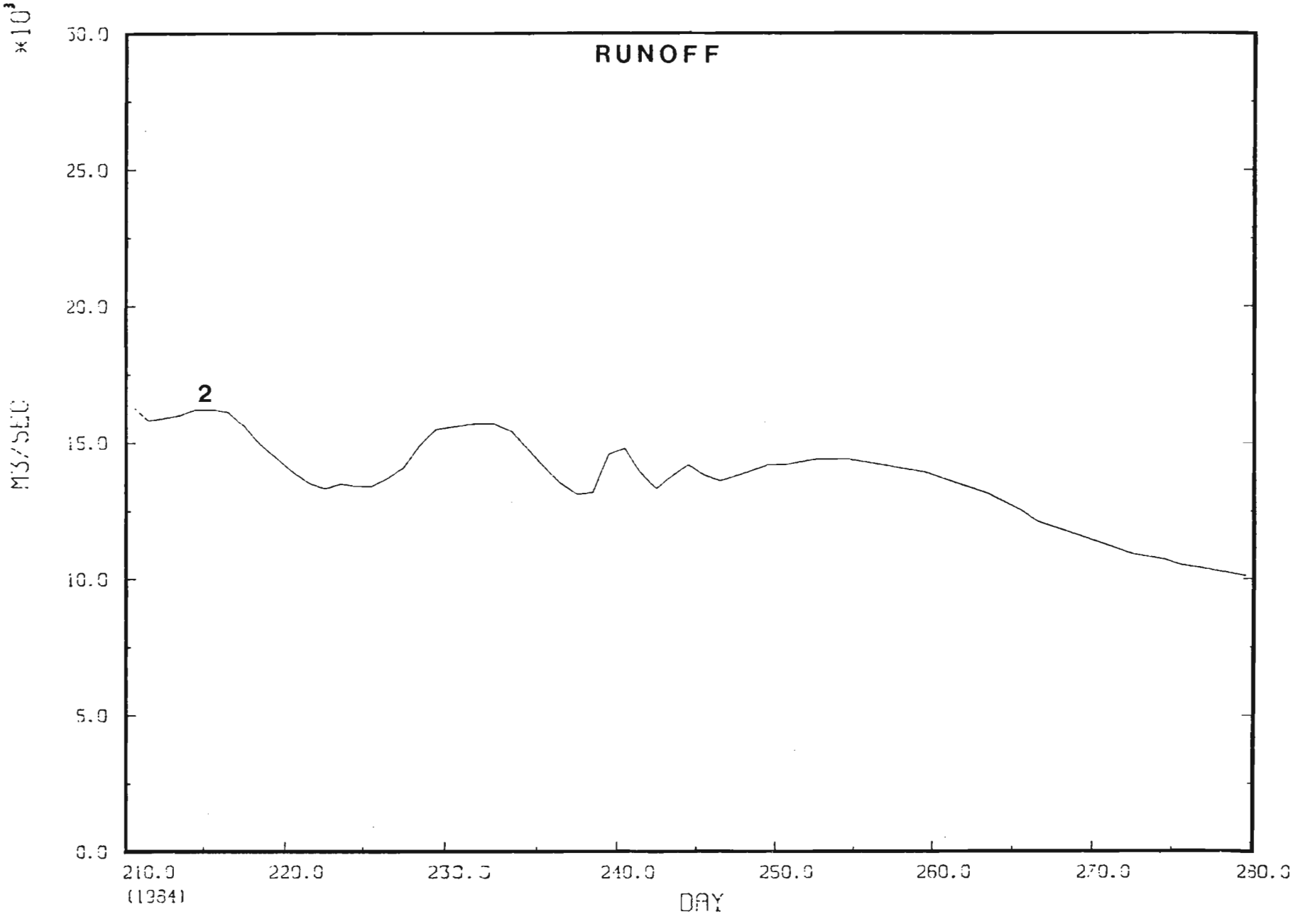
RUNOFF
*10³
M³/SEC
30.0
25.0
20.0
15.0
10.0
5.0
0.0
2
210.0
(1984)
220.0
230.0
240.0
250.0
260.0
270.0
280.0
DAY

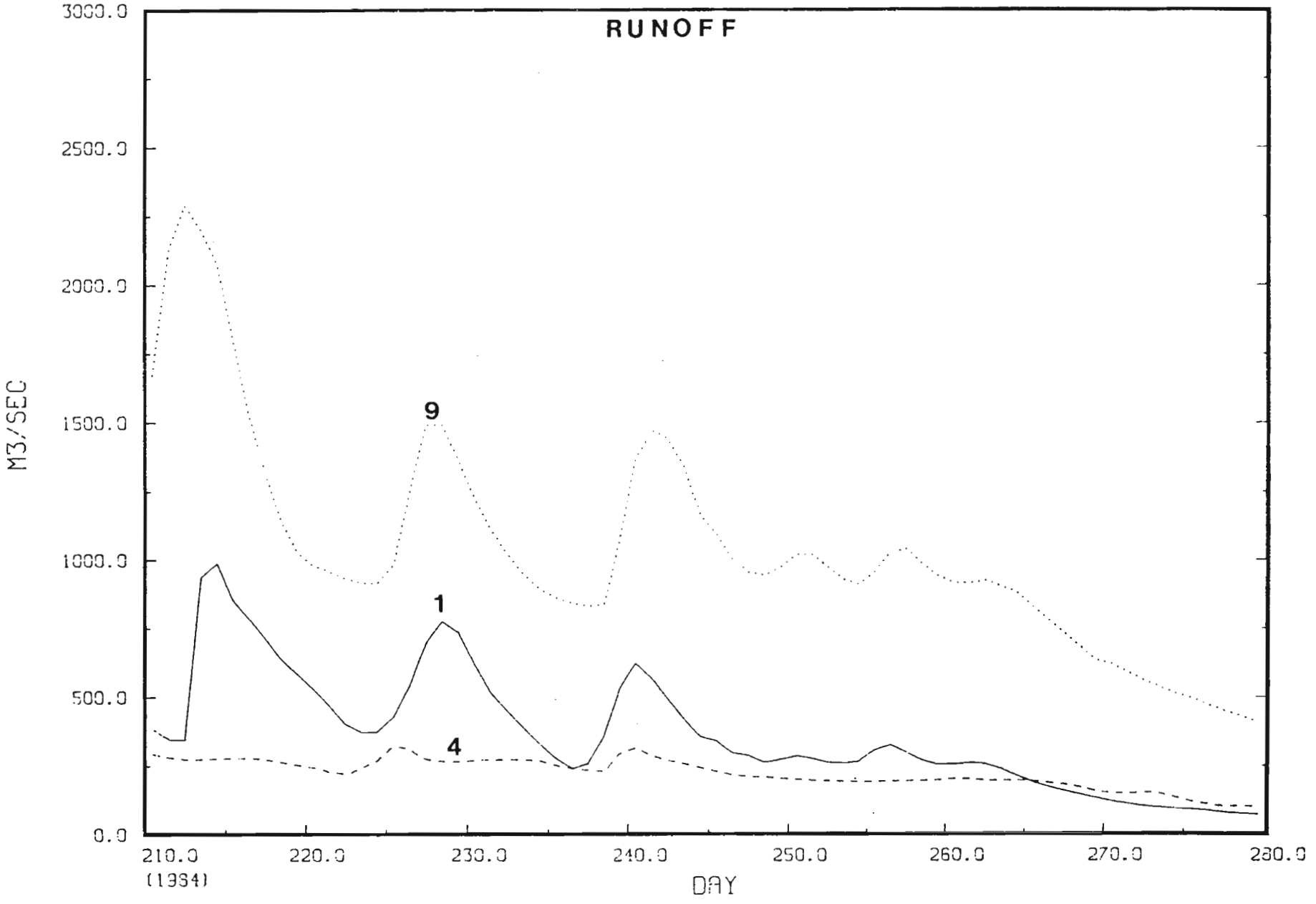
RUNOFF
3000.0
2500.0
2000.0
1500.0
1000.0
500.0
0.0
M3/SEC
9
1
4
210.0
(1984)
220.0
230.0
240.0
250.0
260.0
270.0
280.0
DAY

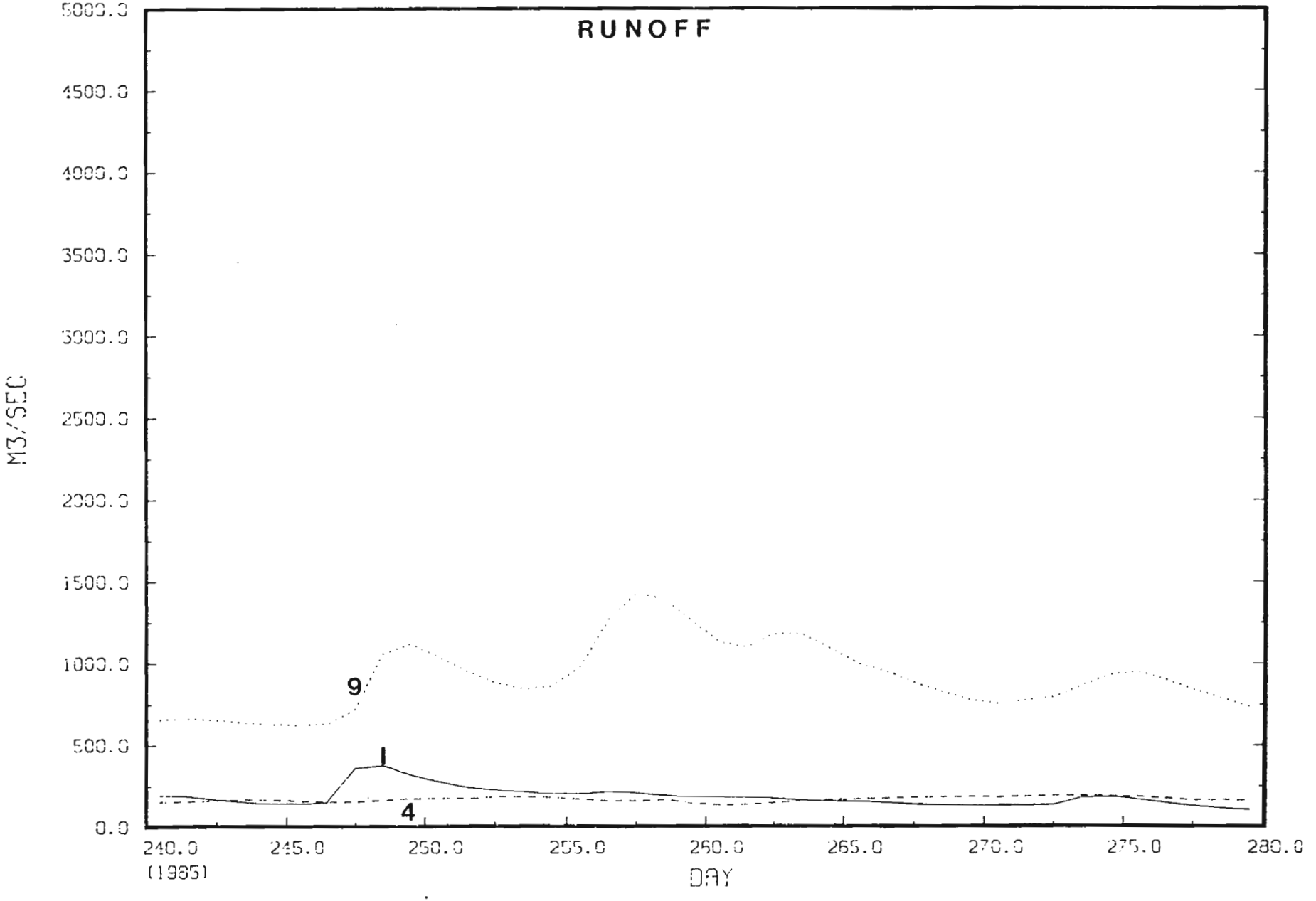
RUNOFF
5000.0
4500.0
4000.0
3500.0
3000.0
2500.0
2000.0
1500.0
1000.0
500.0
0.0
M3/SEC
9
1
4
240.0
(1985)
245.0
250.0
255.0
260.0
265.0
270.0
275.0
280.0
DAY

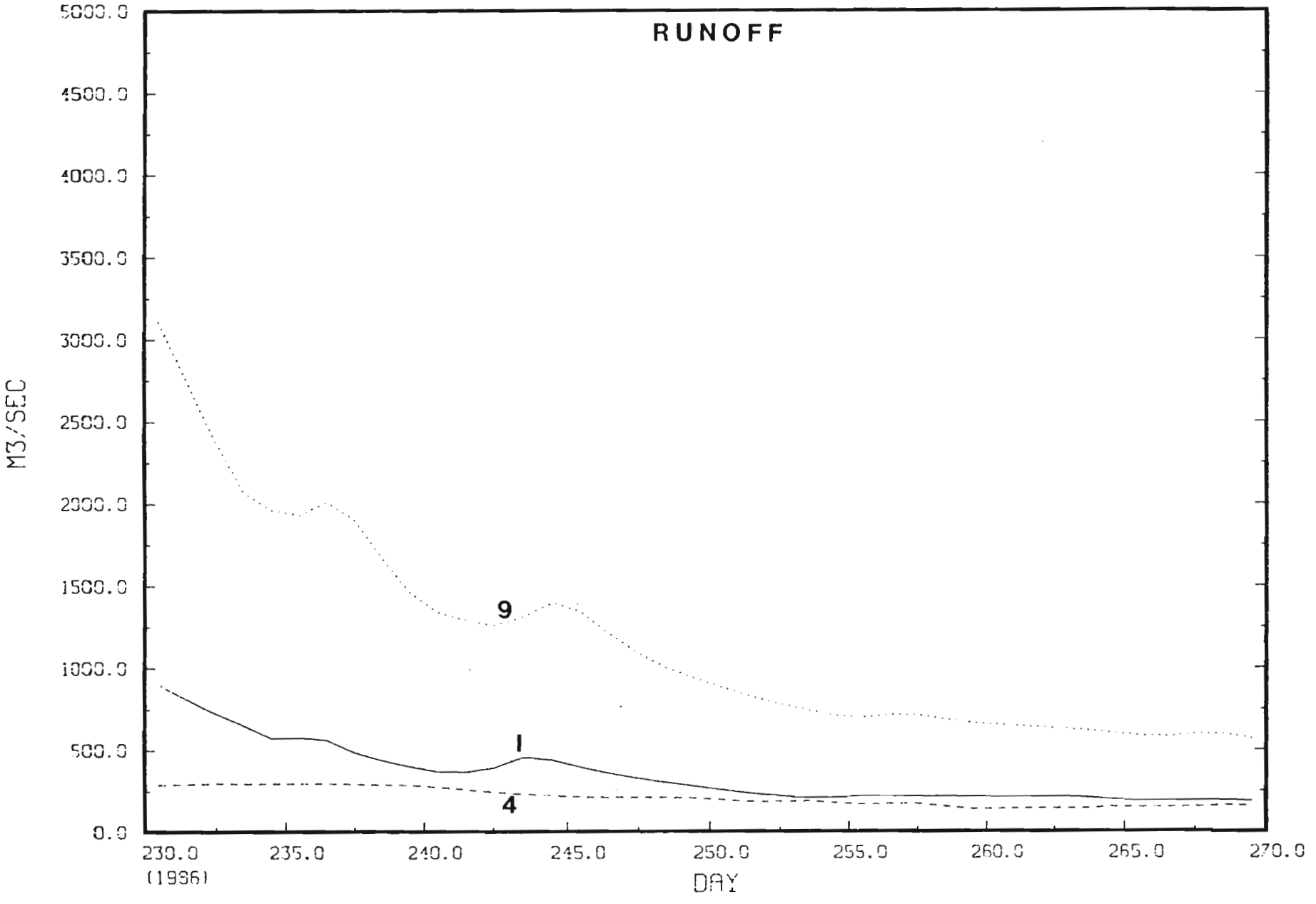
RUNOFF
5000.0
4500.0
4000.0
3500.0
3000.0
2500.0
2000.0
1500.0
1000.0
500.0
0.0
M3/SEC
9
1
4
230.0
(1986)
235.0
240.0
245.0
250.0
255.0
260.0
265.0
270.0
DAY

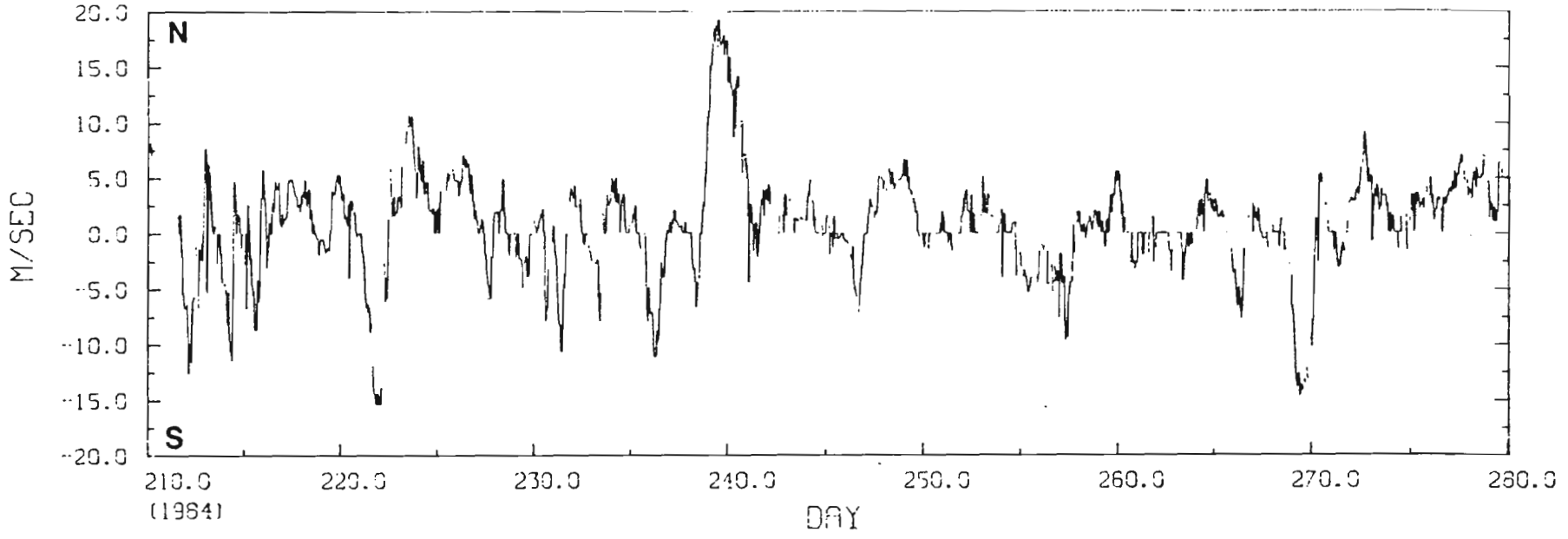
N
S
M/SEC
20.0
15.0
10.0
5.0
0.0
-5.0
-10.0
-15.0
-20.0
210.0
(1984)
220.0
230.0
240.0
250.0
260.0
270.0
280.0
DAY

**1984 WIND**

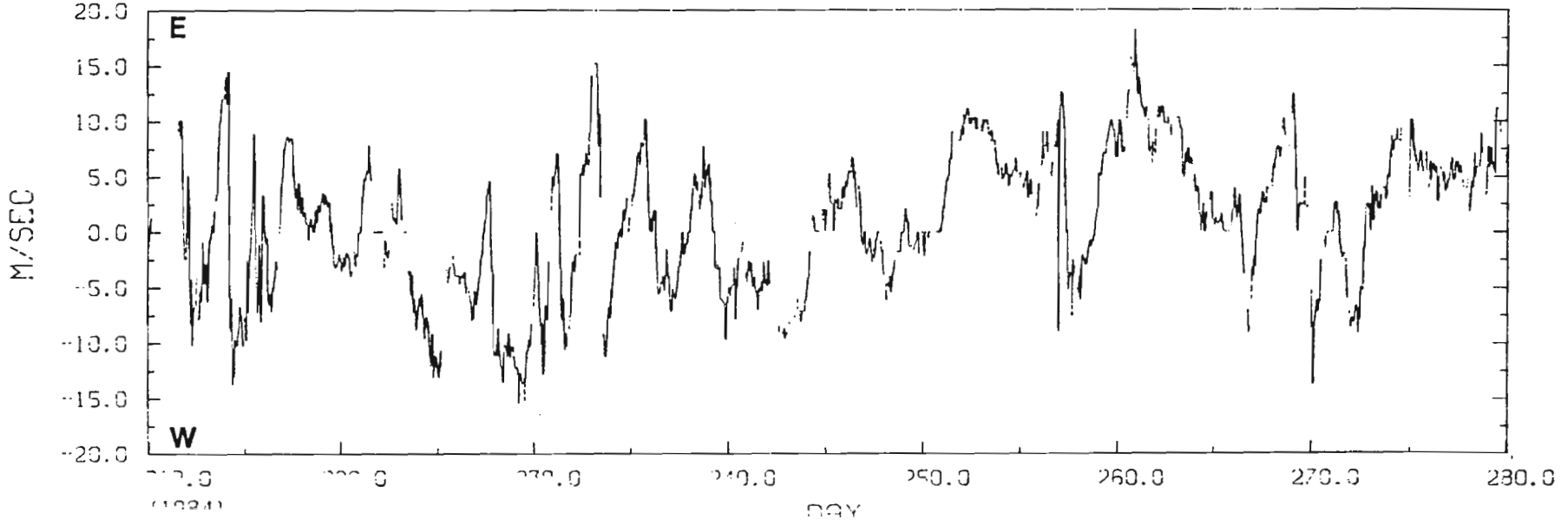
E
W
M/SEC
20.0
15.0
10.0
5.0
0.0
-5.0
-10.0
-15.0
-20.0
260.0
270.0
280.0
DAY

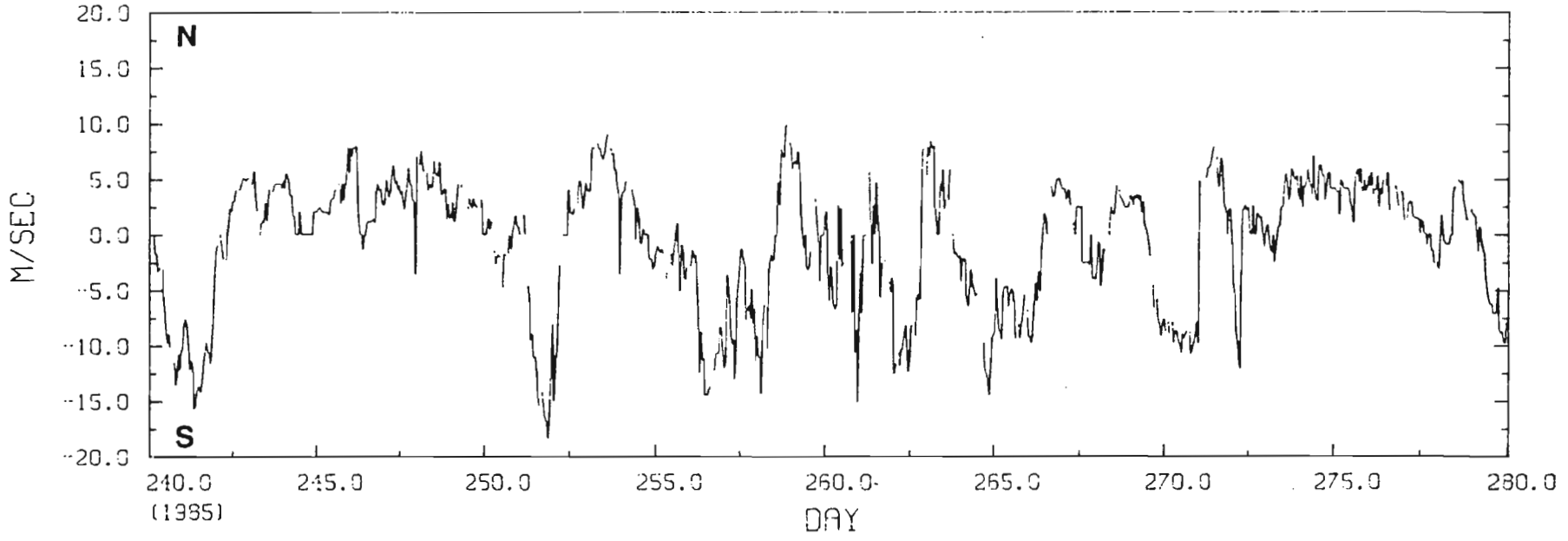
N
S
M/SEC
20.0
15.0
10.0
5.0
0.0
-5.0
-10.0
-15.0
-20.0
240.0
245.0
250.0
255.0
260.0
265.0
270.0
275.0
280.0
(1985)
DAY

**1985 WIND**

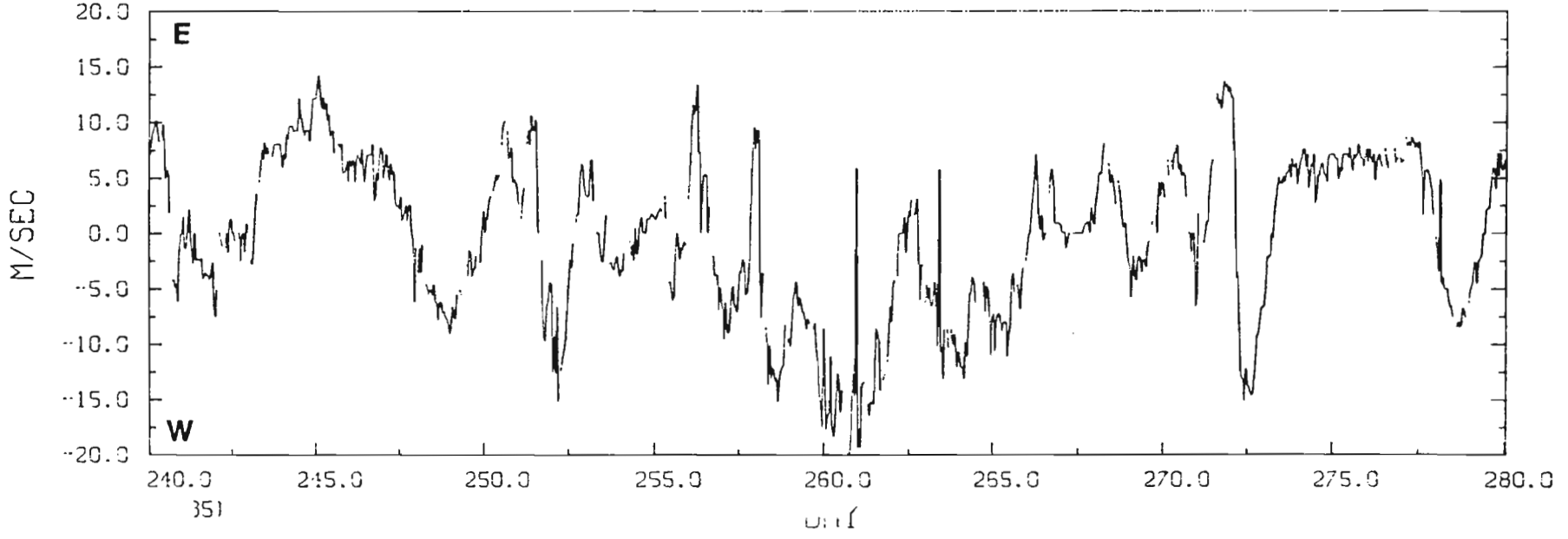
E
W
M/SEC
20.0
15.0
10.0
5.0
0.0
-5.0
-10.0
-15.0
-20.0
240.0
245.0
250.0
255.0
260.0
265.0
270.0
275.0
280.0
DAY

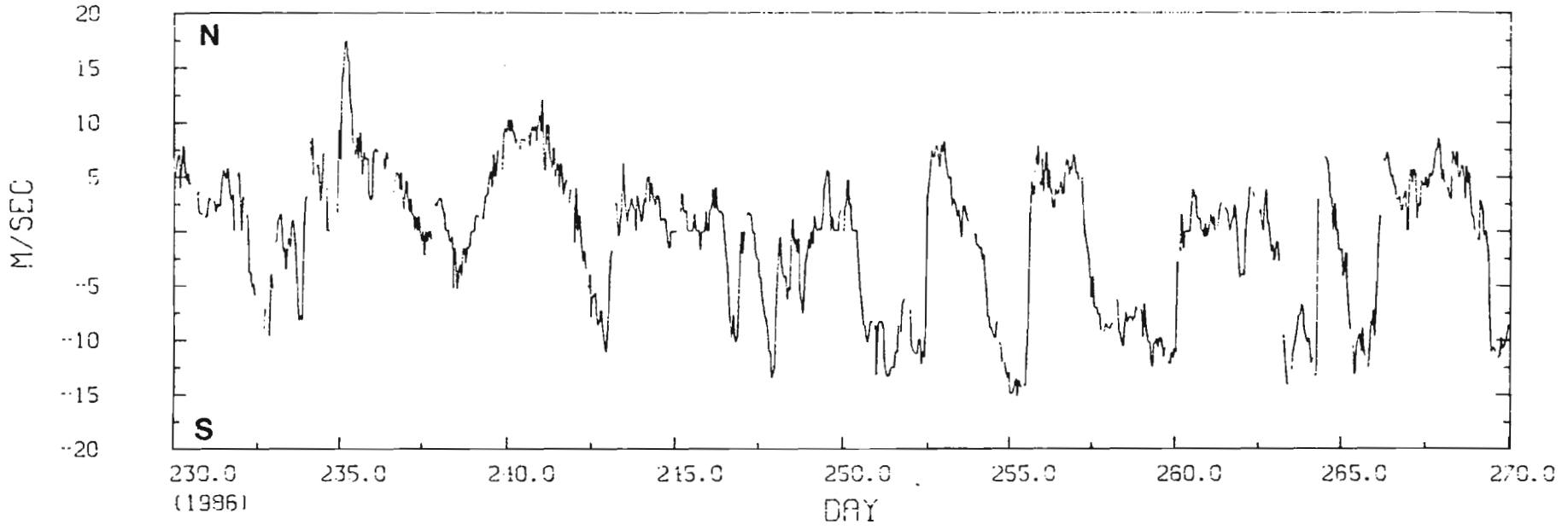
N
S
M/SEC
20
15
10
5
-5
-10
-15
-20
230.0
235.0
240.0
245.0
250.0
255.0
260.0
265.0
270.0
(1986)
DAY

**1986 WIND**

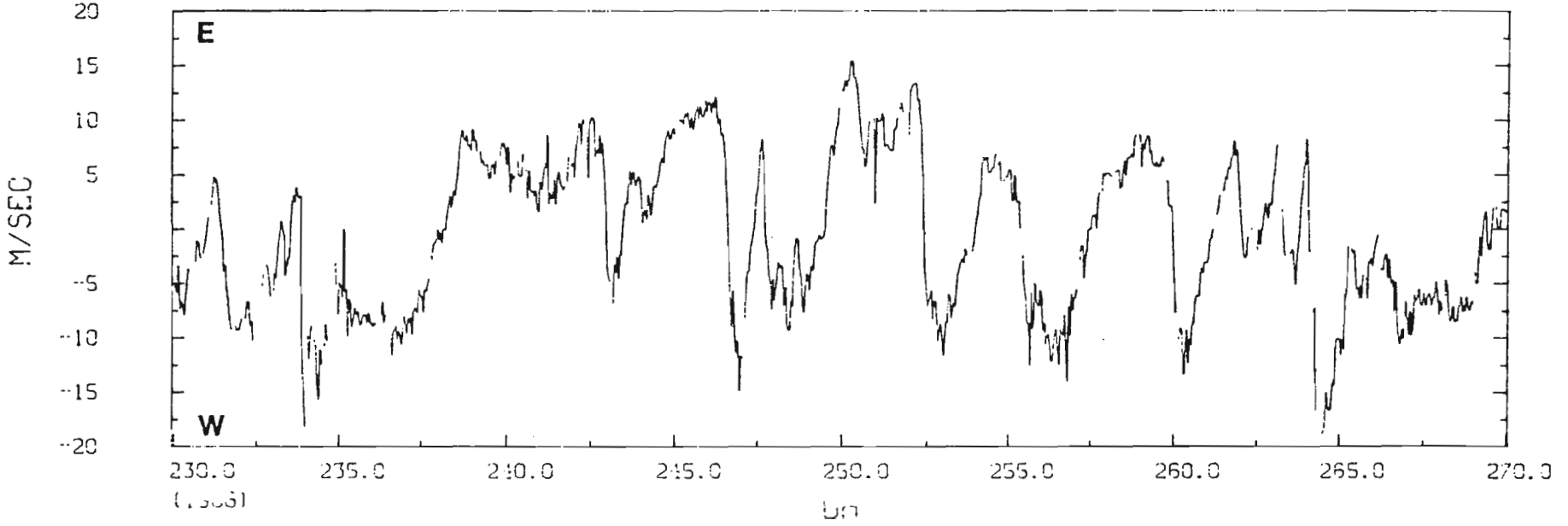
E
W
M/SEC
20
15
10
5
-5
-10
-15
-20
230.0
235.0
240.0
245.0
250.0
255.0
260.0
265.0
270.0

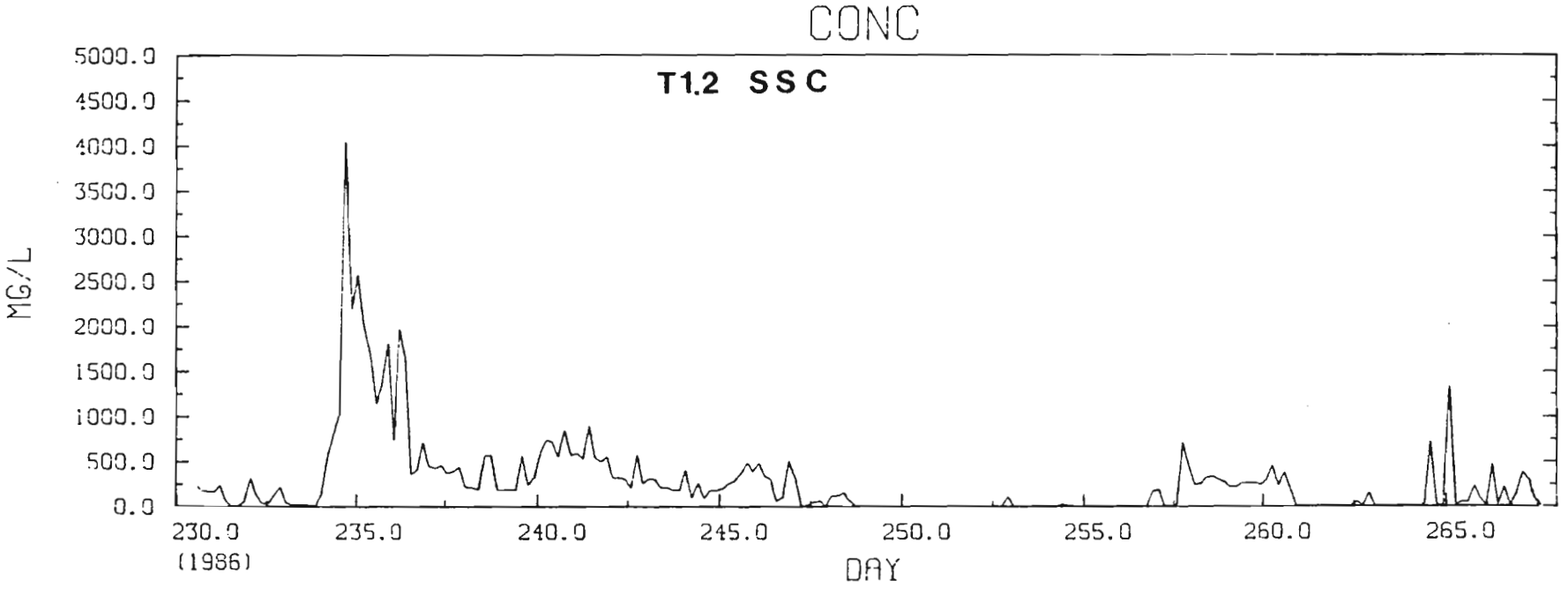
CONC
T1.2 SSC
MG/L
5000.0
4500.0
4000.0
3500.0
3000.0
2500.0
2000.0
1500.0
1000.0
500.0
0.0
230.0
(1986)
235.0
240.0
245.0
250.0
255.0
260.0
265.0
DAY

# WAVE HEIGHT
## $H_{sig}$

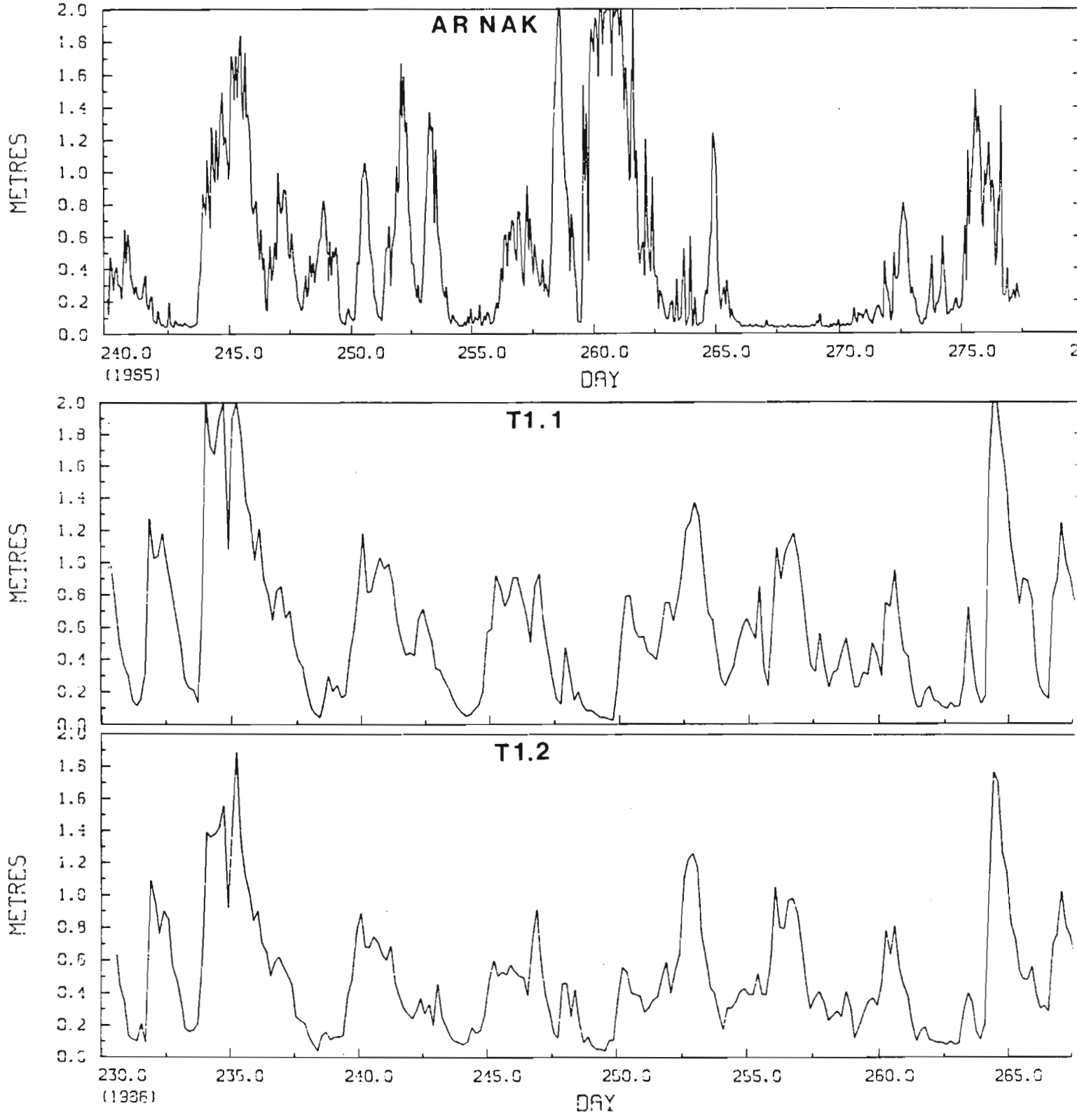

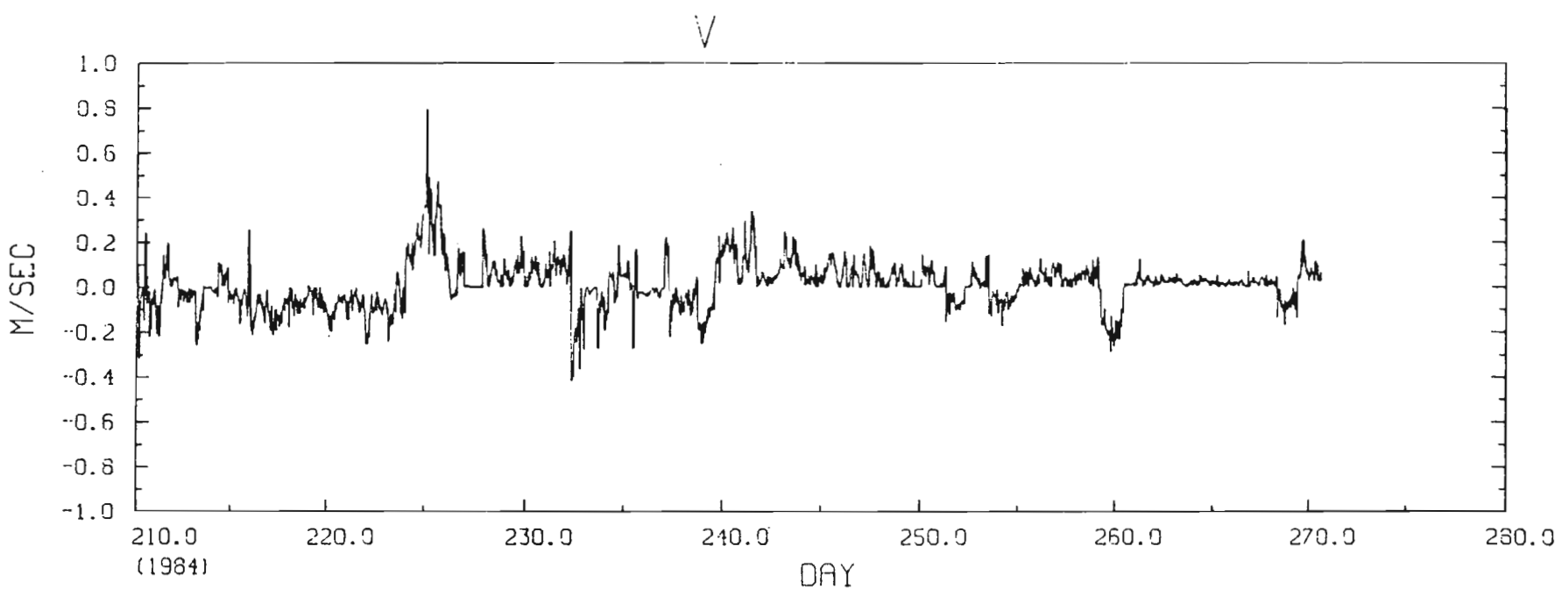
V
1.0
0.8
0.6
0.4
0.2
0.0
-0.2
-0.4
-0.6
-0.8
-1.0
M/SEC
210.0
(1984)
220.0
230.0
240.0
250.0
260.0
270.0
280.0
DAY

**NIPTERK 11m**

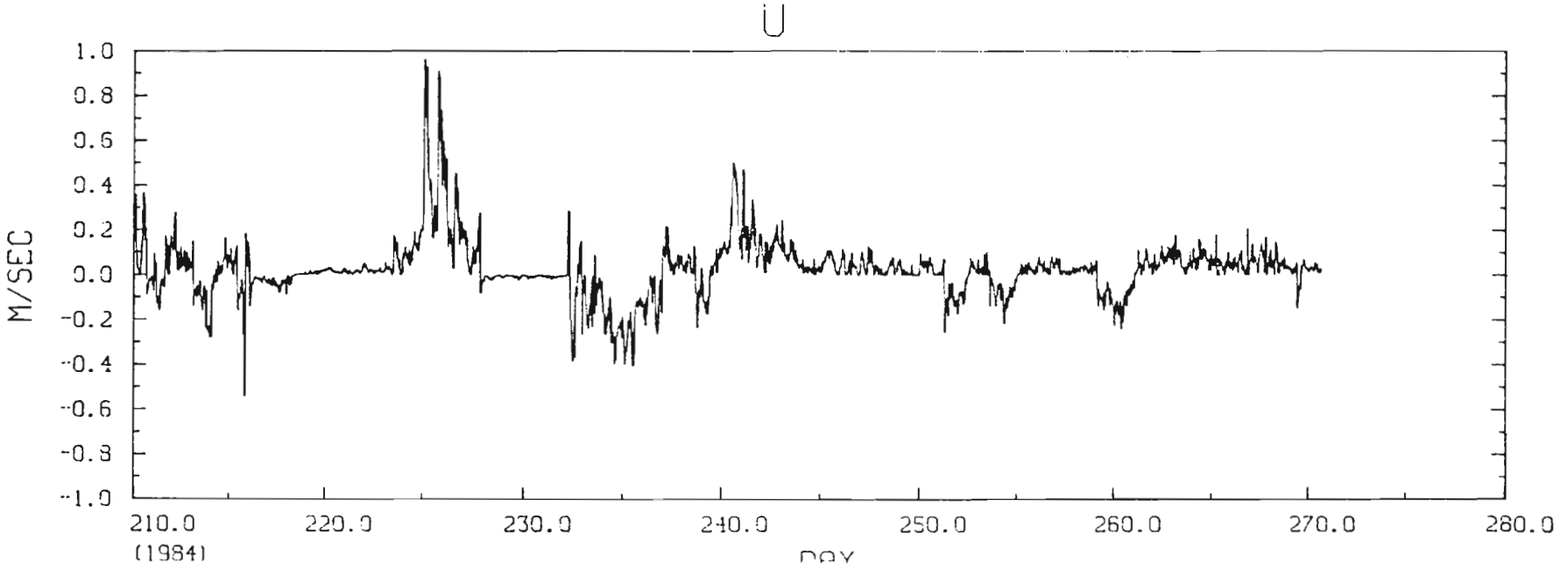
U
1.0
0.8
0.6
0.4
0.2
0.0
-0.2
-0.4
-0.6
-0.8
-1.0
M/SEC
210.0
(1984)
220.0
230.0
240.0
250.0
260.0
270.0
280.0
DAY

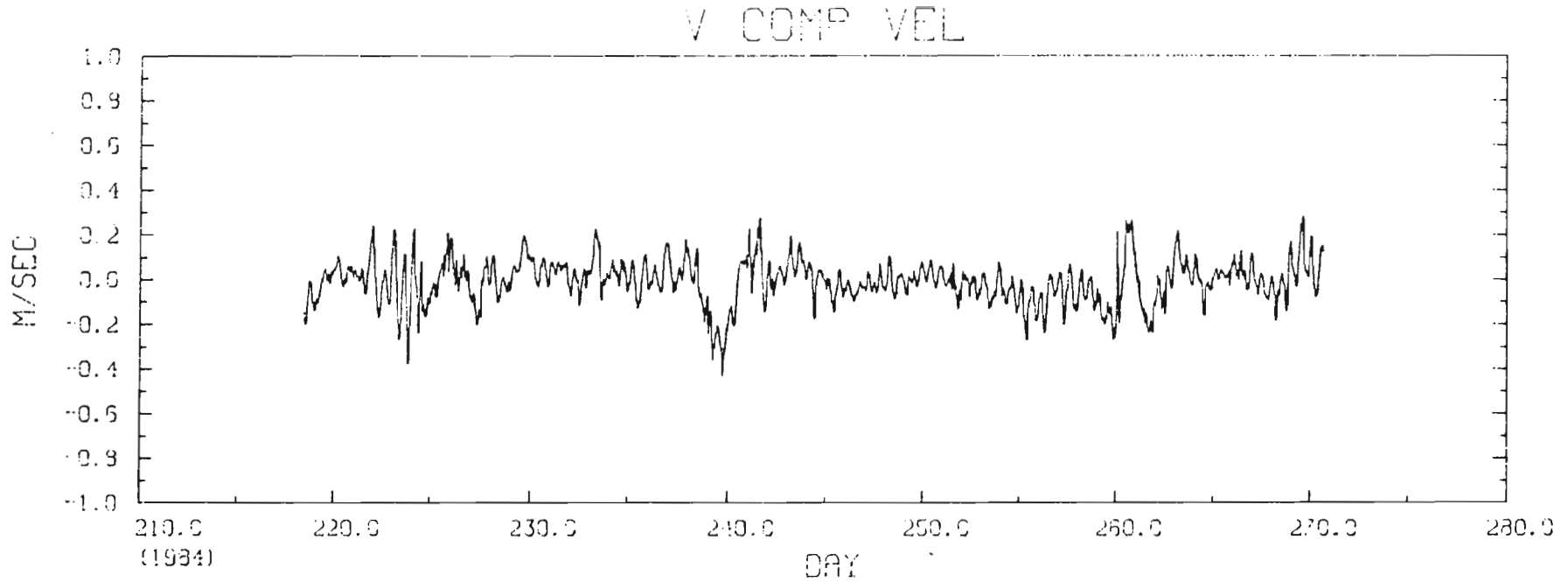
V COMP VEL
M/SEC
1.0
0.8
0.6
0.4
0.2
0.0
-0.2
-0.4
-0.6
-0.8
-1.0
210.0
(1984)
220.0
230.0
240.0
250.0
260.0
270.0
280.0
DAY

**NIPTERK 7 m**

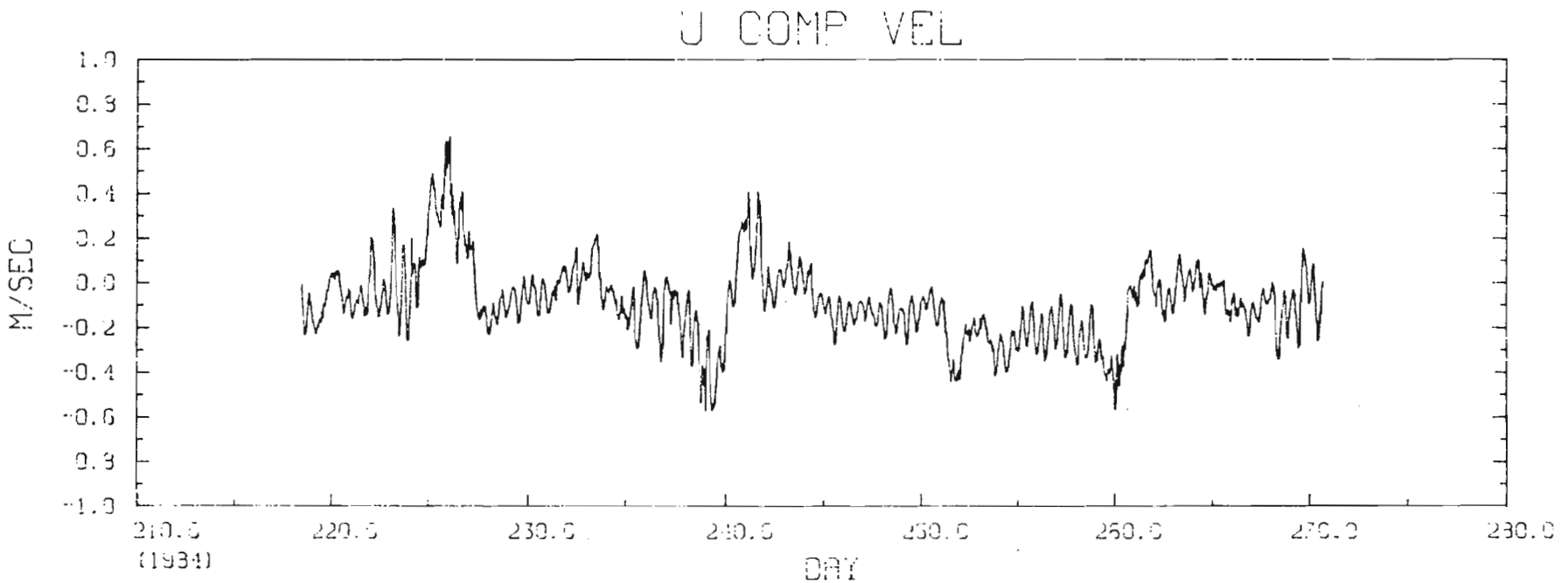
U COMP VEL
M/SEC
1.0
0.8
0.6
0.4
0.2
0.0
-0.2
-0.4
-0.6
-0.8
-1.0
210.0
(1984)
220.0
230.0
240.0
250.0
260.0
270.0
280.0
DAY

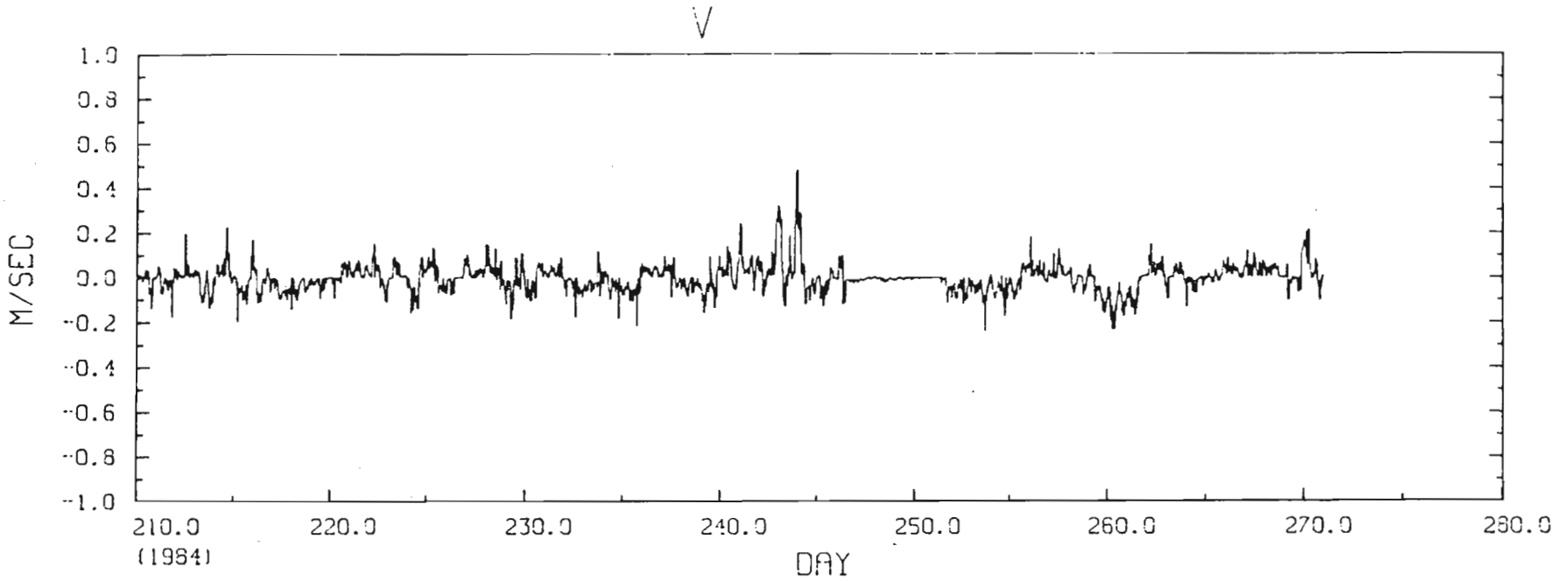
V
1.0
0.8
0.6
0.4
0.2
0.0
-0.2
-0.4
-0.6
-0.8
-1.0
M/SEC
210.0
220.0
230.0
240.0
250.0
260.0
270.0
280.0
(1984)
DAY

**AMERK 19.5 m**

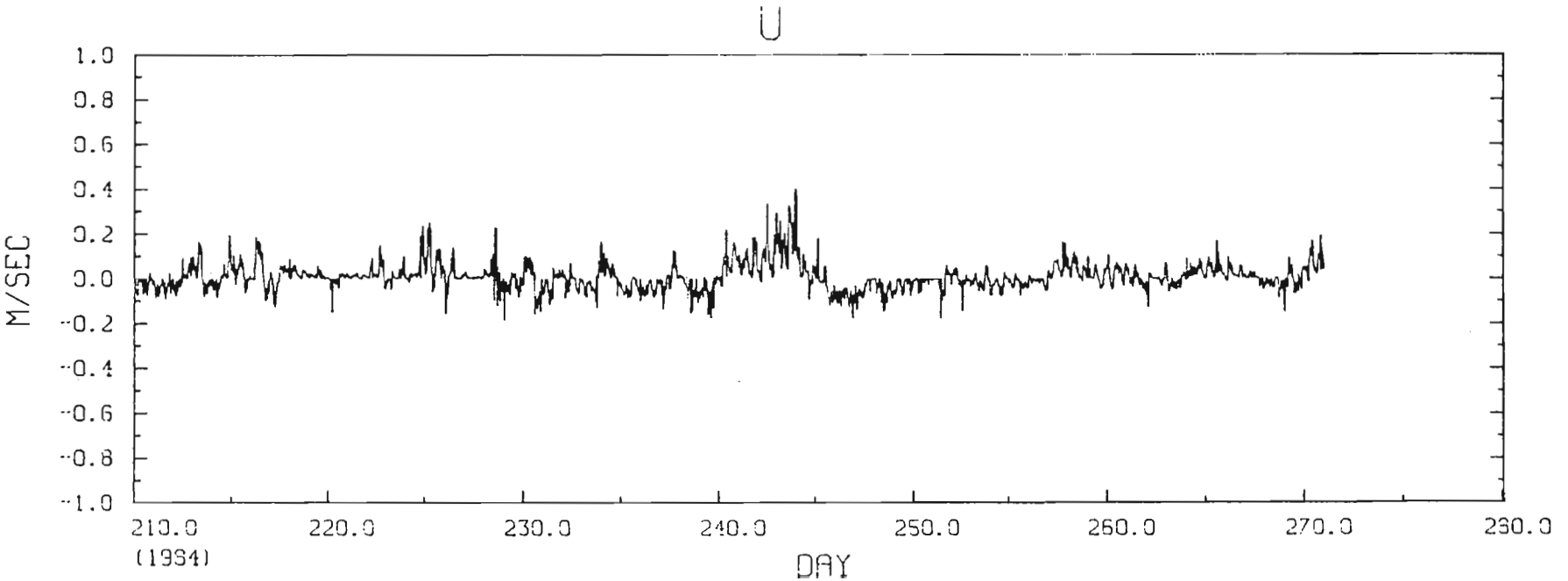
U
1.0
0.8
0.6
0.4
0.2
0.0
-0.2
-0.4
-0.6
-0.8
-1.0
M/SEC
210.0
220.0
230.0
240.0
250.0
260.0
270.0
280.0
(1984)
DAY

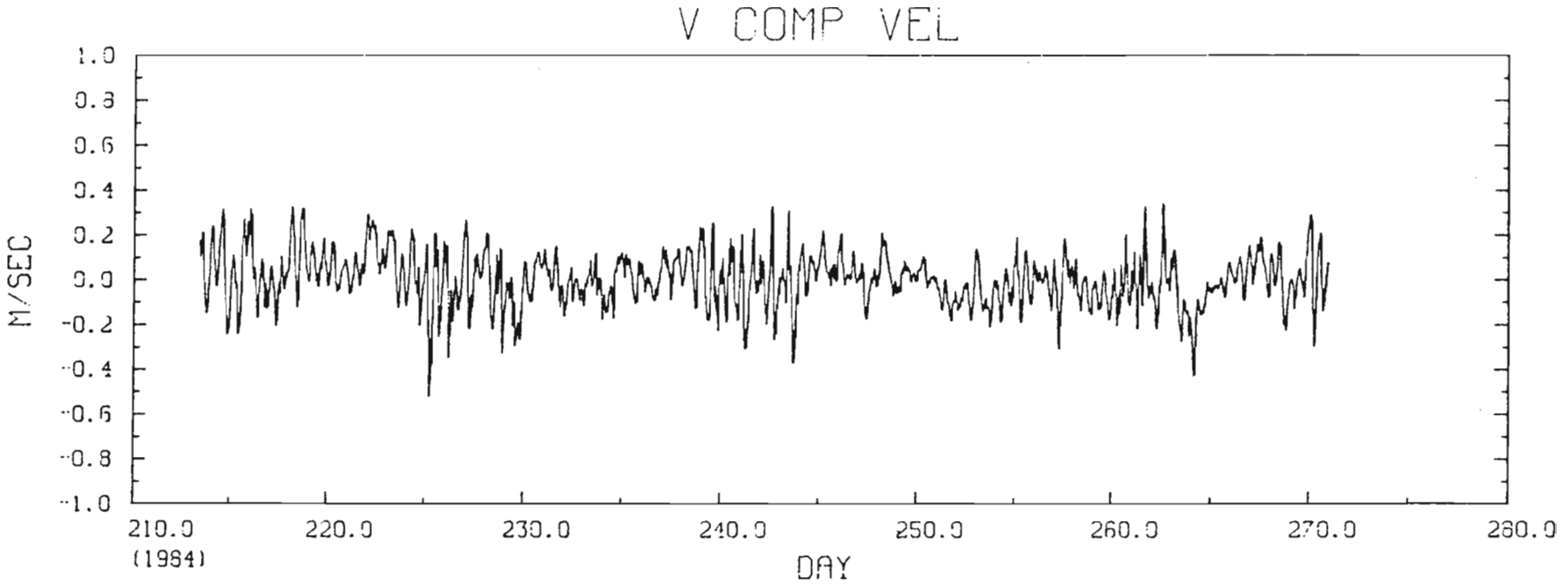
V COMP VEL
M/SEC
1.0
0.8
0.6
0.4
0.2
0.0
-0.2
-0.4
-0.6
-0.8
-1.0
210.0
(1984)
220.0
230.0
240.0
250.0
260.0
270.0
280.0
DAY

**AMERK 7.1 m**

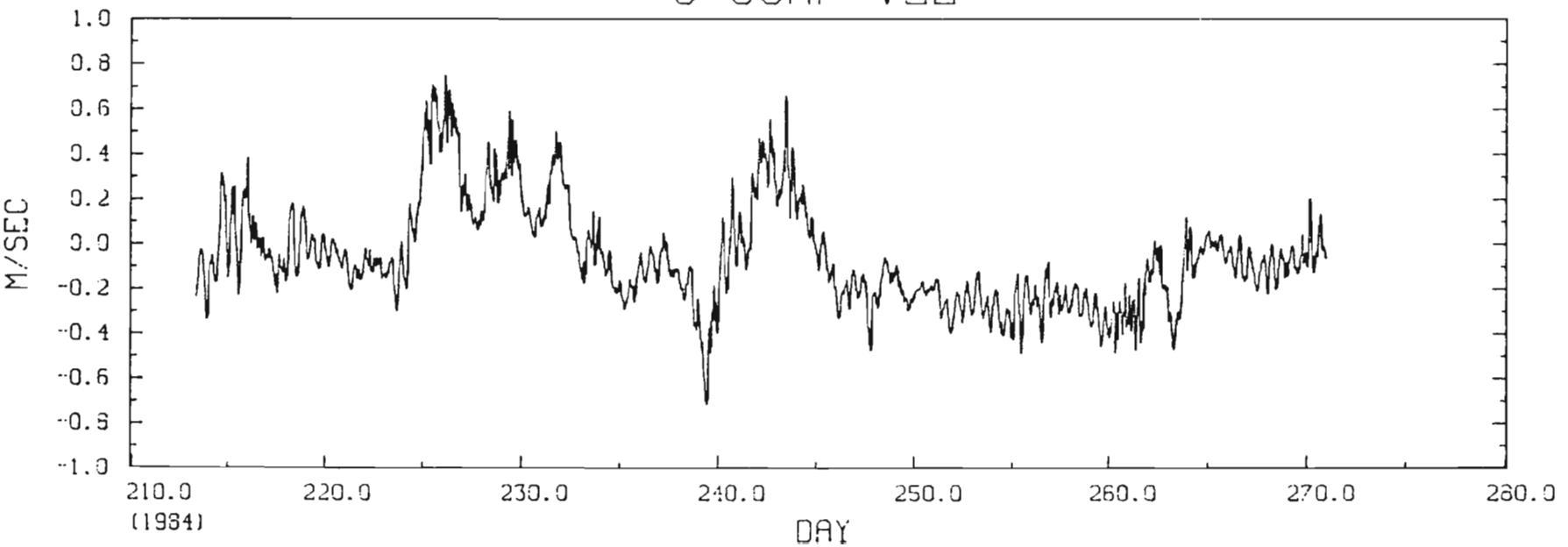
U COMP VEL
M/SEC
1.0
0.8
0.6
0.4
0.2
0.0
-0.2
-0.4
-0.6
-0.8
-1.0
210.0
(1984)
220.0
230.0
240.0
250.0
260.0
270.0
280.0
DAY

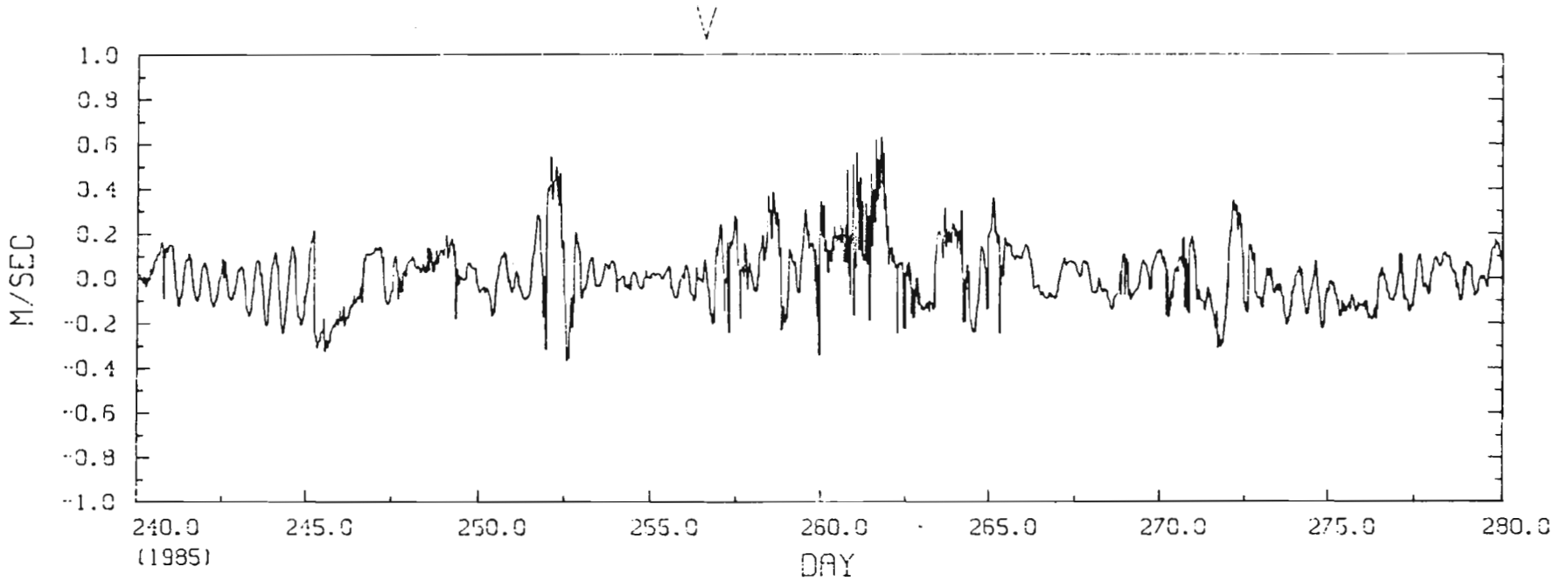
V
1.0
0.8
0.6
0.4
0.2
0.0
-0.2
-0.4
-0.6
-0.8
-1.0
M/SEC
240.0
245.0
250.0
255.0
260.0
265.0
270.0
275.0
280.0
(1985)
DAY

**NIP TERK 7.8m**

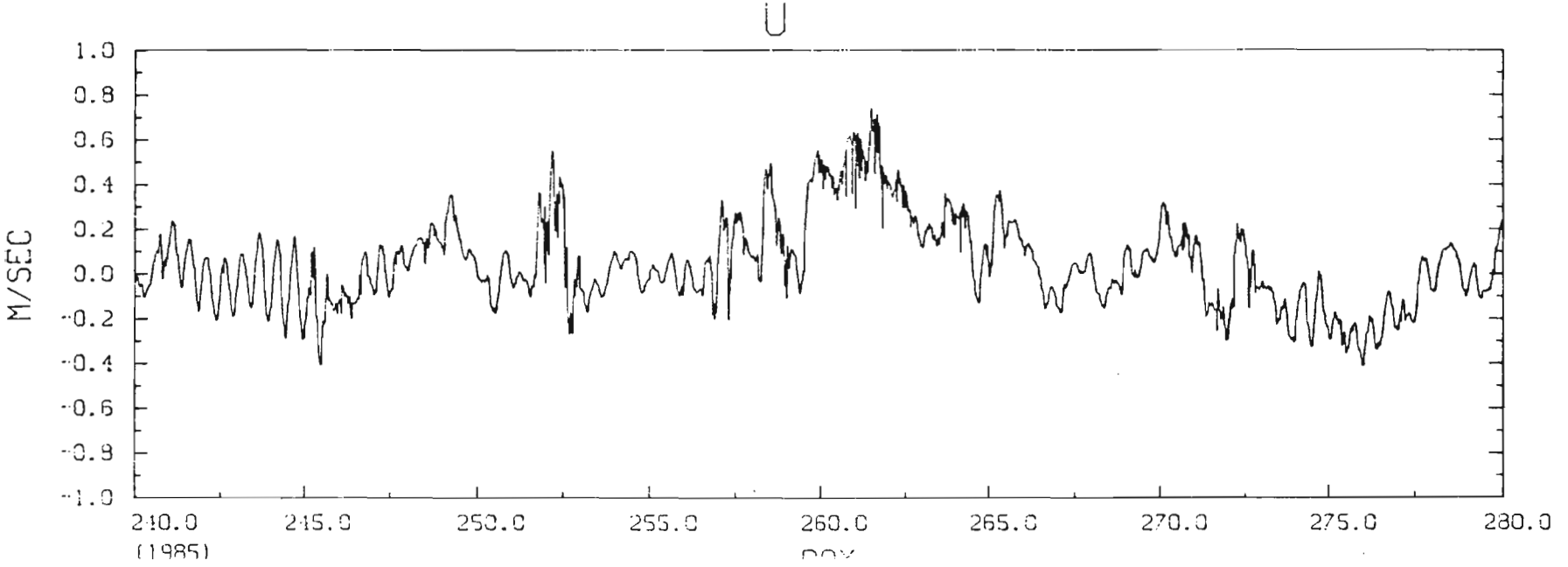
U
1.0
0.8
0.6
0.4
0.2
0.0
-0.2
-0.4
-0.6
-0.8
-1.0
M/SEC
240.0
245.0
250.0
255.0
260.0
265.0
270.0
275.0
280.0
(1985)

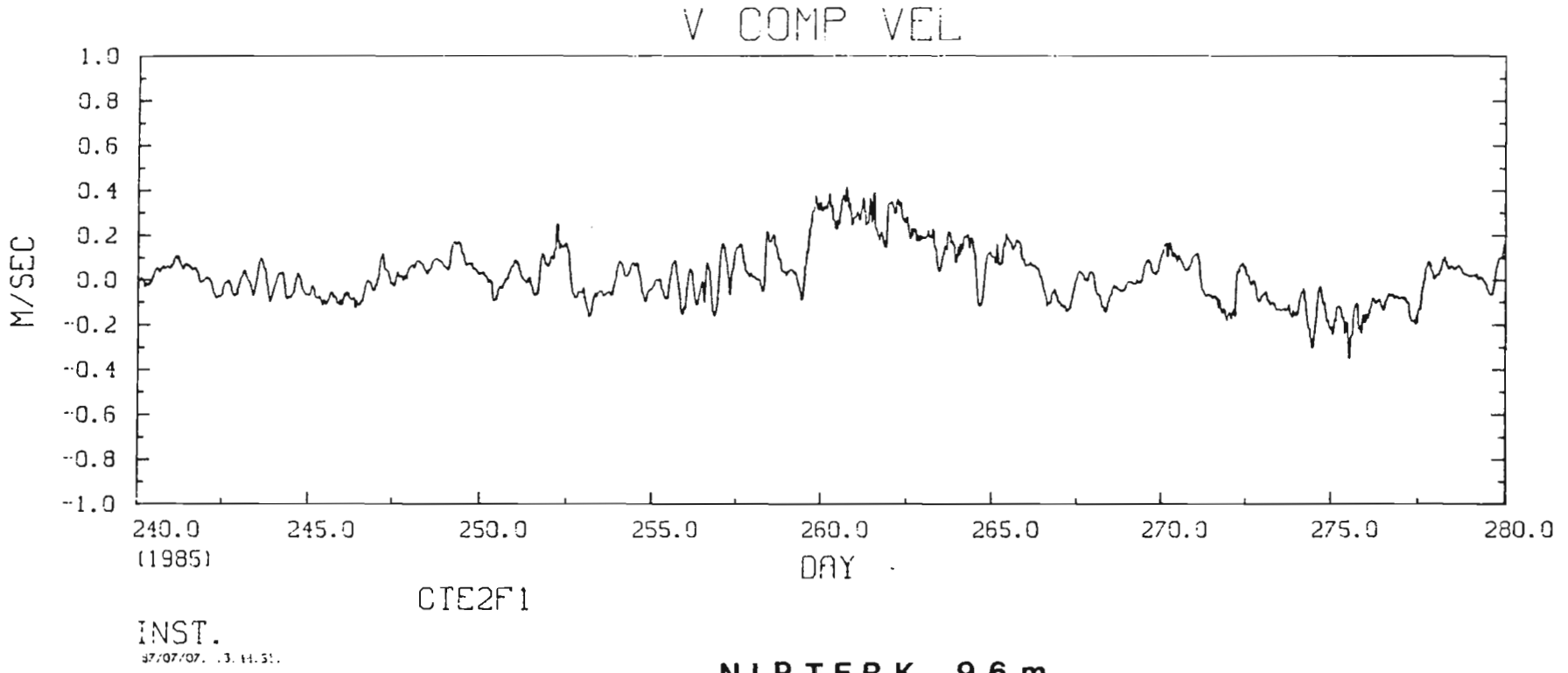
V COMP VEL
1.0
0.8
0.6
0.4
0.2
0.0
-0.2
-0.4
-0.6
-0.8
-1.0
M/SEC
240.0
245.0
250.0
255.0
260.0
265.0
270.0
275.0
280.0
(1985)
DAY
CTE2F1
INST.

**NIPTERK 9.6 m**

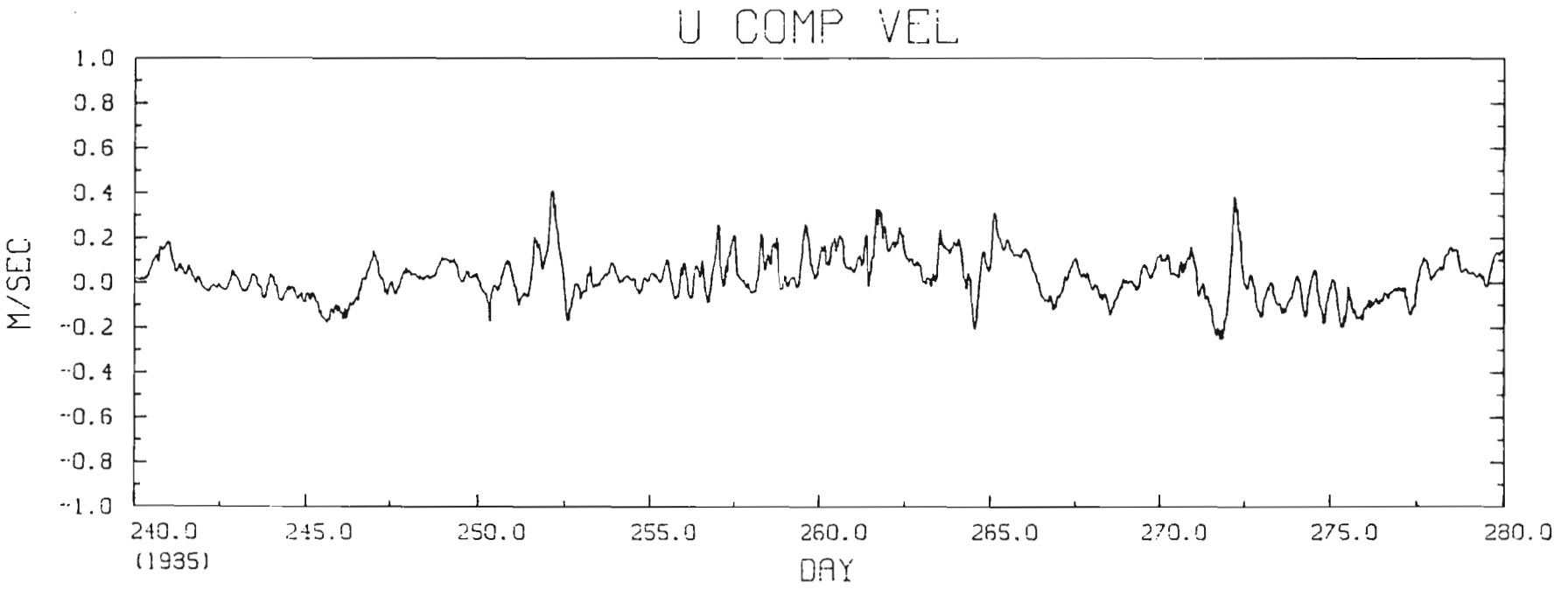
U COMP VEL
1.0
0.8
0.6
0.4
0.2
0.0
-0.2
-0.4
-0.6
-0.8
-1.0
M/SEC
240.0
245.0
250.0
255.0
260.0
265.0
270.0
275.0
280.0
(1985)
DAY

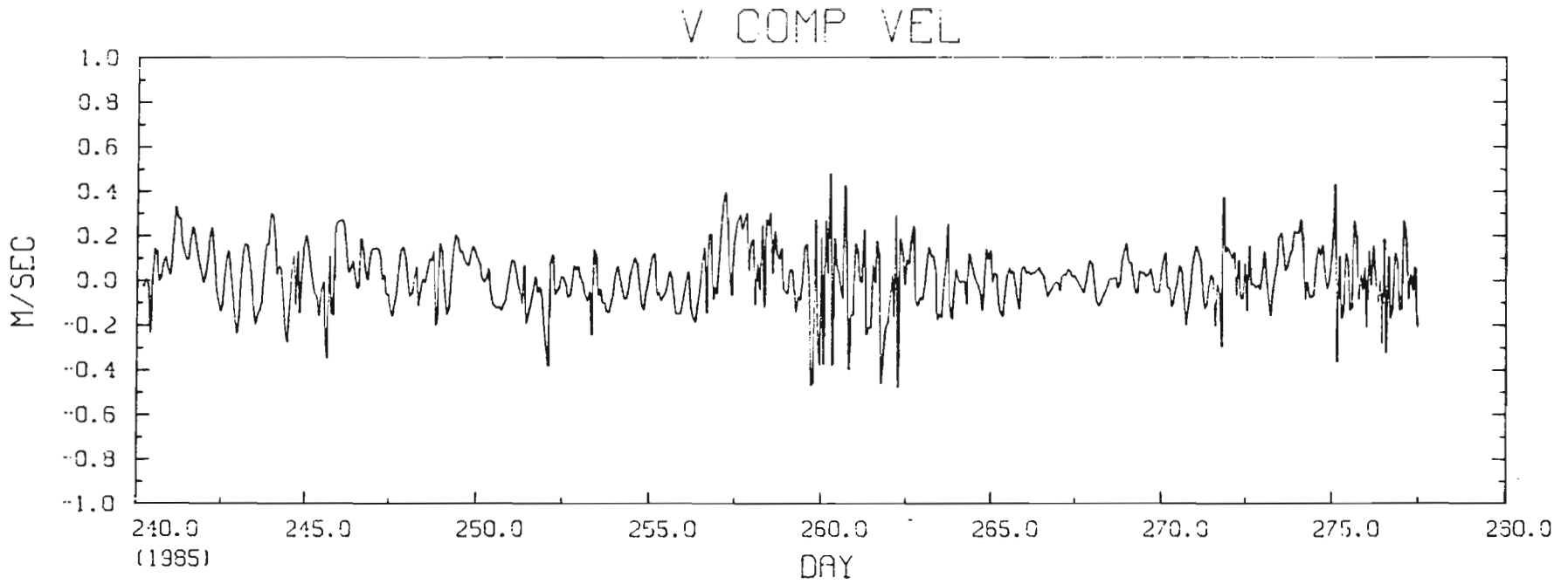
V COMP VEL
1.0
0.8
0.6
0.4
0.2
0.0
-0.2
-0.4
-0.6
-0.8
-1.0
M/SEC
240.0
(1985)
245.0
250.0
255.0
260.0
265.0
270.0
275.0
280.0
DAY

**A R N A K**

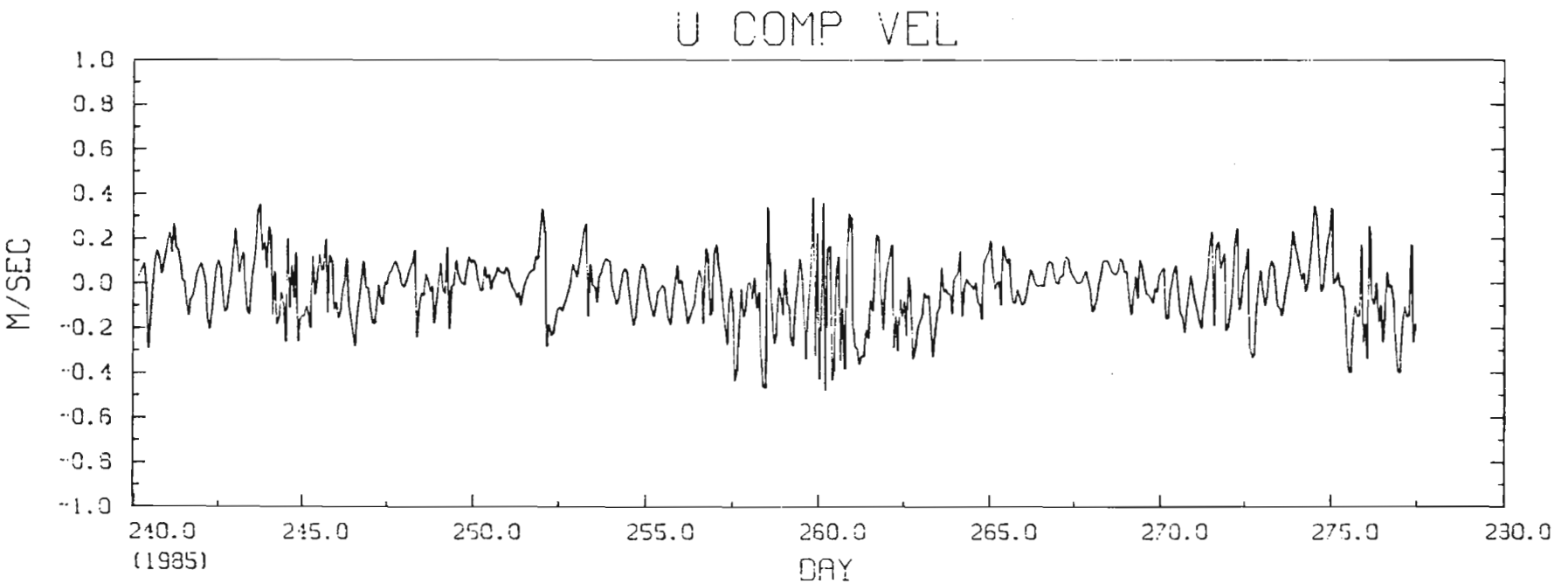
U COMP VEL
1.0
0.8
0.6
0.4
0.2
0.0
-0.2
-0.4
-0.6
-0.8
-1.0
M/SEC
240.0
(1985)
245.0
250.0
255.0
260.0
265.0
270.0
275.0
280.0
DAY

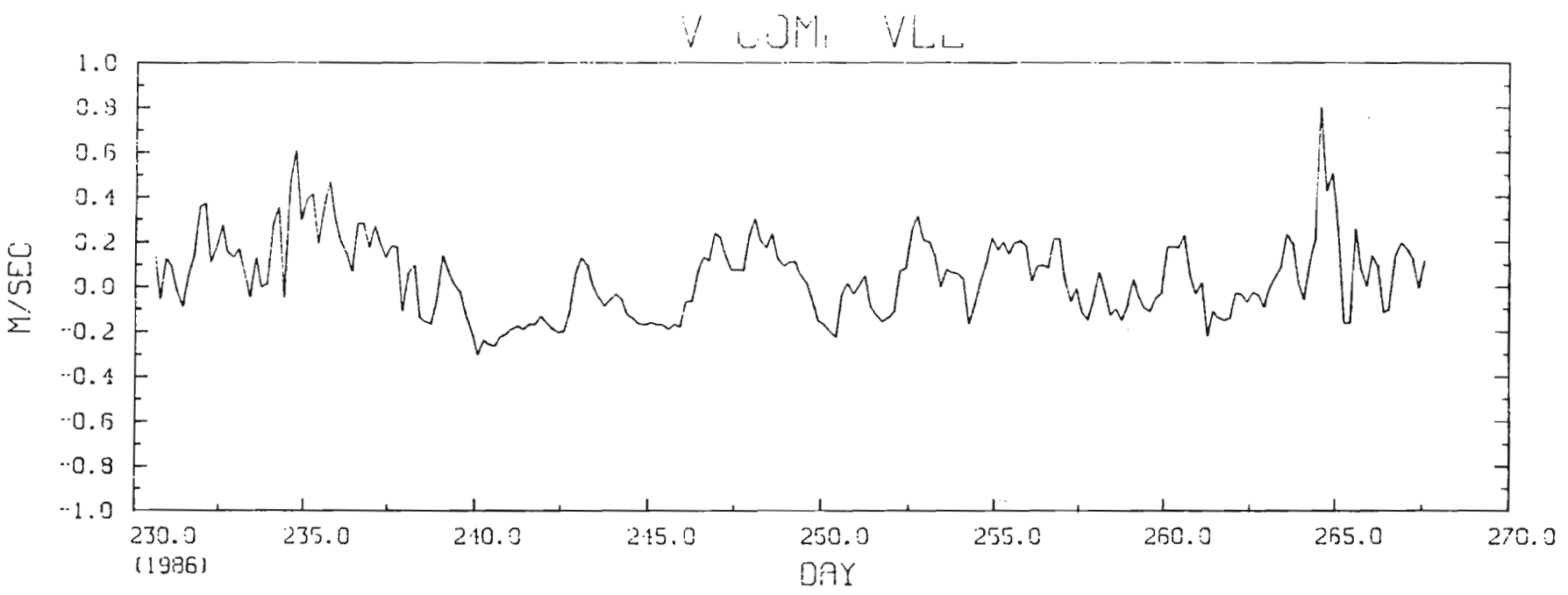
V COMP VEL
M/SEC
1.0
0.8
0.6
0.4
0.2
0.0
-0.2
-0.4
-0.6
-0.8
-1.0
230.0
(1986)
235.0
240.0
245.0
250.0
255.0
260.0
265.0
270.0
DAY

**T1.2**

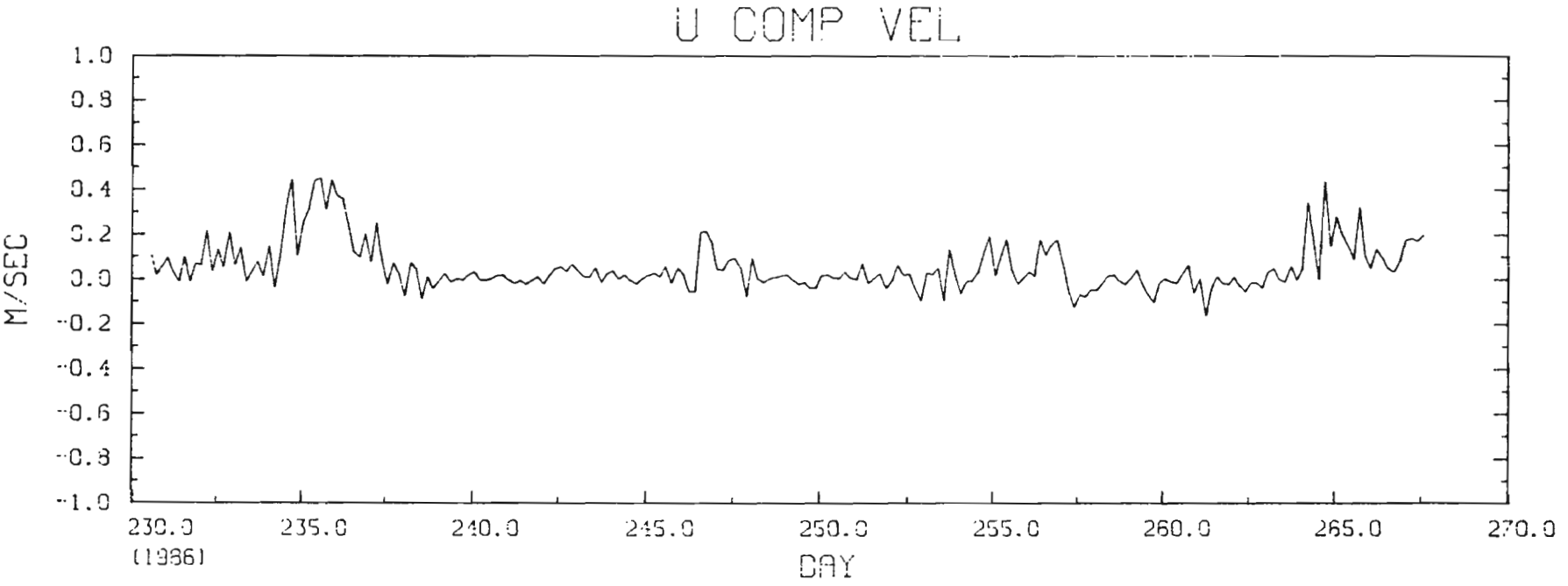
U COMP VEL
M/SEC
1.0
0.8
0.6
0.4
0.2
0.0
-0.2
-0.4
-0.6
-0.8
-1.0
230.0
(1986)
235.0
240.0
245.0
250.0
255.0
260.0
265.0
270.0
DAY

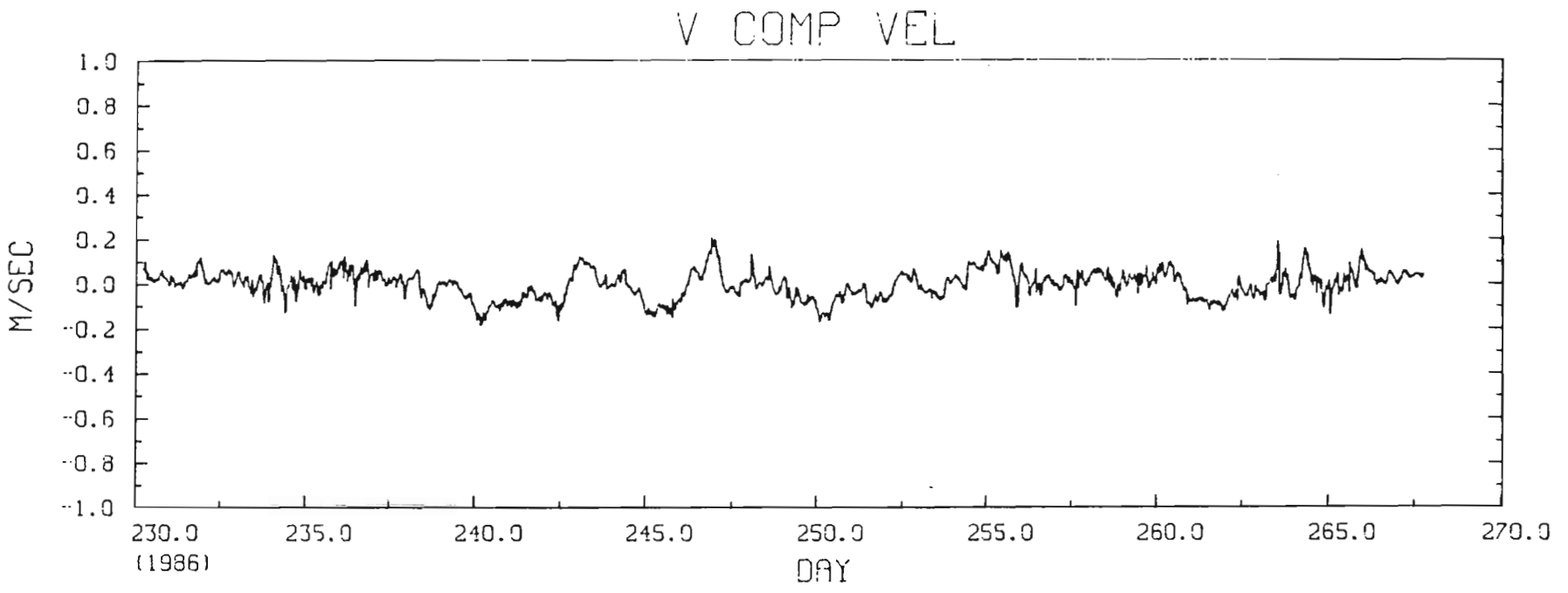
V COMP VEL
M/SEC
1.0
0.8
0.6
0.4
0.2
0.0
-0.2
-0.4
-0.6
-0.8
-1.0
230.0
(1986)
235.0
240.0
245.0
250.0
255.0
260.0
265.0
270.0
DAY

**T1.1**

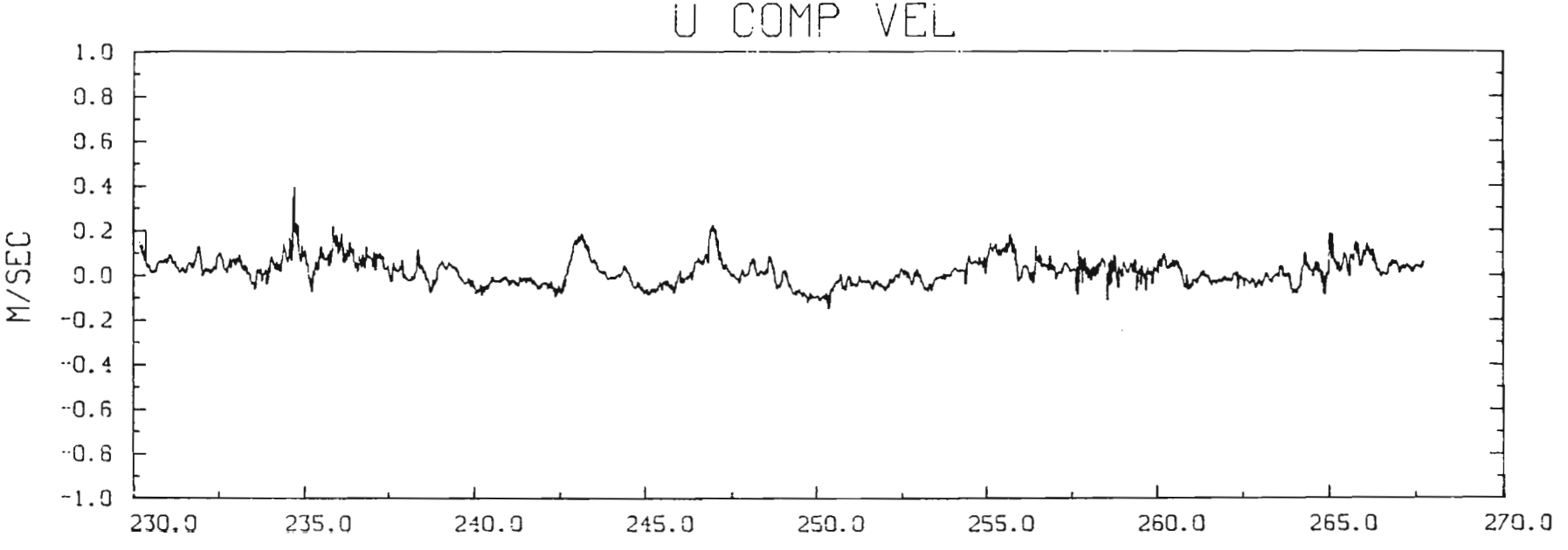
U COMP VEL
M/SEC
1.0
0.8
0.6
0.4
0.2
0.0
-0.2
-0.4
-0.6
-0.8
-1.0
230.0
235.0
240.0
245.0
250.0
255.0
260.0
265.0
270.0

## Appendix B: Bottom stress time series

( Note: 10 Dynes / $cm^2$ = Pa )

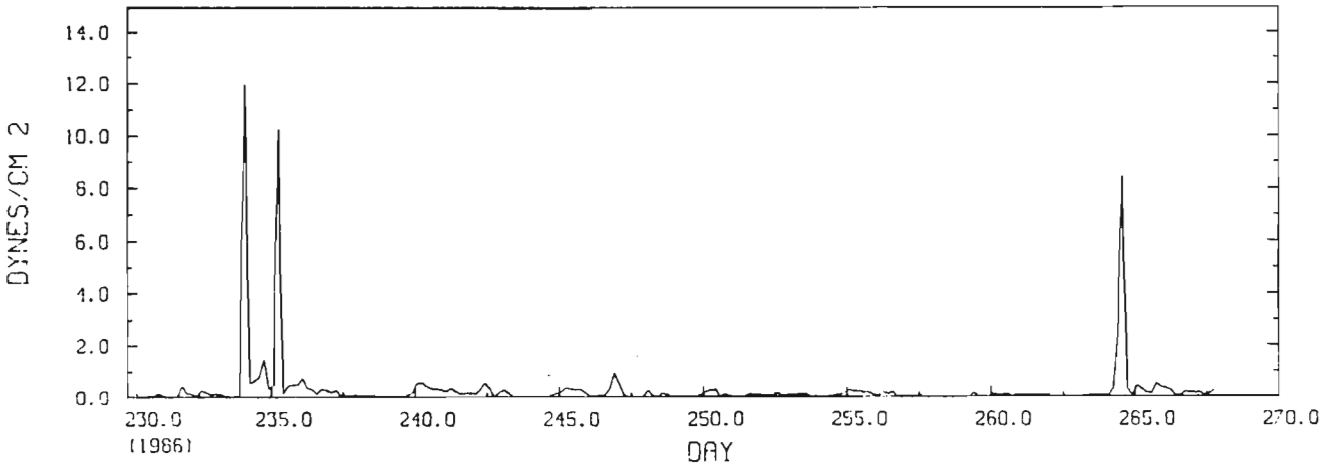


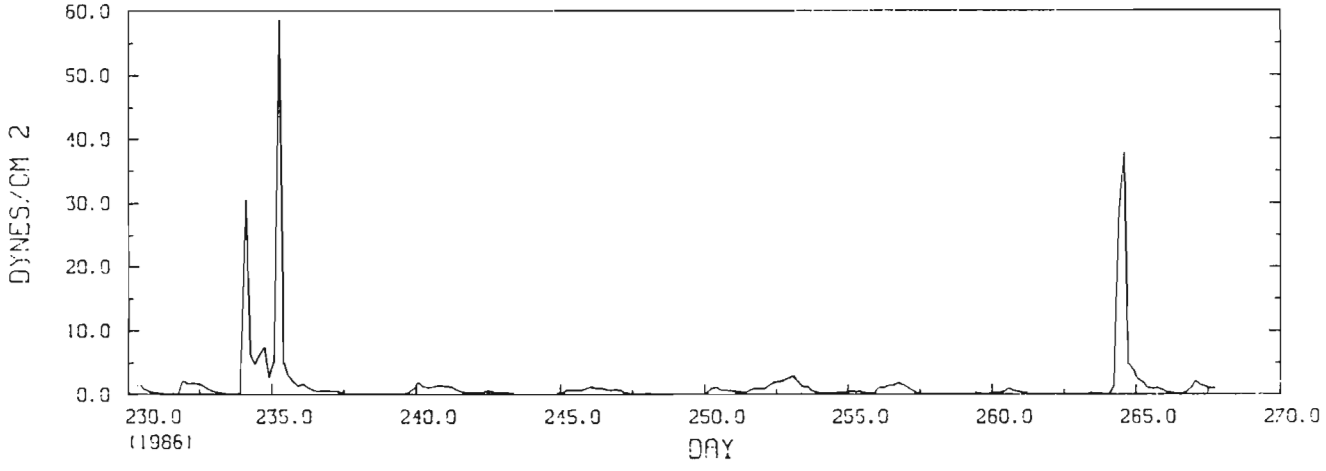


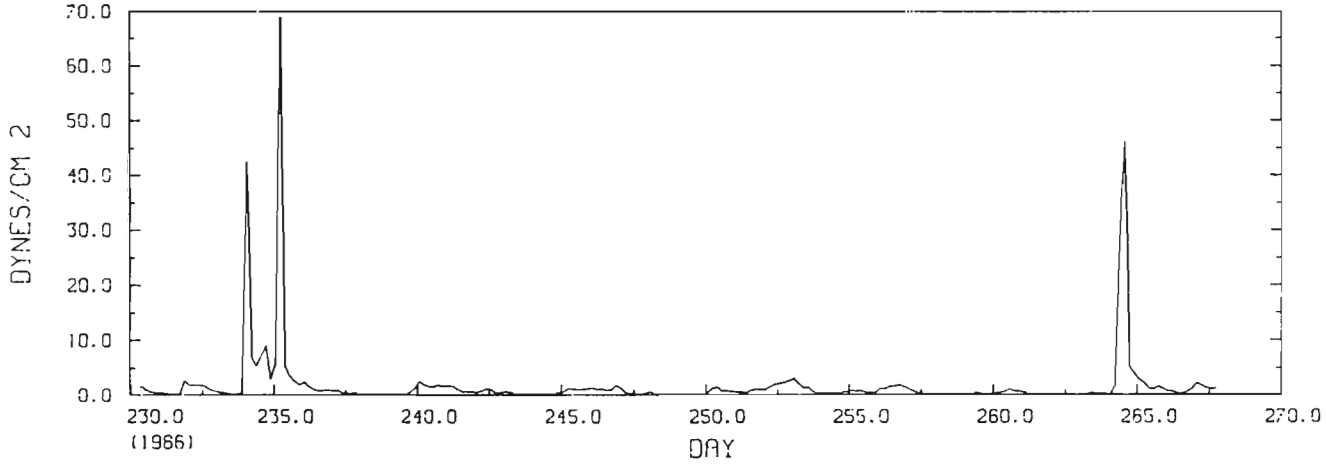


Figure B.1 Time series of bottom shear stress for site T1.1 in 1986: (a) steady component of bottom stress
(b) oscillatory component of bottom stress
(c) total bottom stress

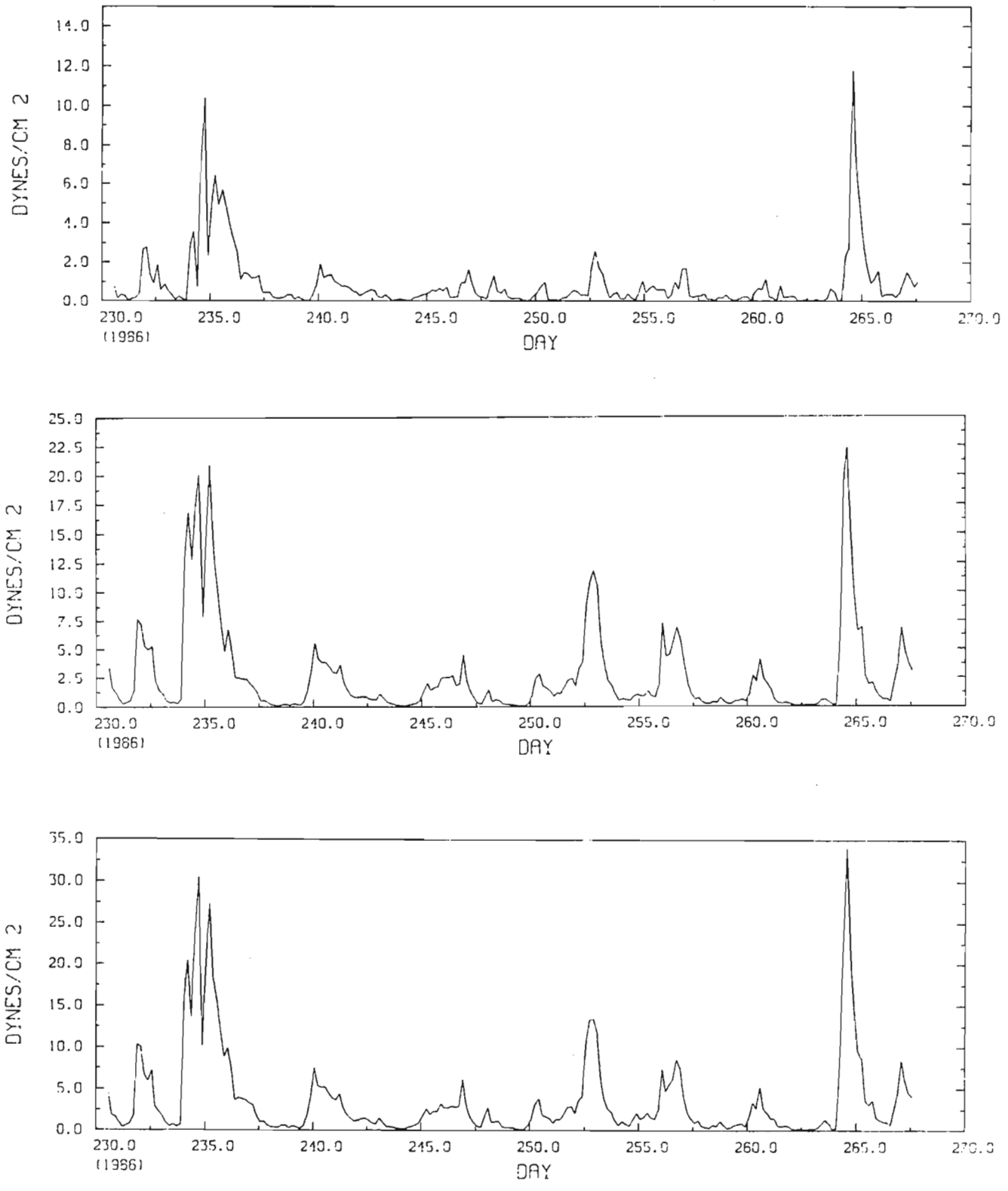


Figure B.2 Time series of bottom shear stress for site T1.2 in 1986: (a) steady component of bottom stress
(b) oscillatory component of bottom stress
(c) total bottom stress

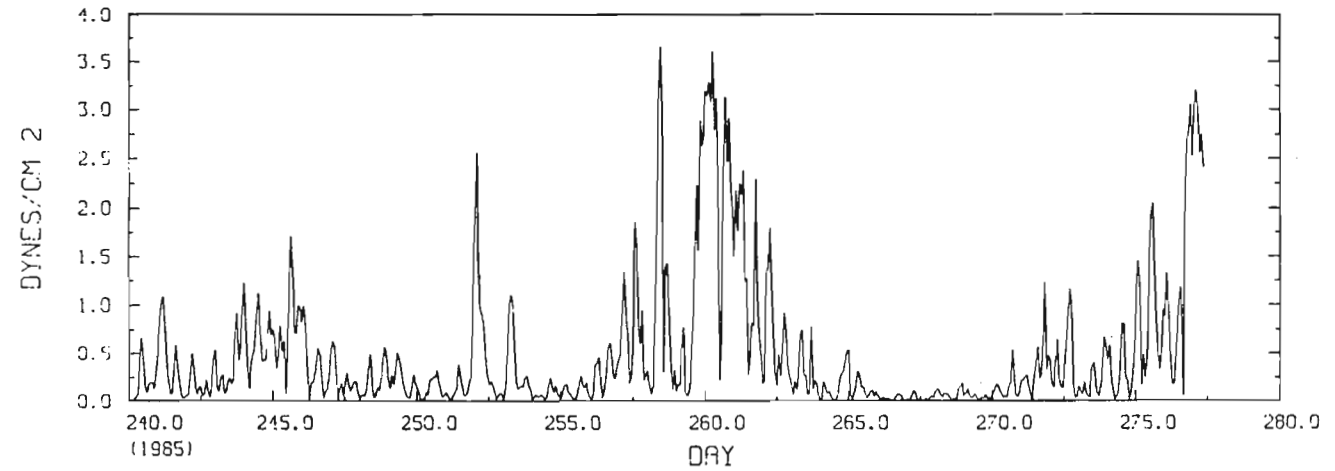


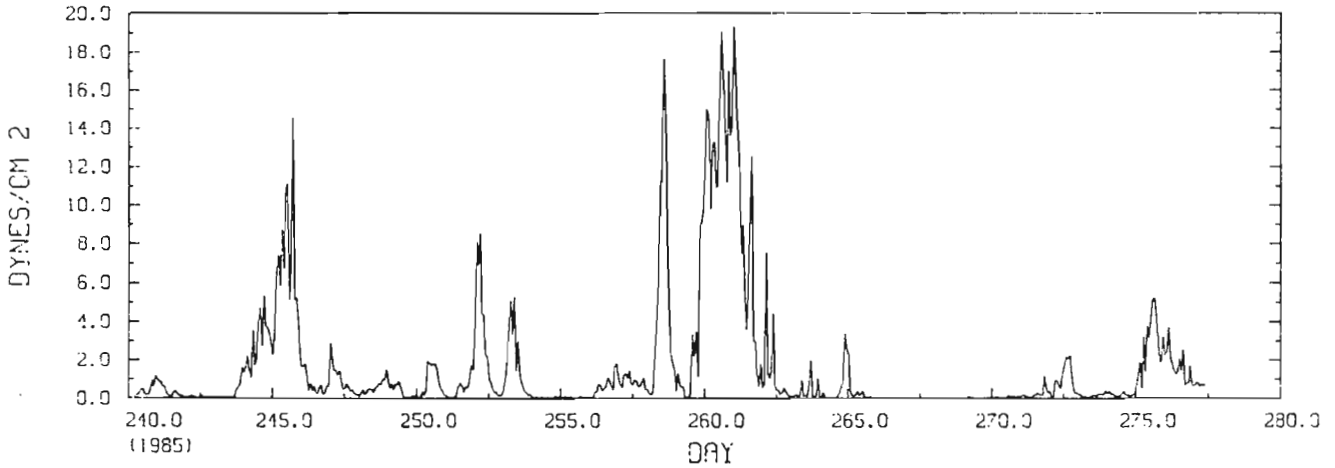


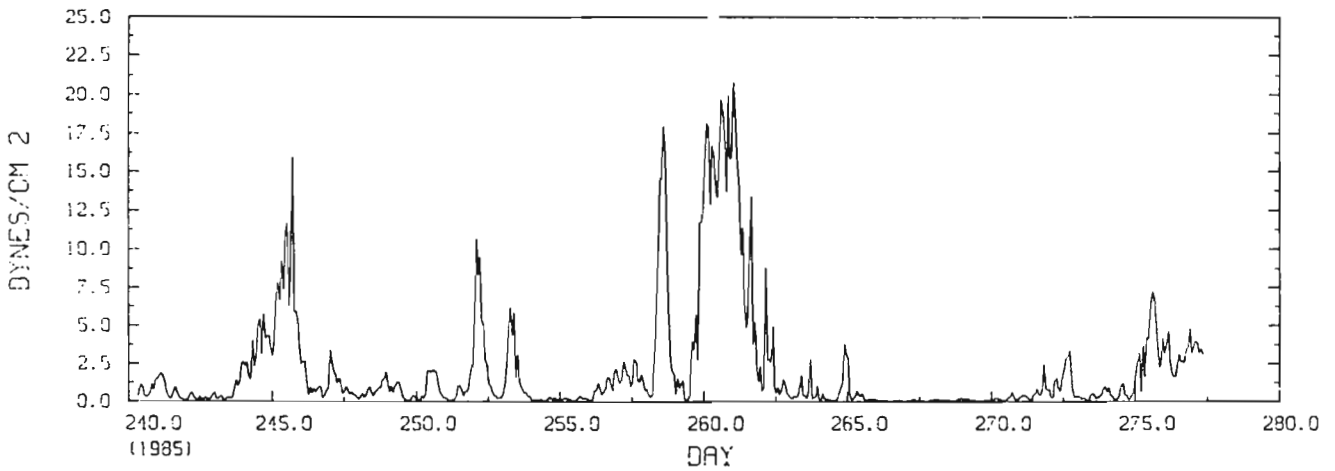


Figure B.3 Time series of bottom shear stress for the ARNAK site in 1985: (a) steady component of bottom stress
(b) oscillatory component of bottom stress
(c) total bottom stress

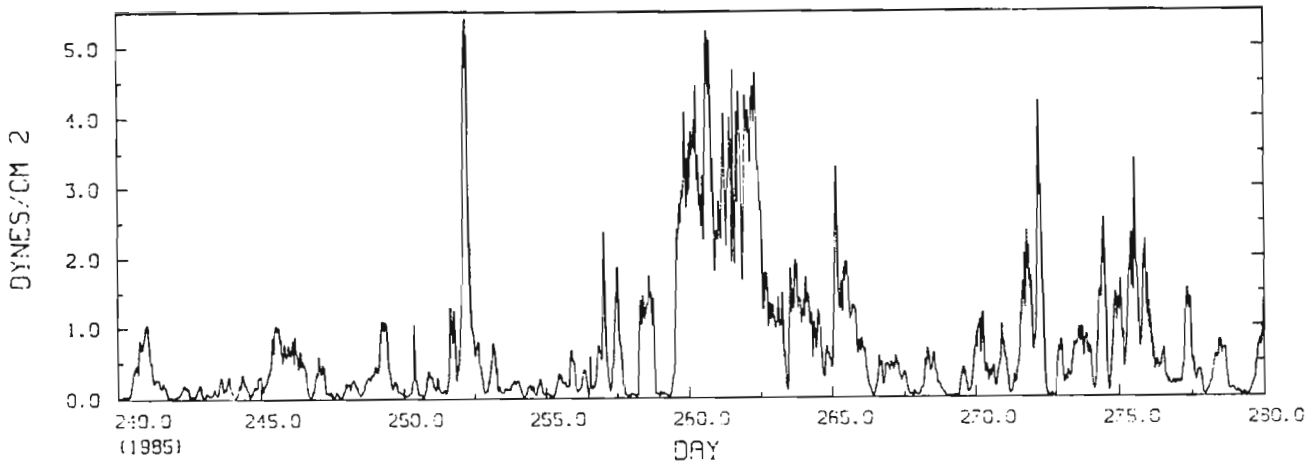


Figure B.4 Time series of bottom shear stress for the steady current component only (no available wave information), for the NIPTERK site in 1985.

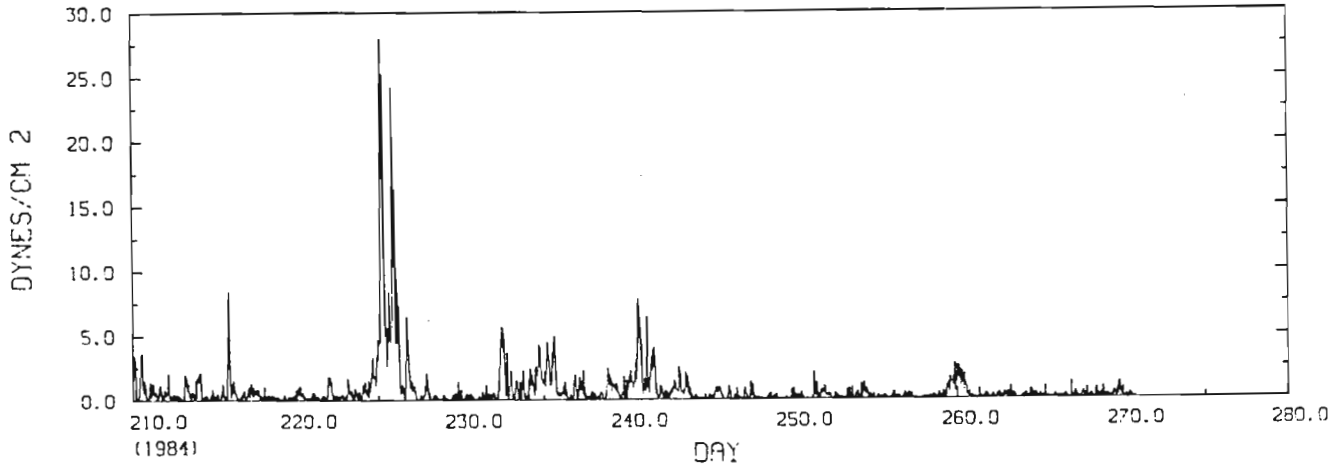


Figure B.5 Time series of bottom shear stress for the steady current component only (no available wave information), for the NIPTERK site in 1984.

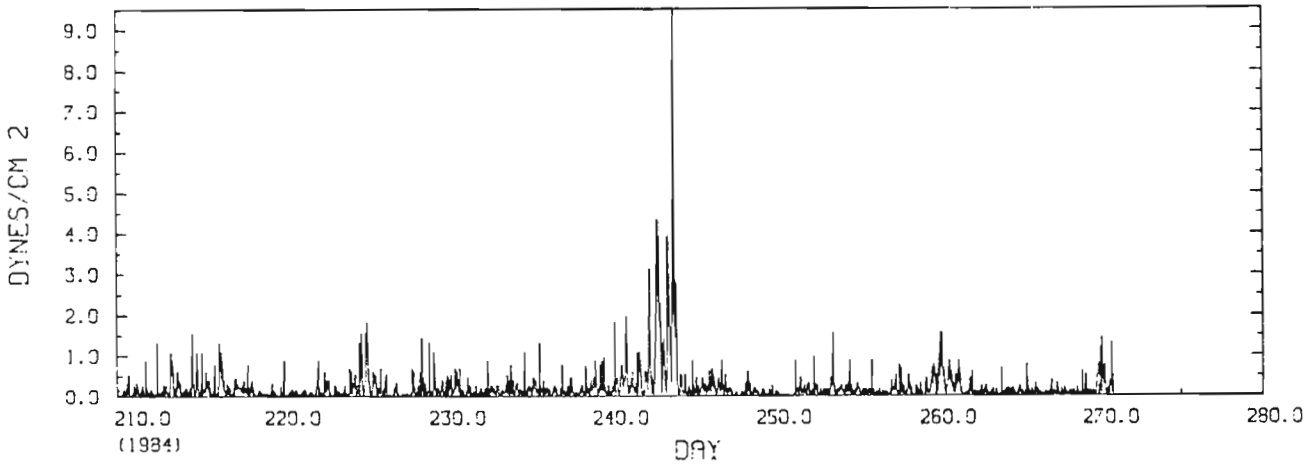


Figure B.6 Time series of bottom shear stress for the steady current component only (insufficient wave information), for the AMERK site in 1984.